Bioresorbable Magnesium Implants for Bone Applications.

Inaugural Dissertation

submitted to the

Faculty of Medicine

in partial fulfillment of the requirements

for the PhD-Degree

of the Faculties of Veterinary Medicine and Medicine

of the Justus Liebig University Giessen

by

Olga Wetterlöv Charyeva

of

Moscow, Russia

Giessen, 2015

From the Laboratory for Experimental Trauma Surgery

Director / Chairman: **Prof. Dr. Christian Heiß**

of the Faculty of Medicine of the Justus Liebig University Giessen

Supervisor:

Prof. Dr. Katrin Susanne Lips

Committee Members:

External reviewer: **Prof. Dr. Annelie-Martina Weinberg**

Chairman: **Prof. Dr. Klaus-Dieter Schlüter**

Vice-Chairman: **Prof. Dr. Jürgen Janek**

Date of Doctoral Defense:

1st December 2015

To my family

TABLE OF CONTENTS

1. Abbreviations

AFM	Atomic Force Microscope
ALP	Alcaline Phosphatase
CPC	Calcium Phosphate Cement
CMPC	Calcium-Magnesium Phosphate Cement
DMEM	Dulbecco's Modified Eagles Medium
FBS	Fetal Bovine Serum
HRD	Human reaming debris-derived cells
Mg	Magnesium
MPC	Magnesium Phosphate Cement
Mg2Ag	Alloy of 98 % magnesium and 2 % silver
Mg10Gd	Alloy of 90 % magnesium and 10 % gadolinium
Mg-HA	Magnesium-Hydroxiapatite
PCL	Polycaprolactone
PMMA	Polymethyl methacrylate
S_a	Average surface roughness
S_{dr}	Developed surface area ratio
S_{ds}	Summit density
SEM	Scanning Electron Microscopy
TEM	Transmission Electron Microscopy
wt	Weight
WE43	Alloy of 4 % yttrium, 3 % rare earth and 93 % magnesium
W4	Alloy of 4 % yttrium and 96 % magnesium

2. Introduction

2.1. Biodegradable Materials for Medical Use

Clinical problems like risk of postoperative infection (Quinn et al. 2009, Hachenberg et al. 2010) and increased incidence of pediatric trauma requiring surgical intervention (Sinikumpu et al. 2012, Sandler et al. 2011) raised the need for temporary medical implants that would resorb after the bone healing is complete. This would decrease high costs associated with repeated surgeries, minimize recovery times, decrease the risk of postoperative infections, and thus promote higher quality of life to each individual patient. The concept of biodegradation is already known in medical practice, resorbable sutures are successfully used in surgery. However, a bone implant that would resorb after the fracture healing is a completely new concept.

Biomaterials used for implants can be metals, ceramics, polymers and composites. Metals have high impact strength, high wear resistance, high ductility and the capacity to absorb high strain energy compared to other materials (Moravej and Montavani 2011). These properties make metals suitable candidates for maxilofacial and orthopedic load-bearing application and fixation devices such as joint replacement, bone plates and screws, as well as dental implants, pacer and suture wires, and coronary stents (Moravej and Montavani 2011, Bhat 2002, Park and Lakes 2007).

The early use of metals as biomaterials for medical applications has been reported in late 18th century when Ag, Fe, Au, and Pt-based alloys were used for bone fracture fixation (Bhat 2002). Elemental magnesium was discovered by Sir Humphrey Davy in 1808 which led to design of metalic biodegradable implants. In 1878, the first implantation of magnesium wires as ligatures to stop bleeding vessels of human patients was performed by Edward C. Huse. He observed that the corrosion of Mg was slower in vivo and that the time period until complete degradation was dependent on the size of the magnesium wire used (Witte 2010).

For metal alloy to be successfully used as a resorbable implant, several criteria must be met. It should provide enough strength to the healing tissues, it should resorb after a set time period, be non-toxic and cause no harm to the organism. Metals proposed for biodegradable implants are magnesium and iron. Iron was mainly suggested for cardiovascular uses like stents for lumen widening (Moravej and Montavani 2011).

Magnesium is considered a suitable material for biodegradable implants because of a number of reasons. First of all, it is biocompatible (Goyer 2001). By term biocompatible it is meant that

material does not cause toxicological tissue reaction (Seal et al. 2009). Secondly, magnesium is natural for humans since our body contains about 25 g of this element and 50-60 % is found in bone (Institute of Medicine 1997). The normal serum magnesium concentration is 0.75 to 0.95 mmol/liter (1.8 to 2.3 mg/dl), we consume about 380-850 mg of magnesium daily (Institute of Medicine 1997). The main sources of magnesium are grains, nuts and green leafy vegetables like spinach and cabbage. Deficiency of these dietary products can cause cardiovascular problems and migraines (Institute of Medicine 1997). Excess magnesium is removed readily by the kidneys (Institute of Medicine 1997). Thirdly, magnesium seems to stimulate bone formation since magnesium ions enhance the cell attachment and proliferation (Li et al. 2008). High amounts of magnesium-containing calcium phosphate were found in the degradation layer around magnesium implants and it was concluded that magnesium stimulates formation of calcium phosphate (Xu et al. 2006, Witte et al. 2005). New bone was seen forming in direct contact to the degradation layer (Xu et al. 2006, Witte et al. 2005). It has been stated that magnesium containing calcium phosphate should have much better osseoconductivity than hydroxyapatite (Kim et al. 2003).

Last but not least, magnesium has excellent mechanical properties which make it a suitable material in trauma patients (Seal et al. 2009). Magnesium based alloys are typically very light since they are 1/3 less dense as titanium based alloys and only 1/5 as dense as stainless steel and cobalt-chrome alloys (Seal et al. 2009). Conventional metallic implants are not well matched, when compared with bone, given the modulus of elasticity for cortical bone is in the order of 3-20 GPa (Staiger et al. 2006). In comparison the modulus of elasticity for stainless steels is typically around 200 GPa, for chrome-cobalt alloys is in the order of 230 GPa, and for titanium alloys is about 115 GPa (Seal et al. 2009). The greater the implant's modulus of elasticity, the higher risk of causing stress shielding of the bone and secondary fracture (Seal et al. 2009). Magnesium alloys, in contrast, have a modulus of elasticity of around 45 GPa, which is much more closely matched to that of bone (3-20 GPa), thus lessening the likelihood of stress shielding (Seal et al. 2009).

2.2. Corrosion

An important problem of magnesium is a high corrosion rate with consistent hydrogen gas formation on contact with fluids:

$$Mg_{(s)} + 2\,H_2O_{(aq)} \rightleftharpoons Mg(OH)_{2\ (s)} + H_{2\ (g)} \qquad (1)$$
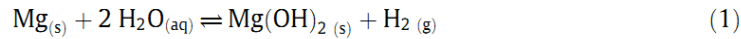
This overall reaction may include the following partial reactions:

$$Mg_{(s)} \rightleftharpoons Mg^{2+}_{(aq)} + 2\,e^- \text{ (anodic reaction)} \qquad (2)$$

$$2\,H_2O_{(aq)} + 2\,e^- \rightleftharpoons H_{2\ (g)} + 2\,OH^-_{(aq)} \text{ (cathodic reaction)} \qquad (3)$$

$$Mg^{2+}_{(aq)} + 2\,OH^-_{(aq)} \rightleftharpoons Mg(OH)_{2\ (s)} \text{ (product formation)} \qquad (4)$$
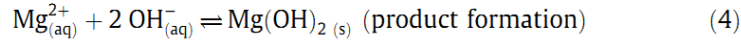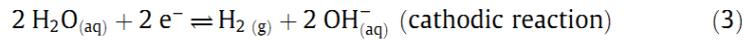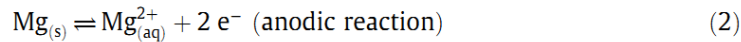
(Witte et al. 2008)

Magnesium hydroxide accumulates on the surface of the magnesium implant to form a mildly protective corrosion layer in water. Although this film slows corrosion under aqueous conditions, it reacts with chlorine ions present in blood to produce a highly soluble magnesium chloride, $MgCl_2$, and hydrogen gas, H_2 (Witte et al. 2008). It was shown that this reaction is achieved when the chloride concentration in the system increases above 30 mmol/l (Shaw et al, 2003). Therefore, severe pitting corrosion can be observed on magnesium alloys where the chloride concentration of the body fluid is about 150 mmol/l (Xu et al. 2007, Witte et al. 2005).

Increase of the pH during this reaction further irritates tissues and makes it more difficult to heal (Witte et al. 2008). The hydrogen bubbles push out the osteoclasts and osteoblasts making it difficult to form new bone in direct proximity to the implant surface. However, hydrogen gas seems to appear within 1 week after implantation, and then disappear after 2-3 weeks (Witte et al. 2005).

It is desirable for magnesium-based alloys to have slow degradation rate so the fractured bone heals before the implant resorbs. It is thus crucial to design alloys with slow corrosion rate and high biocompatibility. Hard-tissue repair typically requires implantation of the fixture for a minimum of 12 weeks (Staiger et al. 2005). In this respect, pure magnesium is undesirable, because it is chemically very active (Xin et al. 2011).

The influence of cells and in vivo environment on magnesium corrosion is not well described in literature. It is known that corrosion is faster in vitro than in vivo by several orders of magnitude (Willumeit et al. 2011). This can be explained by the presence of proteins and other organic molecules in blood which create a protective coating around magnesium slowing down corrosion (Willumeit et al. 2011). Thus, an addition of proteins in form of fetal bovine serum (FBS) into the cell growth media would closer imitate in vivo environment than just using pure media during corrosion studies on magnesium. Dulbecco's modified Eagle's medium (DMEM) contains inorganic salts, calcium, amino acids and vitamins, and is thus very close to physiologic conditions (Willumeit et al. 2011).

It was shown that magnesium facilitates calcification and formation of calcium phosphates (Feyerabend et al. 2012). As mentioned previously, magnesium increases pH of the solution. This shift to more basic pH might interfere with bone healing (Xu et al. 2007), but at the same time high pH promotes Ca^{2+} binding (Willumeit et al. 2011). An adequate supply of calcium is important to ensure that bone laid down by osteoblasts is normally mineralized (Reid 2014).

2.3. Magnesium-Based Alloy Design

Although magnesium is biocompatible, increased degradation rates under physiological pH conditions can locally reduce the biocompatibility on the implant surface. Efforts to control the corrosion rate of Mg have utilized various processing methods such as purification, alloying, anodizing, and surface coating (Brar et al. 2008). Studies have shown that purification of Mg reduces the corrosion rate considerably, however, due to low yield strength of pure magnesium (Witte et al. 2005), its application in medical appliances that require good load bearing properties, is limited.

Alloying elements can be added to improve mechanical properties of pure magnesium but alloying elements should be selected carefully not only in respect to physical properties, but most importantly in respect to their effect on cells and body as whole. This, however, is a difficult task since one must look not only on the element as a single unit, but also consider its interactions with other elements in the magnesium-based alloy. This chapter will discuss some common elements used in Mg alloys in respect to their properties and toxicology.

In general, adding extra elements to the alloy will strengthen material by forming intermetallic phases. These intermetallic phases act as obstacles for the dislocation movement (Witte et al. 2008). Even ductility and corrosion properties might be influenced (Witte et al. 2008, Shaw et al. 2003). Typical impurities in magnesium alloys are iron (Fe), nickel (Ni), copper (Cu), and beryllium (Be) (Witte et al, 2008). They have extremely harmful effects on the corrosion behaviour of Mg and rapidly increase the degradation rate. Elements like cadmium (Cd), manganese (Mn), tin (Sn), and zinc (Zn) have mild effect on the corrosion rate of Mg with their efficacy being dependent on solute concentration (Shaw et al. 2003). Aluminum (Al) is considered to enhance the strength and corrosion resistance of Mg, but in recent years it has been implicated in a variety of disorders including dialysis demential, hypochromic microcytic anaemia, renal osteodystrophy, hepatic disorders and Alzheimer's disease (Kawahara 2005, Shcherbatykh and Carpenter 2007). For that reasons it is unacceptable to use Al in medical implants.

Zirconium, which is added as a grain refiner in Mg-based alloys, has been linked to breast and lung cancer (Brar et al. 2008). It is reported that rare earth (RE) elements have a beneficial effect on the corrosion resistance and mechanical properties of magnesium alloys (Nakatsugawa et al. 1996). Some of these elements like cerium (Ce), lutetium (Lu), and praseodymium (Pr), are, however, considered toxic for the human body (Brar et al. 2008). Still, there are some elements in the RE family that have relatively low chemical toxicity and can be used in very small amounts without toxic effect on the organism. Such elements are yttrium (Y) (Reardon et al. 2009, Kyker and Anderson 1955) and gadolinium (Gd) (Hemmer et al. 2010, Setyawati et al. 2012). Alloying magnesium with yttrium could be an effective measure to improve the bio-corrosion properties of the magnesium alloy for biomedical application (He et al. 2010). Combining magnesium with silver (Ag) might not only strengthen the material but also add antibacterial properties to the alloy (Tie et al. 2013).

Calcium addition to magnesium alloys slows corrosion rate, which is beneficial in terms of hydrogen gas formation (Aghion et al. 2012). Ideally, corrosion would be slowed to allow the mechanical integrity of the metal to remain intact during bone healing. This would also minimize hydrogen production, which has been observed as a (potentially disadvantageous) corrosion by-product when using this material (Shadanbaz et al. 2012). Moreover, calcium ions might contribute to increased viability of magnesium alloys, like in Mg-Ca alloy tested in one Chinese study (Li et al. 2008).

Calcium is natural for humans and it accounts for 1-2 % of adult human body weight. Over 99 % of total body calcium is found in teeth and bones, the rest is present in blood, muscle, and other tissues, where it mediates vascular and muscular contraction and nerve transmission (Institute of Medicine 1997).

In bone, calcium exists primarily in the form of hydroxyapatite (Ca_{10} $(PO_4)_6$ $(OH)_2$), and bone mineral is almost 40 % of the weight of bone (Institute of Medicine 1997). Using materials essential to human body as alloying elements, we can greatly reduce the chance of toxicity (Brar et al. 2008).

For the above mentioned reasons, six types of biodegradable magnesium-based alloys were designed and produced for this study:

- alloy consisting of 98 % Mg and 2 % Ag (Mg2Ag),
- alloy of 90 % Mg and 10 % Gd (Mg10Gd),
- alloy of 4 % yttrium, 3 % rare earth and 93 % magnesium (WE43),

- pure 99.8 % magnesium (pure Mg),
- magnesium-hydroxyapatite composite implant (Mg-HA),
- alloy of 96 % Mg and 4 % Y (W4).

2.4. Surface

Corrosion of magnesium implants also has an effect on material's surface characteristics. Surface plays an important role for cell attachment. Both too rough and too smooth surfaces are not beneficial and hinder bone formation around implants (Wennerberg and Albrektsson 2000). Several parameters can describe implant surface topography, such as average surface roughness (S_a), developed surface area ratio (S_{dr}) and summit density (S_{ds}). S_a is defined as an arithmetic mean of the departures of the roughness area from the mean plane (Wennerberg and Albrektsson 2000). S_{dr} is a ratio between the 3-D measurement and a 2-D reference plane (Wennerberg and Albrektsson 2000). S_{ds} is the number of summits per unit area making up the surface (Stout et al. 1993). Parameters describing spatial properties, like S_{ds}, as well as hybrid properties, like S_{dr}, might further differentiate surfaces with similar S_a characteristics (Stout et al. 1993).

It was shown by previous studies that an optimal S_a value, representing average surface roughness, lies between 1-1.5 μm for titanium implants (Wennerberg and Albrektsson 2000). However, positive effect on the bone response was also seen for S_a of ~ 0.5 μm up to ~ 8.5 μm (Shalabi et al. 2006). Long-term corrosion effect on surface roughness of magnesium-based alloys has not been studied yet.

It also seems that bacterial adhesion to surface is highly dependent on surface roughness (S_a) and developed surface area ratio (S_{dr}) (Dorkhan et al. 2012, Bürgers et al. 2010). The level of bacterial adherence to moderately rough titanium surfaces (S_{dr} 58 %) was five times greater than to smooth titanium surfaces (S_{dr} 2.8 %) (Dorkhan et al. 2012). Magnesium resorbs mainly by pitting corrosion (Witte et al. 2005) which results in surface changes and might promote bacterial adhesion. Thus, it is important to compare whether any correlation between biofilm adhesion and surface changes which occur during resorbtion exist.

2.5. Bacterial Infections

Postoperative wound infections are the third most common type of nosocomial infection in German emergency hospitals after pneumonia and urinary infections (Hachenberg et al. 2010). They accounts for 14-16 % of all nosocomial infections among hospital patients and are associated with increased morbidity and mortality, prolonged hospital stay and increased costs

(Smyth et al. 2008, Smyth and Emmerson. 2000). The most important risk factors include the microbiological state of the skin surrounding the incision, delayed or premature prophylaxis with antibiotics, duration of surgery, emergency surgery, poorly controlled diabetes mellitus, malignant disease, smoking and advanced age (Hachenberg et al. 2010). If the implant could biodegrade then all those risk associated with repeated surgeries could be avoided. Thus, development of such implant is of importance.

Implant-associated infections are the result of bacteria adhesion to an implant surface and subsequent biofilm formation at the implantation site (Ribeiro et al. 2012). Sources of infectious bacteria include the environment of the operating room, surgical equipment, clothing worn by medical and paramedical staff, resident bacteria on the patient's skin and bacteria already residing in the patient's body (Ribeiro et al. 2012, Frank et al. 2013). Thus, the secondary operation on implant removal highly increases the risk of nosocomial infection.

Enterococci, specifically *Enterococcus faecalis*, are the third most common cause of nosocomial infection, and most infections in hospitalized patients are associated with the use of indwelling medical devices (Paganelli et al. 2013). *E. faecalis*, a Gram-positive constituent of the human intestinal microbiome, has become a prominent pathogen of health care-associated infections over the past 3 decades (Frank et al. 2013). Between 1980 and 2008, the frequency of nosocomial infections caused by *Enterococcus faecium*, the other frequently encountered enterococcal pathogen, increased by 8.8 % (Kang et al. 2012). *E. faecalis* and *E. faecium* infections together accounted for 16.0 % of central line-associated bloodstream infections, 14.9 % of catheter-associated urinary tract infections, and 11.2 % of surgical site infections reported to the United States National Healthcare Safety Network between 2006 and 2007 (Hidron et al. 2008). *E. faecalis* is also the primary causative agent of enterococcal endocarditis (McDonald et al. 2005, Fernández Guerrero et al. 2007) and is the most frequently isolated in secondary endodontic infections (Tennert et al. 2014).

Staphylococcus epidermidis and *Staphylococcus aureus* represent, in absolute, the main causative agents of infection in orthopedics (Campoccia et al. 2006). *S. epidermidis* is the most frequently isolated member of the group of coagulase-negative staphylococci from implant-associated infections and they are associated with nosocomial infections (Ribeiro et al. 2012). *S. epiderimidis*, a Gram-positive, nonspore forming facultative anaerobe that grow by aerobic respiration or fermentation, with diameters of 0.5−1.5 mm, belong to the normal microbiota of

the human skin (Ribeiro et al. 2012). They are characterized by individual cocci, which divide in more than one plane to form grape-like clusters (Ribeiro et al. 2012).

2.6. Ethical Aspects in Experiment Planning for in vitro and in vivo Studies

In 1959, Russell and Burch published "The Principles of Humane Experimental Techniques", which idea was the humanest possible treatment of experimental animals (Russell and Burch 1959). The authors suggested the principles of *Replacement, Reduction and Refinement*, commonly abbreviated to 3R's principle, as the main guideline to achieve as humane experimental techniques as possible. Today the principles of the 3R's is used internationally to govern the use of animals in life science.

By *replacement* meant Russell and Burch the use of non-animal methods over animal methods if this allows to achieve the same scientific aims. Replacement strategies include: a) tissue culture, b) perfused organs, c) tissue slices, d) cellular experiments, e) subcellular fractions (Russell and Burch 1959).

Reduction method enables scientists to obtain data from fewer animals, or to gain more data from the same number of animals (Russell and Burch 1959). Careful study design is crucial for this method to be successful. Development of computer technologies and modern imaging techniques greatly facilitate this principle.

Refinement means minimization of animal suffering during experiment. This includes proper anaesthetic and analgesic regimes for pain relief, non-invasive study techniques, as well as proper housing and environmental enrichment meeting the animals' needs (Russell and Burch 1959).

The current Thesis is based on 3 R's principle. In vitro methods were used on the first place in order to understand the processes which happen to magnesium-based alloys without involving animals. That is why the cellular experiment, the in vitro biofilm formation study design and in vitro corrosion were chosen. The last stage was to see the tissue reaction to magnesium-based implants. The implants were carefully chosen and the animal number was kept to as low as possible.

Unfortunately, in vitro methods have their disadvantages compared to in vivo methods. In case with magnesium implants it is known that corrosion is faster in vitro than in vivo by several orders of magnitude (Willumeit et al. 2011). This can be explained by the presence of proteins

16

and other organic molecules in blood which create a protective coating around magnesium slowing down corrosion (Willumeit et al. 2011). Thus, carefully planning the experiment is crucial. In our study, an addition of proteins in form of fetal bovine serum (FBS) into the cell growth media during corrosion study was chosen in order to closer imitate in vivo environment than just using pure media. Dulbecco's modified Eagle's medium (DMEM) contains inorganic salts, calcium, amino acids and vitamins, and is thus very close to physiologic conditions (Willumeit et al. 2011). The majority of studies on magnesium's biocompatibility in vitro assess short-term magnesium extract's effect on the cells (Tie et al. 2013, Feyerabend et al. 2010, Yang et al. 2013). The aim of our cell study was to evaluate the long-term influence of direct exposure of magnesium alloys on the bioactivity of bone-forming cells. This, in our opinion, closer mimics the in vivo conditions.

2.7. Applications of Magnesium Implants

Two magnesium alloys are currently used today in orthopedic and cardiovascular medicine – WE43 and MgYREZr.

WE43 alloy has shown good results in cardiovascular medicine with no evidence of stent particle embolization, thrombosis, excess inflammation, or fibrin deposition and neointimal area was significantly less in magnesium alloy stent segments as compared with the stainless steel stent segments (Waksman et al. 2006). It was shown that biodegradable magnesium stents can achieve an immediate angiographic result similar to the result of other metal stents and can be safely degraded after 4 months in human patients (Erbel et al. 2007). However, modifications of stent characteristics with prolonged degradation and drug elution are still required and currently in development (Moravej and Montavani 2011).

Orthopedic screws consisting of MgYREZr alloy are commercially available under the name MagneZix and are distributed by the medical company Syntellix ("MagneZix Compression Screw 3.2" 2013). MagneZix is an aluminum-free magnesium alloy that is classified as an MgYREZr alloy. This alloy contains rare earth elements and is compositionally similar to WE43 (Windhagen et al. 2013). It has already demonstrated good biocompatibility and osteoconductive quality in vivo (Waizy et al. 2014) and is recommended for treatment of among others hallux valgus, smaller bone fractures, pseudarthrosis and arthrodesis ("MagneZix Compression Screw 3.2" 2013). These screws have shown positive results in the pilot study on 13 patients (Windhagen et al. 2013).

One of the limitations of Windhagen et al.'s study is the relatively low statistical power. Another limitation of MgYREZr alloy is that formation of fibrous tissue was observed in direct contact with the implant at some areas (Waizy et al. 2014). Furthermore, Windhagen et al. were not able to verify complete screw degradation after 6 months (Windhagen et al. 2013). MagneZix was still present after 12 months in the rabbit model (Waizy et al. 2014). The manufacturer thus promises complete degradation in up to 24 months ("MagneZix Compression Screw 3.2" 2013). Although slow degradation of magnesium is desirable, for some areas of medical applications such as pediatric and maxillofacial fields, shorter degradation times than 24 months are required. For pediatric and maxillofacial medicine 6 months degradation would be optimal. Shorter degradation time would minimize allergic reactions and also be beneficial in pediatric patients that are constantly growing and thus should have implants with faster degradation to prevent interference with the growing bone.

Several articles have reported increase in the incidence of paediatric bone fractures (Sinicumpu et al. 2012, Sandler et al. 2011, Delaney et al. 2009). Plays and sports are the common reasons to fractures with trampoline, which can now be seen in almost every household, being the main reason to such an increase (Sandler et al. 2011). Up to 41 % of all paediatric injuries are related to trampoline (Sinicumpu et al. 2012). In about 61-68 % of children with bone fractures, surgical intervention is required (Sandler et al. 2011, Delaney et al. 2009). The most common site for injury are upper limbs, their prevalence lies between 3-27.9 % in different studies (Sinicumpu et al. 2012, Sandler et al. 2011), and the number surgical treatment for diaphyseal fractures increased 4.2-fold (Sinicumpu et al. 2012). Children are a specific group of patients and their treatment is often hampered since their bodies are in a constant process of growing and implants must be adjusted to the bone development so that the growth pattern is uniform and symmetrical. All repeated surgeries carry risks as discussed previously, and it is thus desired to avoid such procedures. Magnesium-based implants could therefore aid even in the pediatric field.

The possible application areas of magnesium in maxillofacial field are screws and plates for fixation of traumatic orbital defects (Izuka et al. 1991), treatment of zygomatic fractures (Bergsma et al. 1993), fixation of mandibular fractures (Quereshy at al. 2000), and fixation in orthognathic and pediatric craniofacial surgeries (Edwards et al. 2001).

3. Aims

The main aim of this Thesis was to investigate magnesium implants' biocompatibility in vitro and in vivo, as well as to study their ability to resist biofilm formation. Additionally, this Thesis examines resorption of magnesium materials and its effect on surface and surrounding environment.

Study I: Degradation

- To determine the corrosion rates of pure Mg, Mg2Ag, Mg10Gd and WE43.
- To analyze magnesium's effect on osmolality, Ca^{2+} concentration, pH and on surface changes.

Study II: Cellular Reactions

- To evaluate the long-term influence of direct exposure of pure Mg, Mg2Ag, Mg10Gd and WE43 on the bioactivity of human reaming debris-derived cells.

Study III: Biofilm

- To investigate pure Mg, Mg2Ag, Mg10Gd and WE43's ability to resist bacterial adhesion as well as further biofilm formation.
- To examine the possible correlation between the early stages of biofilm formation and the surface characteristics.

Study IV: Histological Examination

- To determine the bone response to pure Mg, Mg-HA and W4.
- To evaluate the amount of gas in the bone tissue and the implant resorption behavior.

4. Material and Methods

4.1 *In vitro*

4.1.1. Sample production

The following materials were used to produce alloys for this study: magnesium (99.99 %, Xinxiang Jiuli Magnesium Co. Ltd., China), yttrium (99.95 %, Grirem Advanced Materials Co. Ltd., China), gadolinium (99.95 %, Grirem Advanced Materials Co. Ltd., China), rare earth mixture (Grirem Advanced Materials Co. Ltd., China), and silver (99.99 %, ESG Edelmetall-Handel GmbH & Co. KG, Germany).

Three magnesium-based materials were produced: Mg2Ag (1.89 % Ag, the rest was Mg), Mg10Gd (8.4 % Gd, the rest was Mg), and WE43 (3.45 % Y, 2.03 % Nd, 0.84 % Ce, the rest was Mg). Pure magnesium (99.97 % Mg) was used as a control. The concentrations of magnesium Mg, Y, Nd and Ce were determined by spark emission spectrometer (Spectrolab M, Spektro, Germany) and the concentrations of Ag and Gd were determined by X-ray fluorescence spectrometer (Bruker AXS S4 Explorer, Bruker AXS GmbH., Germany). The materials were cast at Helmholtz Zentrum Geesthacht, Magnesium Innovation Center (HZG-MagIC).

The three magnesium alloys (Mg2Ag, Mg10Gd, WE43) were produced by permanent mould gravity casting. After melting the pure Mg the melt was held at 720 °C and the preheated alloying elements were added with continuous stirring for 15 minutes. The melt was poured into a preheated (550 °C) permanent steel mould treated with boron nitride. During the casting process cover gas was used (SF_6 and Ar mixture). The alloys were homogenized with a T4 heat treatment prior to extrusion in Ar atmosphere at 550 °C (Mg10Gd and WE43) and at 420 °C (Mg2Ag) for 6 hours (h). Afterwards the alloys were extruded indirectly with an extrusion ratio of 4:25. The chamber of the extrusion machine was set to 370 °C and the billets (d = 30 mm) were preheated for one hour at 370 °C (Mg2Ag), at 390 °C (WE43) and at 430 °C (Mg10Gd). The extrusion speed was between 3 and 4.5 mm/sec. Pure Mg was cast by permanent mould direct chill casting (Peng et al. 2010). The cast billet (d = 110 mm) was extruded indirectly with an extrusion ratio of 1:84. The billet temperature was 340 °C and the speed of the extrusion was 0.7 mm/sec. Discs (10 mm diameter and 1.5 mm thickness) were machined from the extruded bars and then polished with Grit 400 silicone carbide sandpaper.

4.1.2. Sample sterilization

The samples were sonicated for 20 minutes (min) in dry isopropanol, dried and gamma-sterilized at the BBF Sterilisationservice GmbH facility (Kernen, Germany) with a total dosage of 29 kGy.

4.1.3. Corrosion Measurements

Corrosion measurements were performed by two methods: immersion test and hydrogen gas evolution test. The immersion tests were performed following in general the ISO 10993, but with modifications: per 0.2 g of sample 3 mL medium consisting of DMEM (DMEM, Life Technologies) with 10 % FBS (PAA Laboratories, Linz, Austria) was used. In total, 6 samples per time point were used. Incubation was performed at 37 °C, 5 % CO_2, and 95 % humidity in an incubator (Heraeus BBD 6620, Thermo Fisher Scientific, Schwerte, Germany), oxygen content was set to 20 %. The exposition time of the samples was up to 240 h with medium change every 48 h. After immersion, the corrosion products were removed by chromic acid (180 g/L in distilled water, VWR International, Darmstadt, Germany) at room temperature. The average corrosion rate was calculated using the formula:

$$CR = (8.76 \times 10^4 \, \Delta g) / (A \cdot t \cdot \rho)$$

where Δg is the weight change in grams, A is the surface area in cm^2, t is the immersion time in h, and ρ is alloy's density in g/cm^3.

The experimental set up for gas evolution method is depicted in Figure 1. All samples were first weighed and then immersed in DMEM containing 10 % FBS. Gas production was measured by eudiometer (400 ml, Rettberg, Germany) at room temperature and atmospheric conditions. The graded cylinders were filled with distilled water. The reading was taken every 24 h. The observation time was 96 h.

4.1.4. Determination of Osmolality and pH

The samples were immersed into DMEM with 10 % FBS with medium change every 48 h. At established time points the medium from 6 wells per group was collected and analzyed. Osmolality was measured by an osmometer (Osmomat 030, Gonotec, Berlin, Germany) and pH measurements were performed by a pH-meter (Titan X, Fisher Scientific GmbH, Schwerte, Germany) for each time point.
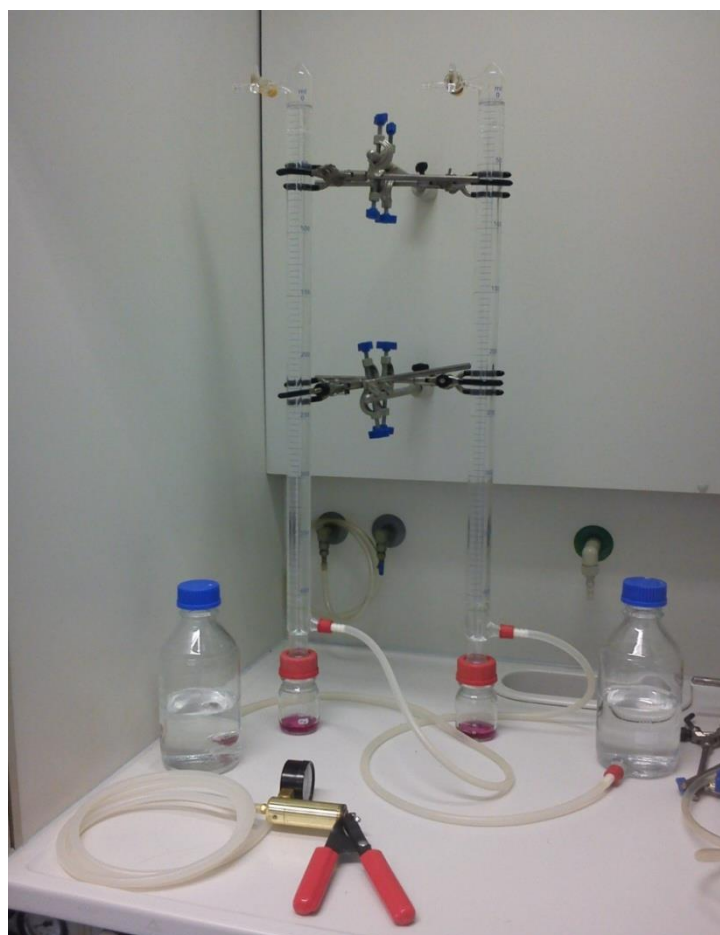
Figure 1. Eudiometer set up for gas evolution measurements.

4.1.5. Determination of Ca^{2+} concentration

Concentration of Ca^{2+} in the solution was measured by a calcium analyzer (9180 Electrolyte Analyser, Roche, Mannheim, Germany) after immersion of tested alloys into DMEM containing 10 % FBS with medium change every 48 h. In total, the medium from 6 wells per group were tested.

4.1.6. Surface Characterization

For the study of *Degradation*, the samples were immersed into DMEM with 10 % FBS and let to corrode in incubator at 37 °C, 5 % CO$_2$, and 95 % humidity for 3, 5, 7 and 10 days. The medium was changed every second day. At different time points the discs were removed and let dry at room temperature. Surface characterization was performed by atomic force microscope (AFM, XE-100, Park Systems Corp, Suwon, Korea). Measurement areas of 10×10 µm in three random positions were selected for each disc. The measurements were performed at a scan rate of

0.50 Hz. The images acquired from AFM were subjected to leveling and applied Gaussian filtering with a cut-off of 2.5 µm using the software MountainsMap® Universal 6.2 (Digital Surf, Besancon, France) and 3-D parameters such as S_a, S_{dr}, S_{ds} were analyzed. In total, 9 surfaces per material group were studied.

For the study of *Biofilm,* the magnesium discs which were pre-coated in human serum for 18 h and then washed twice in 2 ml potassium phosphate buffer (PBS) for 10 min at 37 °C. The micro titer plates with magnesium discs in human serum but without bacteria were incubated at 37 °C on a rotary shaker at 300 cycles per hour in 5 % CO_2 for 2, 24, 72 and 168 h. The human serum was changed every second day. At different time points the discs were removed and let dry at room temperature after which the surface characterization was performed by AFM with the same settings as described in previous paragraph.

4.1.7. Isolation of human reaming debris-derived cells

Human reaming debris-derived cells (HRD) were cultured from human reaming debris from various patients, with the approval of the local Ethics Commission, approval number AZ 103/13, as described by Wenisch (Wenisch et al. 2005). The adult patients were of different gender and different ages and did not display any disease related to bone metabolism. In total, the cells from six different patients were taken for this study.

The reaming debris was cultured in Petri dishes with F12K medium including 20 % FBS, 100 U/ml penicillin and 100 µg/g streptomycin. After 4–7 days the HRD started to grow out of the debris. When the cells reached confluence after 2–3 weeks they were trypsinized and transferred to cell culture flasks. All cells were kept at 37 °C in a 5 % CO_2 atmosphere.

4.1.8. Cell viability

To determine cell viability a MTT assay was conducted according to Mosmann (Mosmann et al. 1983). Briefly, 10,000 cells per cm^2 were seeded into 12-well plates containing pre-incubated magnesium discs and F12K medium with 20 % FCS and 100 µg/g streptomycin. The cell medium was changed every second day during the experiment. Duplicates were used for each material and patients, and in total 12 wells per specimen were tested. After 24 h, 7 days and 21 days MTT solution was added to the cell medium. The cells were then incubated in the dark for 4 h at 37 °C. Subsequently the cell medium was discarded and the cells were lysed with 0.004 N HCl in isopropanol. The cell lysates were centrifuged and supernatants were transferred

as triplets to a 96-well plate. The adsorption was measured at 570 and 630 nm using a Synergy HT Microplate Reader (BioTek, Bad Friedrichshall, Germany). The MTT assay was also performed for magnesium discs which were not seeded with the cell culture in order to exclude material's effect on the test and see only how the cells react during the assay.

Additionally, cell morphology was studied by inverted light microscopy using a Leica microscope type 090-135.002 (Leica Microsystems GmbH, Wetzlar, Germany) equipped with a Nikon Ds-Fi1 digital camera (Nikon, Duesseldorf, Germany).

4.1.9. Alkaline phosphatase (ALP) content

As an indicator of changes in the differentiation behavior of the bone-forming cells caused by the test substances a SensoLyte® pNPP Alkaline Phosphatase assay (AnaSpec, Fremont, CA, USA) was applied after 24 h and 7, 14, 21 and 28 days of culturing in DMEM low glucose with l-glutamine, 10 % FCS, 100 U/ml penicillin, 100 μg/g streptomycin, 0.1 μM dexamethasone, 0.005 μM ascorbic acid and 10 mM β-glycerol phosphate to induce osteogenic differentiation. The cell medium was changed every second day during the experiment. Duplicates were used for each material and patients and in total 12 wells per specimen were tested.

The cells were washed and frozen at −80 °C. After thawing the cell number was measured using a PicoGreen® dsDNA quantitation assay (Invitrogen, Eugene, OR, USA) according to the manufacturer's protocol. Cells were lysed with 1 % Triton X-100 in phosphate-buffered saline. The cell lysates were centrifuged and the supernatants were mixed with the PicoGreen® working solution in a 96-well plate. The samples were excited at 485 nm and the fluorescence emission intensity measured at 528 nm. The cells that were lysed for the PicoGreen assay, were centrifuged and the supernatants were diluted in specific assay buffer included in the assay kit. ALP substrate was applied to the diluted samples and the absorbance measured at 405 nm. The absolute amounts of ALP were correlated with the cell numbers obtained from the PicoGreen® assay.

4.1.10. Transmission Electron Microscopy (TEM)

Human HRD seeded in chamber slides (Nalge Nunc International, Rochester, NY, USA) were incubated with magnesium discs for 21 days. The cell layer was fixed for 30 min with 2 % paraformaldehyde (EMS, Hatfield, PA, USA) in 0.1 M sodium phosphate buffer (pH 7.2–7.4) with 2 % glutaraldehyde (EMS, Hatfield, PA, USA) and 0.02 % picric acid (EMS, Hatfield, PA,

USA), followed by 20 min fixation with 1 % osmium tetroxide (EMS, Hatfield, PA, USA) in 0.1 M sodium cacodylate buffer (pH 7.2–7.4). The samples were dehydrated and embedded in Epon (Pelco, Redding, CA, USA) before ultrathin sections (80–100 nm) were applied to collodion-coated copper grids. Analysis was done with a Leo 912 transmission electron microscope (Carl Zeiss AG, Oberkochen, Germany) at 80 kV accelerating voltage and equipped with a TRS Sharpeye slow scan dual speed CCD camera (Albert Troendle Prototypentwicklung, Moorenweis, Germany).

4.1.11. Scanning Electron Microscopy (SEM)

Human HRD were cultivated on magnesium discs for 7 and 21 days. Subsequently the cells were fixed in 2 % glutaraldehyde in 0.1 M sodium phosphate buffer for 1 h at room temperature, followed by dehydration in graded series of ethanol and critical point drying. The specimens were mounted together on aluminum pin stubs with the help of adhesive carbon pads. The specimens were then sputter-coated with gold/palladium (SC7640 Sputter Coater, VG Microtech, Uckfield, East Sussex, GB) and assessed in a LEO 1530 (LEO Elektronenmikroskopie GmbH, Oberkochen, Germany) field emission scanning electron microscope operated at 7.5 or 15 kV.

4.1.12. Determination of Ca^{2+} Consumption and pH

At established time points the medium was collected and analyzed for Ca^{2+} in the solution and pH. The concentration of Ca^{2+} was measured using a calcium analyzer (9180 Electrolyte Analyzer, Roche, Mannheim, Germany) and pH measurements were performed by a pH-meter (Titan X, Fisher Scientific GmbH, Schwerte, Germany) for each time point. The control group for this investigation consisted of the well-plates which contained only the HRD and the medium but no magnesium.

4.1.13. Bacterial Strains and Culture

The strains used for biofilm assays were *E. faecalis* ATCC 29212 and *S. epidermidis* C121 isolated from the external side of peritoneal dialysis catheter as described by Pihl (Pihl et al. 2010). All strains were routinely maintained on blood agar or in Todd–Hewitt broth (30 g/l, Difco Laboratories, Becton Dickinson & Co, Sparks, MD, USA) at 37 °C in 5 % CO_2.

4.1.14. Biofilm Formation Assays

The magnesium discs were pre-coated in human serum for 18 h and then washed twice in 2 ml PBS for 10 min at 37 °C. Overnight broth cultures of *S. epidermidis* or *E. faecalis* were transferred by 1:10 dilution into fresh, pre-warmed Todd–Hewitt broth and incubated at 37 °C in 5 % CO_2 to the mid-exponential growth phase (optical density at 600 nm $\approx$ 0.6). The bacterial suspension was centrifuged at 3000 rpm for 10 min at 5 °C washed once in PBS and re-suspended in 10 % human serum to a final concentration of approximately 1×10^8 cells ml^{-1}. The bacterial suspension was added to a microtiter plate with the magnesium discs and the bacteria were allowed to adhere for 2 h at 37 °C on a rocking platform at 300 cycles per hour. Following incubation for 2 h, the surfaces were rinsed twice in 2 ml PBS with pH 7.5 to remove loosely bound cells. *S. epidermidis* was then further incubated for 24, 72 and 168 h respectively. Adhered cells were stained using the Live/Dead BacLight staining kit (Molecular Probes, Eugene, OR, USA) and then visualized using Aristoplan fluorescent microscope (Leitz, Wetzlar, Germany). Ten images per surface were recorded with a digital camera and the number of bacteria on each image was counted by hand in a field area of 15600 μm^2. All experiments were carried out three times for each surface.

4.1.15. Statistical Analysis

Data were analyzed using the Statistical Package for the Social Sciences (SPSS, v18, SPSS Inc, Chicago, USA). The significance level was set at 5 %. Standard analyses comparing more than two treatments were conducted via one-way repeated measures analysis of variance (ANOVA). One-way repeated measures ANOVA was performed with the Dunn or Holm–Sidak post-hoc test. Surface characterization values (S_a, S_{ds}, S_{dr}) had non-normal distribution and Kruskal-Wallis test was performed. The graphs were plotted with Microsoft Excel® computer software (MS Excel 2003, Washington, USA).

4.2 *In vivo*

4.2.1. Sample Production

Three types of magnesium-based implants were used in this study: a) pure Mg (99.8 % of Mg by weight (wt)), b) W4 alloy, VMWO 061 R116986, c) Mg-hydroxyapatite (HA) (80 % W4, 20 % HA). The HA powder was produced by spray drying a HA slurry. Mg-HA samples were manufactured by high-energy milling of a mixture of HA and Mg granules and extruding the homogenate (Witte et al. 2007).

Pure Mg and W4 were cut from cast ingots and machined into rod samples with a dimension of 5.0 mm in length and 5.5 mm in diameter. Implants were ultrasonically cleaned and packed into airtight pouches. Gamma-sterilization was performed at the BBF Sterilisationservice GmbH facility (Kernen, Germany) with a total dosage of 29 kGy.

4.2.2. Implantation

All animal experiments were conducted according to the European Commission Directive 86/609/EEC for animal experiments. A total of 24 female New Zealand white rabbits (Manfred Bauer, Neuenstein, Germany) were used. There were 8 animals in each group. The pre-anesthetic procedure included an intramuscular administration of Ketamine (50 mg/kg) and Xylazine (1 mg/kg). General anesthesia was then achieved with intravenous administration of Ketamin (25 mg/kg) as well as Midazolam 0.5-1 mg/kg. Post-operative anesthesia was achieved with Buprenorphin 0.05 mg/kg.

An incision at the skin level was performed followed by a muscle layer and a periosteal incision. Next, a flap was reflected, and the bone exposed. The samples were implanted by lateral approach to the left distal femur condyle after predrilling with a 5.5 mm hand-operated diamond bone cutting system under constant irrigation with saline solution. Implantation was performed pressfit into the spongiosa. One magnesium-based implant was implanted per rabbit. The periosteum, muscle, and dermis layer were closed with 4-0 vicryl (Ethicon Johnson, Miami, FL, USA) resorbable suture, using single interrupted nodes. The skin was sutured with 4-0 nylon (Ethicon Johnson) sutures. After the surgical procedures, the animals were kept in their cages under controlled lighting and temperature.

After the operation, all the animals received 128 mg of Veracin as an antibiotic prophylaxis. Postoperatively, the rabbits were allowed to move freely in their cages without external support. Four rabbits per group were sacrificed randomly at 6 and 12 weeks post-operation, respectively.

4.2.3. Histological Preparations

The bone samples were embedded in paraffin and in methyl methacrylate based resin (Technovit® 9100, Heraeus Kulzer, Hanau, Germany).

For the paraffin embedding, the specimens were first fixed in 4 % phosphate-buffered paraformaldehyde (Merck, Darmstadt, Germany), then decalcified with 10 % ethylenediaminetetraacetic acid (EDTA, pH 8.0, Sigma, Taufkirchen, Germany) in 3.5 M Tris buffer (pH 7.4, Sigma) for 21 days, dehydrated with graded ethanol concentrations, saturated in xylene, and finally embedded in paraffin. Sections of 3–5 μm thickness were cut with a rotator microtome (Leica, Bensheim, Germany), deparaffinized, and then stained with hematoxylin and eosin (HE) (Shandon Scientific Ltd, Cheshire, UK).

For the Technovit® 9100 new embedding, the samples were prepared according to the manufacturers protocol (Heraeus Kulzer GmbH, Wehrheim, Germany) and then grinded into 50 μm thick specimens using EXAKT 400CS microgrinding system (Exakt GmbH, Norderstedt Germany). The grindings were stained with toluidine blue (TB) and tartrate-resistant acid phosphatase (TRAP). Briefly, the grindings were first deplastified. For TB, they were etched in 20 % hydrogen peroxide for 40 minutes, stained with TB solution containing Sodium Tetraborate (Merck, Darmstadt, Germany), Pyronin G (Merck) and Toluidine blue (Chroma, Olching, Germany). The grindings were then let to dry for 24 h washed in 100 % ethanol and xylene, and coverslipped with DePeX mounting medium (Serva Electrophoresis Life Science Products, Heidelberg, Germany). For TRAP the sections were treated with 0.1 M Sodium Acetate buffer and incubated in Napthol-AS-TR phosphate (N6125-1G, Sigma) in N–N-Dimethyl formamide (Sigma Aldrich) and sodium tartrate (Merck) with Fast Red TR salt (Sigma Aldrich) at 37 °C for 60 minutes. Coverslipping was performed using DePeX.

4.2.4. Histomorphometric Analysis

Image capturing used Axioplan 2 Imaging system (Carl Zeiss, Germany) associated to a DC500 camera (Leica, Germany). Image evaluation was performed on Image-Pro® Plus (Weiss Imaging and Solutions GmbH, Germany) and Photoshop CS3 Extended® (Adobe, v.10.0.1, 2007, USA). The region of interest (ROI) was defined as 2 mm from the implant surface since we were mainly interested in implant stability in the surrounding bone and the reaction of the nearby tissues. Briefly, circles with diameter 7.5 mm were created in Photoshop CS3 Extended® and placed in the implant area. The implant was centered in the middle of the circle. All histomorphometric analysis was then limited to the ROI inside the circle. For measuring the amount of gas voids,

corrosion layer and new bone, all areas containing these structures were first selected and then the total area calculated. For quantification of TRAP-positive cells, all cells were counted in the ROI and then the resultant number was divided by the circle area (mm^2) to get the mean number of cells per mm². In order to determine the implant-bone contact, the interface between material and trabeculae was measured in mm for each animal.

4.2.5. TEM

Examination under TEM was performed in order to study the cell morphology and bone response to magnesium materials. The same protocol as for in vitro study was applied to prepare the samples for examination (p.24) and then ultrathin sections of about 60–80 nm were cut using the ultramicrotome (Reichert-Jung, Vienna, Austria). Examination was done with the transmission electron microscope Leo EM 912 (Zeiss). Images were recorded with a 2k × 2k slow scan CCD camera (Albert Troendle Prototypentwicklung, Moorenweis, Germany).

4.2.6. Statistical Analysis

Data were analyzed using SPSS®. The significance level was set at 5 %. ANOVA test was used to determine whether any significant differences in hydrogen gas production, bone contact, corrosion layer and implant resorption existed between the three groups. The graphs were plotted in Microsoft Excel® computer software.

# 5. Results

5.1. Degradation

Degradation of magnesium is a complex process which consists of material's mass loss, hydrogen gas production, change in osmolality, pH and Ca^{2+} concentration of the surrounding medium, as well as of surface changes of degrading implants. These changes were measured in this study and are presented below.

5.1.1. Corrosion

An important problem of magnesium is a high corrosion rate with consistent hydrogen gas formation on contact with fluids (Witte et al. 2008). Corrosion is determined by the changes in sample mass, and/or the produced gass volume. Thus, both the mass loss and eudiometer methods were performed in this study.

WE43 alloy showed the fastest degradation of all materials measured both by immersion and gas evolution methods, followed by Mg10Gd (Fig 2 A). Corrosion of Mg2Ag and pure Mg was comparable, but was somewhat lower for Mg2Ag. Figure 2 B illustrates the mass loss at different time points during degradation under cell culture conditions. It can be seen that the mass loss increases up to day 7 for all samples. At day 7 a slight mass loss was observed for Mg10Gd and a rapid mass loss for WE43. For Mg2Ag and pure Mg a slight mass gain after day 7 could be due to crystal formation on samples' surface. The mean corrosion rate was lowest in Mg2Ag, but it was not highly significantly different compared to WE43 (p = 0.09).

Gas evolution test has shown that corrosion tends to slow down after day 3 for all but WE43 alloy (Fig 2 C). WE43 was corroding fast in vitro and its degradation did not slow down even after 4 days. The graph of mass loss (Fig. 2 B) and the graph showing gas emission (Fig. 2 C) have quite similar pattern with significantly higher values for WE43 compared to the other groups (p ≤ 0.05).
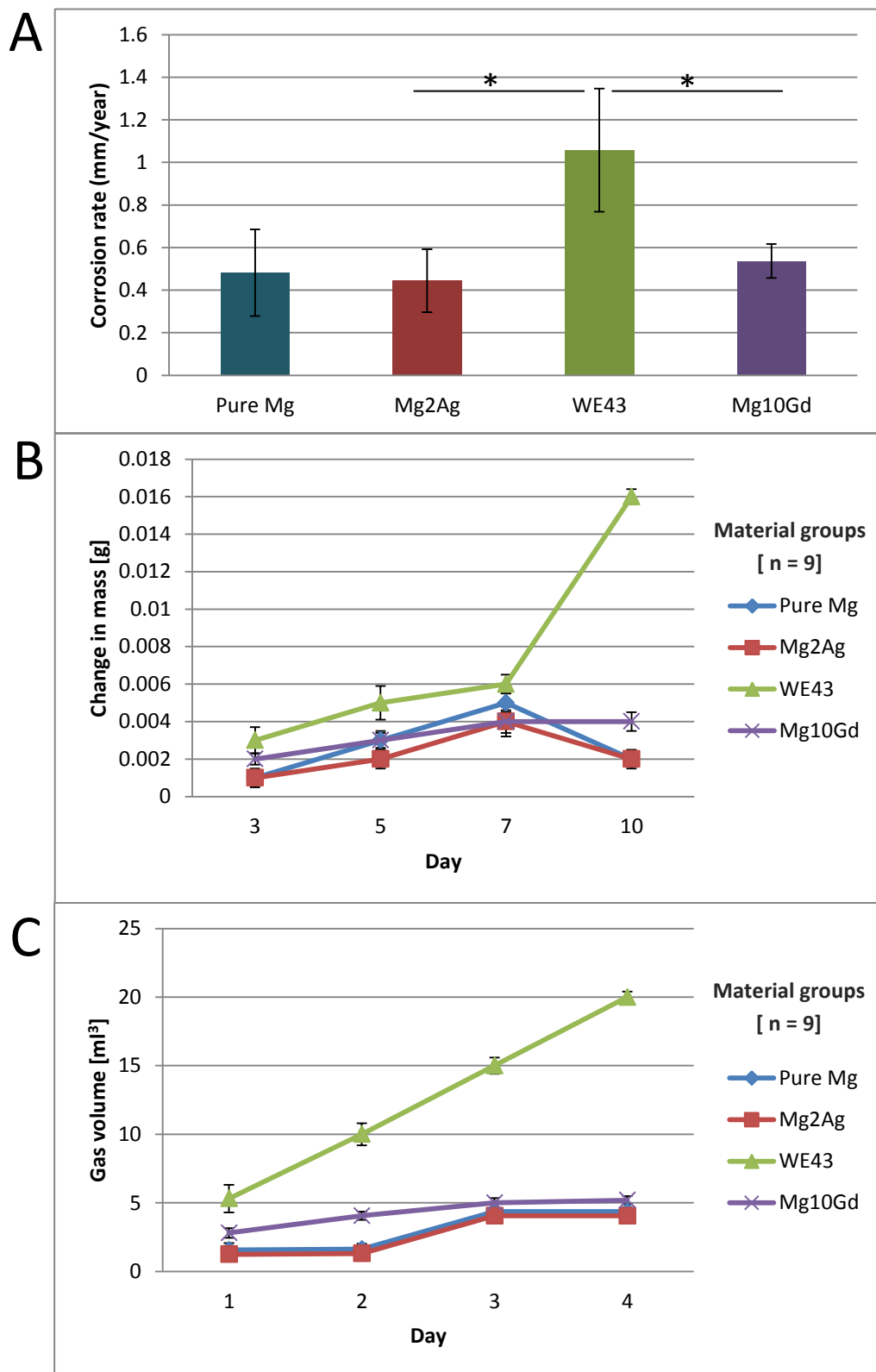
Figure 2. A. Mean corrosion rates of pure Mg, Mg2Ag, WE43 and Mg10Gd. **B.** Mass loss at different time points during degradation. Note highly significant difference between WE43 and other groups at day 10 ($p \leq 0.005$). **C.** Gas evolution. Observe highly significant difference between WE43 and other groups starting at day 1 ($p \leq 0.005$).

5.1.2. Osmolality

For pure Mg and Mg10Gd osmolality was generally on constant level up to day 7 (Fig 3 A). After day 7 osmolality dropped for all tested materials. For Mg2Ag osmolality increased between day 3 and 5, but then decreased already after day 5. WE43's osmolality values varied but the lowest osmolality value was reached at day 10.

5.1.3. pH – measurements

The original control pH of the medium was 7.9. It was observed that pH of the medium in which the samples were immersed was fluctuating over the observation period (Fig. 3 B). Generally, pH increased starting from day 3 and reaching its peak at day 7. After day 7 it decreased for all groups. The highest mean pH was found for WE43 (1.05 ± 0.23), whereas the lowest mean pH was measured for Mg2Ag (0.44 ± 0.17) at all time points. No significant differences were found between the groups at various observation periods.

5.1.4. Ca^{2+} Concentration

Concentration of Ca^{2+} ions in the original control solution was 1.1 mM/L. It was observed that Ca^{2+} concentration generally decreasing for all samples (Fig. 3 C). This decrease was fastest for Mg2Ag and WE43, whereas for pure Mg and Mg10Gd it was more uniform. There was observed a signisignificantly lower concentration of Ca^{2+} for pure Mg and Mg10Gd at day 3 compared to the other groups ($p \leq 0.01$). No correlation was found between Ca^{2+} and pH of the solution.
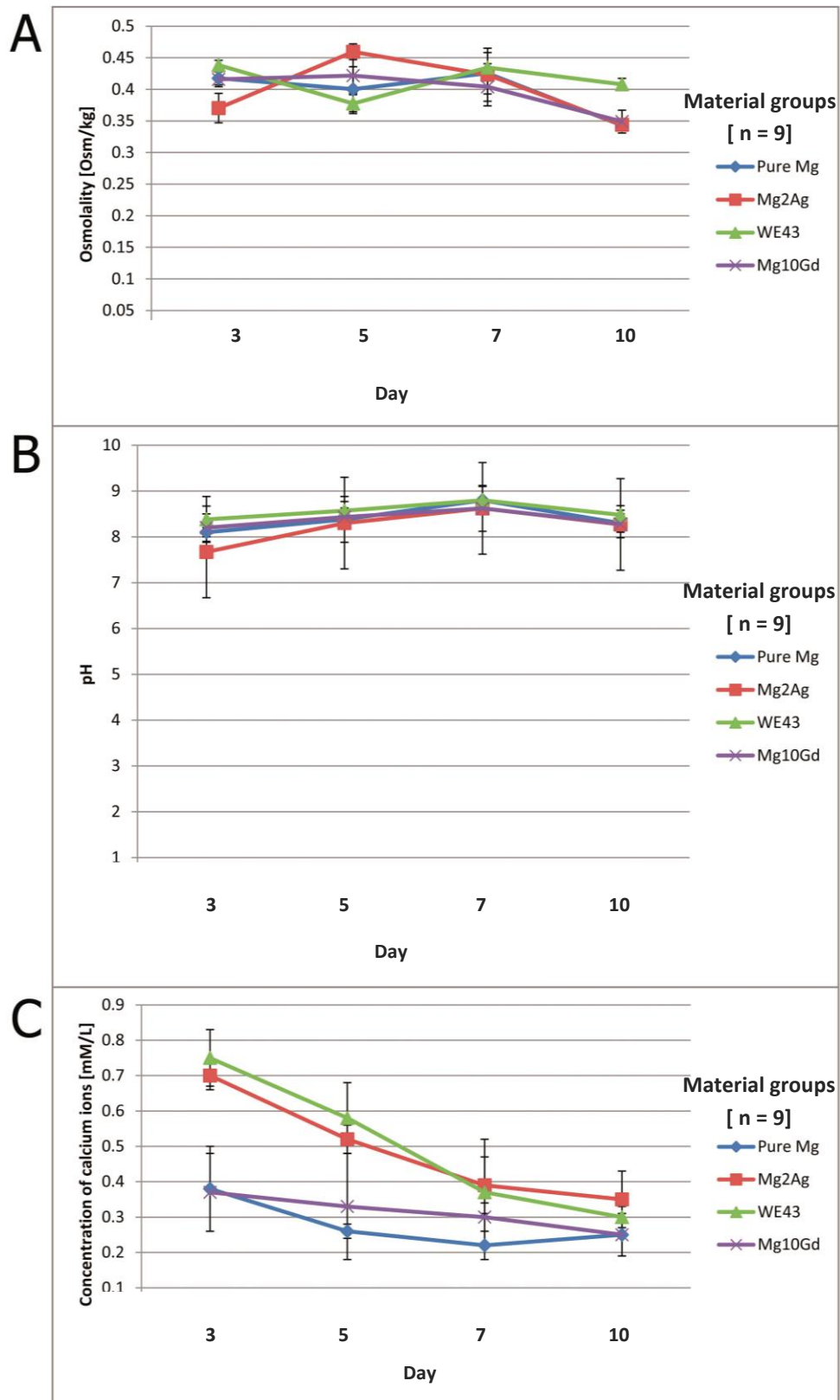
Figure 3. A. Osmolality over 10 days of observation period. **B.** pH during the observation time. **C.** Concentration of free Ca^{2+} ions; note signisignificantly lower concentration of Ca^{2+} for pure Mg and Mg10Gd at day 3 compared to the other groups (p ≤ 0.01).

5.1.5. Surface Characterization

Corrosion of magnesium implants influences material's surface characteristics. Surface plays an important role for cellular and bacterial attachment. Both too rough and too smooth surfaces are not beneficial and hinder bone formation around implants (Wennerberg and Albrektsson 2000). Several parameters can describe implant surface topography, such as average surface roughness (S_a), developed surface area ratio (S_{dr}) and summit density (S_{ds}) (Wennerberg and Albrektsson 2000, Stout et al. 1993).

The AFM-measurements have revealed that S_a values of Mg2Ag, WE43 and Mg10Gd formed a similar pattern (Fig. 4). For these groups, S_a was lowest at day 0 but increased from day 0 to day 3, reaching a peak at day 3. Afterwards S_a decreased at day 5 but then started to increase slowly up to day 10, but this fluctuation was not statistically significant. In contrast, S_a values of pure Mg were rather constant.
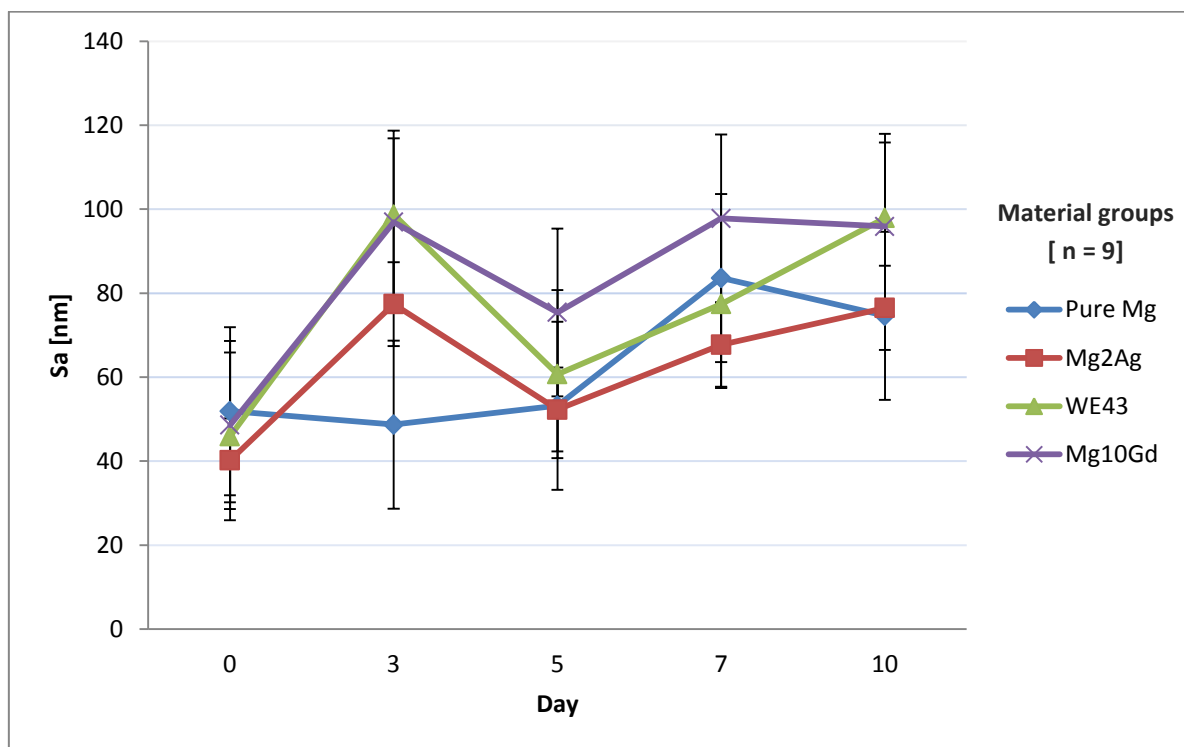

Figure 4. S_a, average surface roughness, of magnesium alloys over time.

S_{dr} values of Mg2Ag, WE43 and Mg10Gd showed a similar pattern as S_a for the same materials (Fig. 5). The values reached a maximum at day 3 for all but pure Mg groups, then decreased at day 5 and then started to grow slightly up to day 10. Increase in S_{dr} values from day 5 to day 10 was not found to be statistically significant inside the group. Mg10Gd had significantly higher S_{dr} compared to all other groups at day 10 ($p \leq 0.01$). S_{dr} and S_a of pure Mg had alike constant pattern.
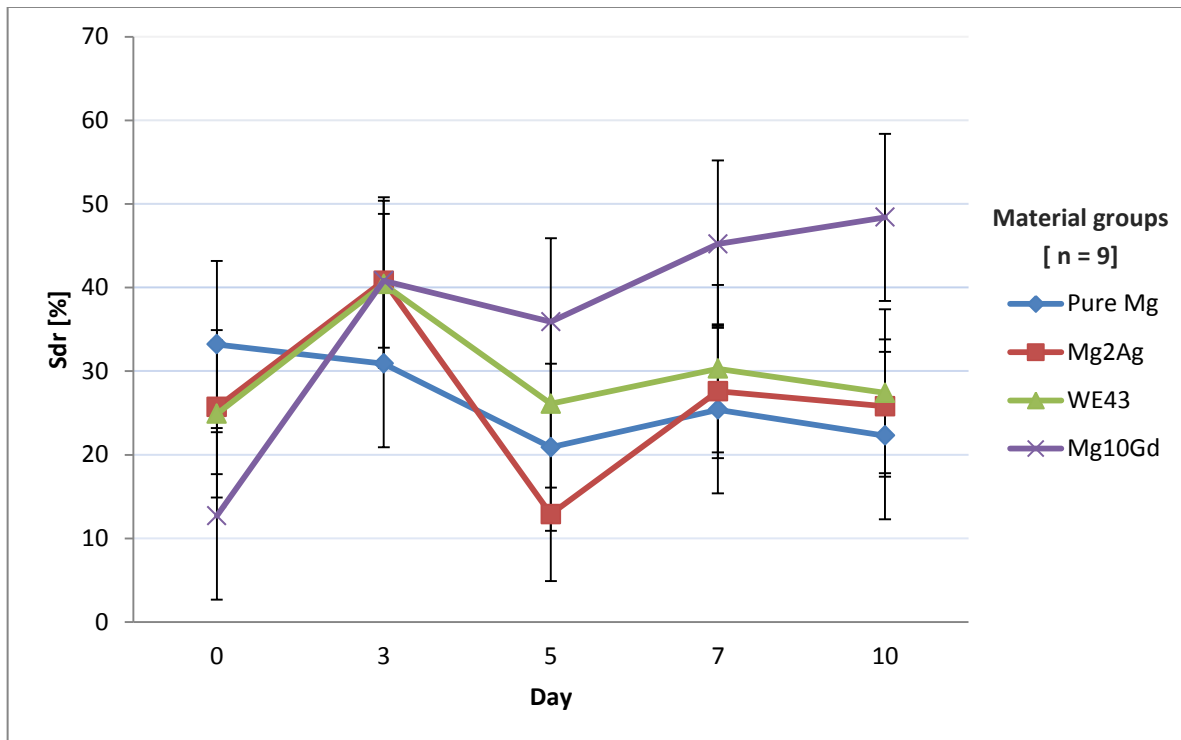

Figure 5. S_{dr}, a ratio between the 3-D measurement and a 2-D reference plane, of magnesium alloys over time. Note significant difference between Mg10Gd and other groups at day 10 ($p \leq 0.01$).

S_{ds} of WE43 was rather constant over the observation period and no statistical differences were found between different observation points (Fig. 6). For the other groups, S_{ds} was fluctuating over observation period. Pure Mg and Mg2Ag had a similar pattern of surface change over time. For both of these materials S_{ds} decreased and reached its minimum at day 5. It then increased again at day 7 but started to fall until day 10, but this decrease was not significant. For Mg10Gd, S_{ds} was minimal at day 3 and maximal at day 5, and was then decreasing until day 10. Pure Mg values for S_{ds} were significantly lower at day 5 compared to all other groups at this time point ($p \leq 0.01$).
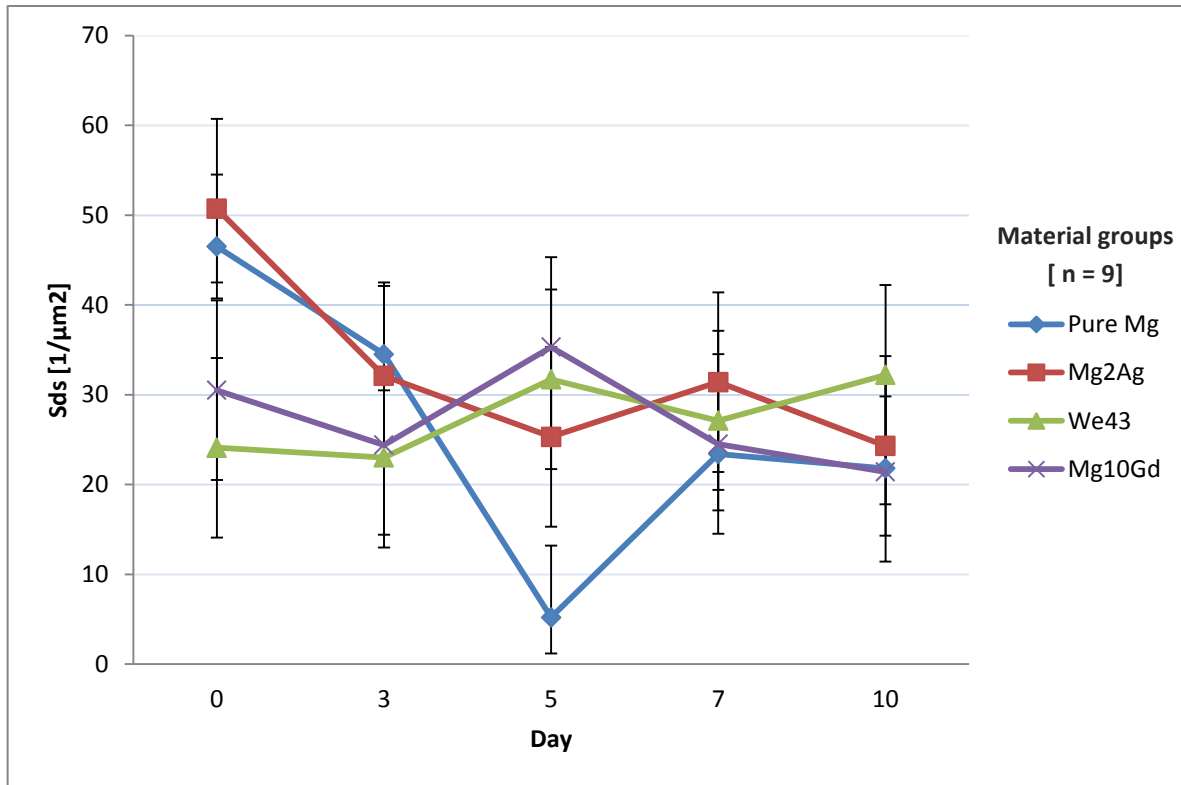
Figure 6. S_{ds}, the number of summits per unit area making up the surface, of magnesium alloys over time. Note significantly lower values for pure Mg compared to all other groups at day 5 ($p \leq 0.01$).

5.2. Cellular reactions

Cell viability, differentiation, morphology, intracellular appearance and attachment to materials' surface have been investigated in this study along with the pH changes and Ca^{2+} concentration in order to evaluate magnesiums influence on the primary HRD cells.

5.2.1. Cell Viability

The aim of this study was to evaluate magnesium alloys' effect on the bioactivity of HRD cells up to 28 days of direct exposure. Pure magnesium, Mg2Ag, WE43, Mg10Gd induced cytotoxicity to HRD were determined by conducting an MTT assay. After 24 h there was no statistical difference in the number of viable cells between the groups (Fig. 7). After 7 days the significant difference between the control group without magnesium and all other tested materials could be observed with higher number of viable cells in the control. After 21 days this difference was even more obvious with $p \leq 0.001$ (Fig. 7). It was observed that the number of viable cells increased in the control group from day 1 to day 21, while in all other groups the cell viability was suppressed and no significant difference was seen inside and between the groups over the study period.
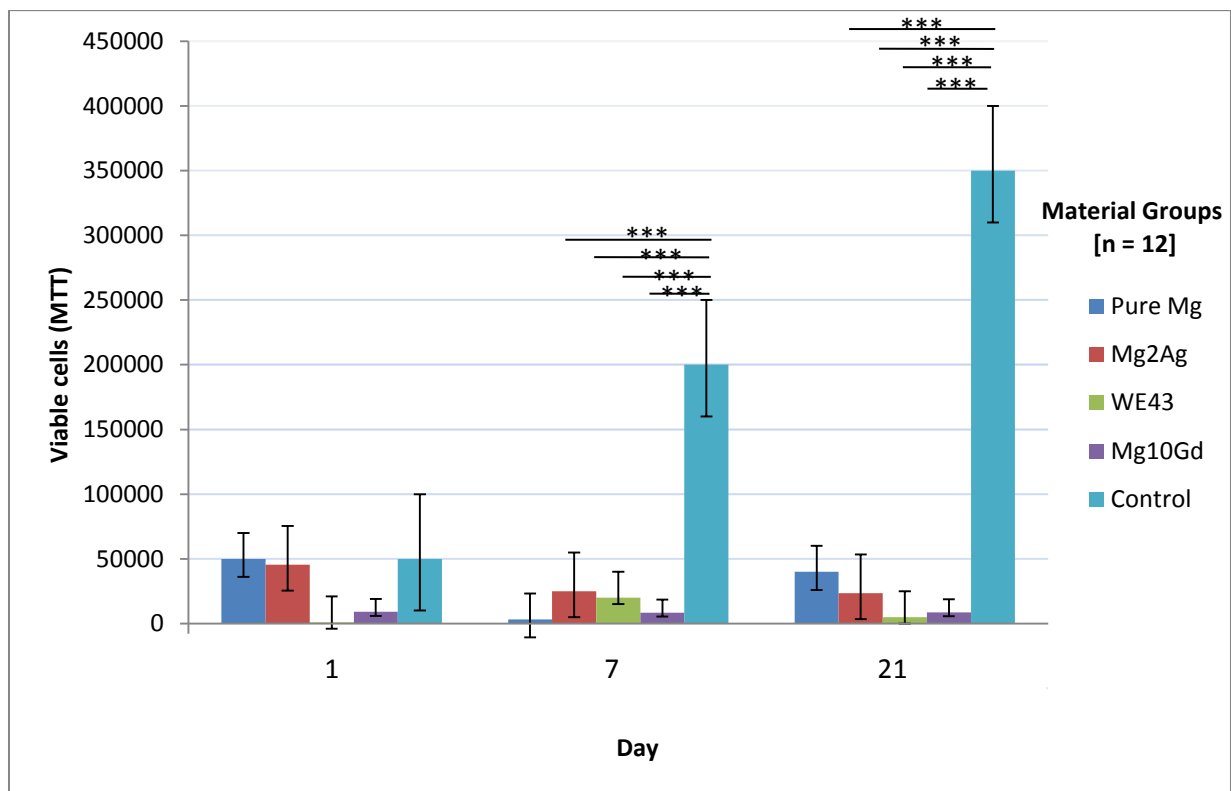

Figure 7. MTT results for HRD after exposure to different magnesium materials over time.

5.2.2. Alkaline Phosphatase Content

The ALP content in HRD is an important factor in bone mineral formation and shows a scale of changes during differentiation. The results for ALP content are presented in Fig. 8. No inhibition of the ALP content caused by Mg2Ag, Mg10Gd and WE43 was observed in osteogenic differentiating HRD at days 14 and 28. At day 1 the ALP content was significantly higher for Mg2Ag ($p = 0.004$) and WE43 ($p = 0.003$) compared to the control. The significantly low values for the ALP content compared to the control group were observed in pure Mg at day 14 ($p = 0.005$) and 28 ($p = 0.001$).
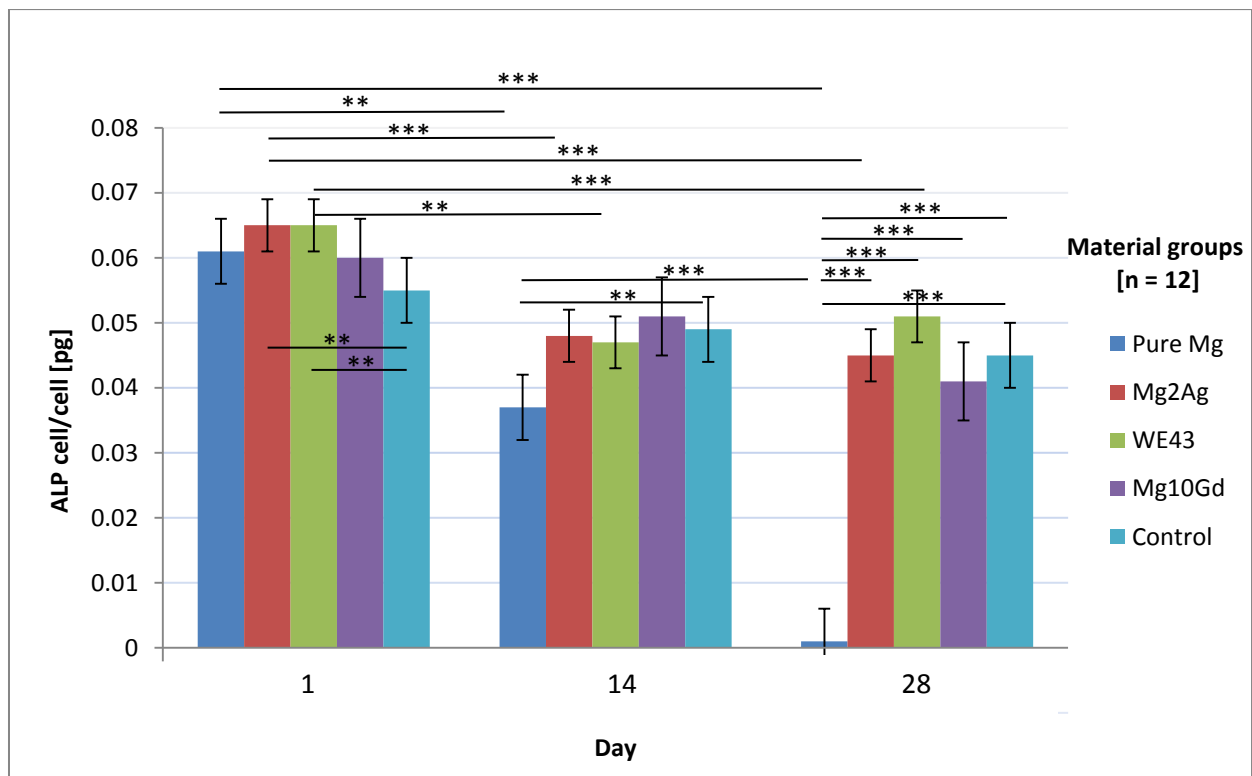

Figure 8. ALP contents after exposure to different magnesium materials over time.

5.2.3. Cell Morphology

Changes in the cell morphology were detected by inverted light microscopy for HRD and for osteogenic differentiating HRD. After 7 days of exposure to pure Mg, Mg10Gd and WE43 HRD showed a reduction in cell number and an increasing amount of cell debris in the medium (Fig. 9).

Few or no cells were seen in direct proximity to pure Mg, Mg10Gd or WE43. Instead, the cells were found on the edge of the wells (Fig. 9 f). The reduction in cell number was more apparent in pure Mg than in any other group. The cell morphology in presence of Mg2Ag was similar to the control and the cells were directly contacting the Mg2Ag discs (Fig. 9 c).
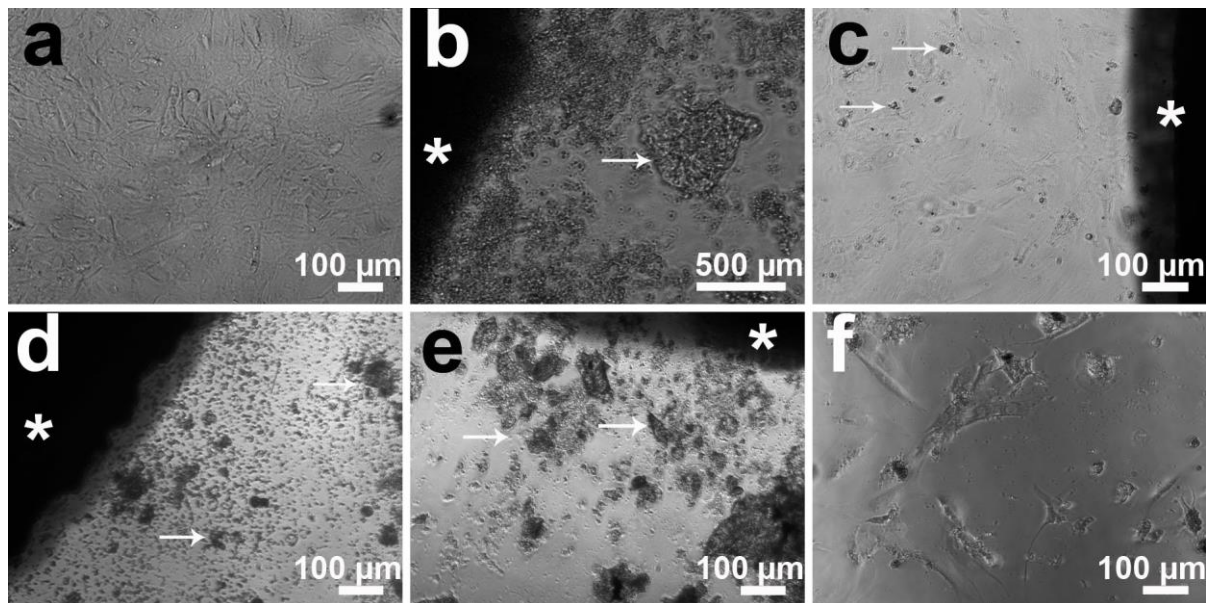

Figure 9. Morphology of HRD at 7 days. **a.** Control group, the well is densely covered with the cells. **b.** Pure Mg, much fewer cells compared to control. **c.** Mg2Ag, the well is densly covered with the cells. **d.** Mg10Gd, much fewer cells compared to control. **e.** WE43, similar in appearance to pure Mg and Mg10Gd with very few cells observed in material's proximity.**f**. For pure Mg, Mg10Gd and WE43 the cells were found mainly at the wells'edge. The image shows Mg10Gd's well edge. *Legend:* asterix = magnesium disc, arrows = products of degradation.

The cell appearance at day 21 is presented in Figure 10. At 21 days the HRD in WE43 and Mg10Gd started to appear closer to the disc although their number was still low compared to control and to Mg2Ag. In pure Mg the cells were still only found around the edge of the well and not in material's proximity. In Mg2Ag the cell morphology was closest to the control with high cell density directly contacting the discs.
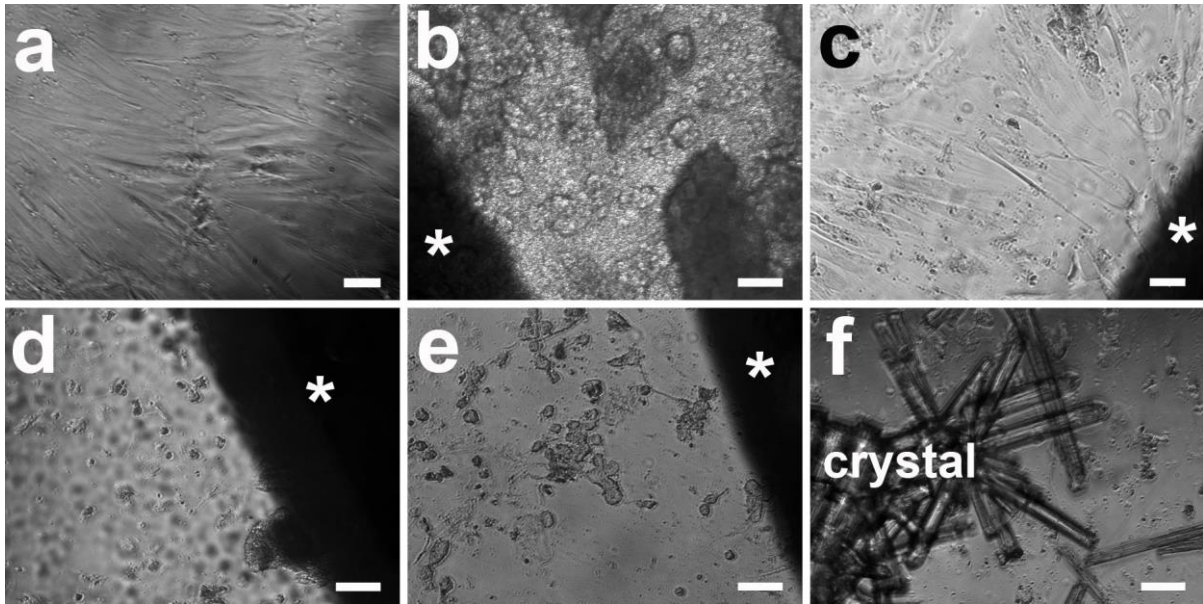
Figure 10. Morphology of HRD at 21 days. **a.** Control group, the well is densely covered with the cells. **b.** Pure Mg, almost no cells compared to control. **c.** Mg2Ag, the well is densely covered with the cells. **d.** Mg10Gd, much fewer cells compared to control but more than at day 7. **e.** WE43 similar appearance to Mg10Gd with somewhat more cells than at day 7. **f**. Crystal formation was observed for all materials. The image shows pure Mg's well. *Legend:* asterix = magnesium disc. Scale bar represents 100 μm.

The osteogenic differentiating HRD showed a similar pattern of cell morphology and cell number as HRD (Fig. 11). No cells were found in direct contact to pure Mg (Fig. 11 b). Mg2Ag was the closest to control at all time points regarding morphology and cell density. At day 28 the osteogenic differentiating HRD in Mg2Ag group were still closest to control regarding the cell number (Fig. 11 c). More cells appeared around Mg10Gd and WE43 at day 28 compared to other time points for these materials (Fig. 11 d and e).
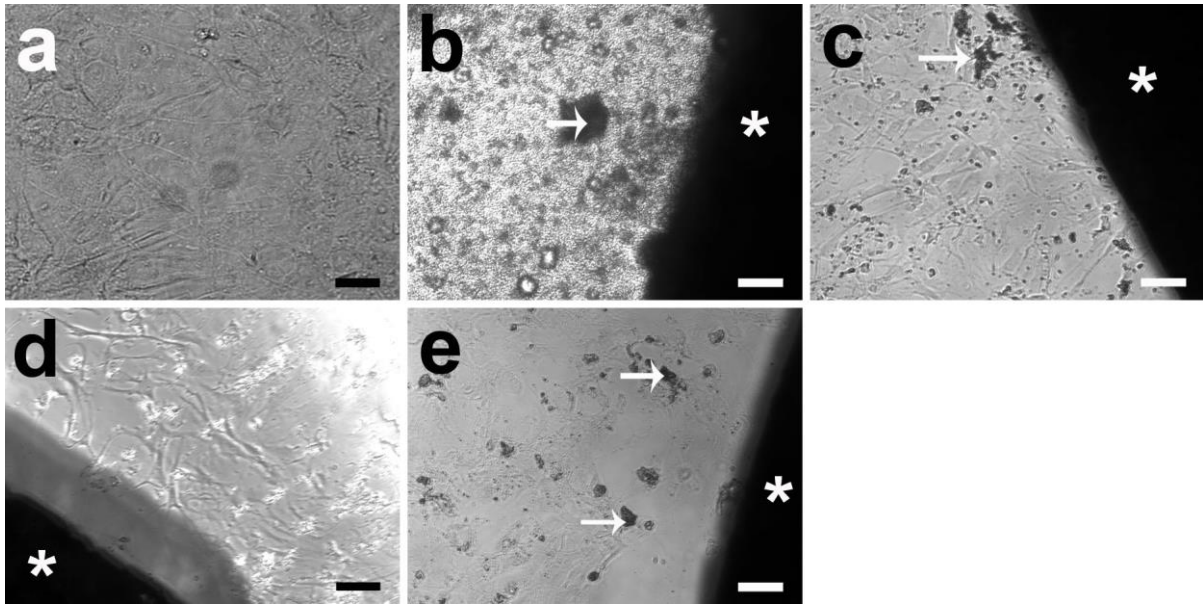
Figure 11. Morphology of osteogenic differentiating HRD at 28 days. **a.** Control group, the well is densely covered with the cells. **b.** Pure Mg, few cells compared to control. **c.** Mg2Ag, the well is densely covered with the cells. **d.** Mg10Gd, the well is densely covered with the cells. **e.** WE43, the well is densely covered with cells. *Legend:* asterix = magnesium disc, arrows = products of degradation. Scale bar represents 100 μm.

5.2.4. TEM

Intracellular structure was examined after exposure of HRD to magnesium samples for 21 days. It was observed that the number of lysosomes and endocytotic vesicles was higher in the HRD exposed to magnesium alloys than in the control (Fig. 12). In Mg2Ag degraded material particles were found inside the lysosomes (Fig. 12 e) and in the cytoplasm (Fig. 12 f). The degradation particles were not observed in the other groups.
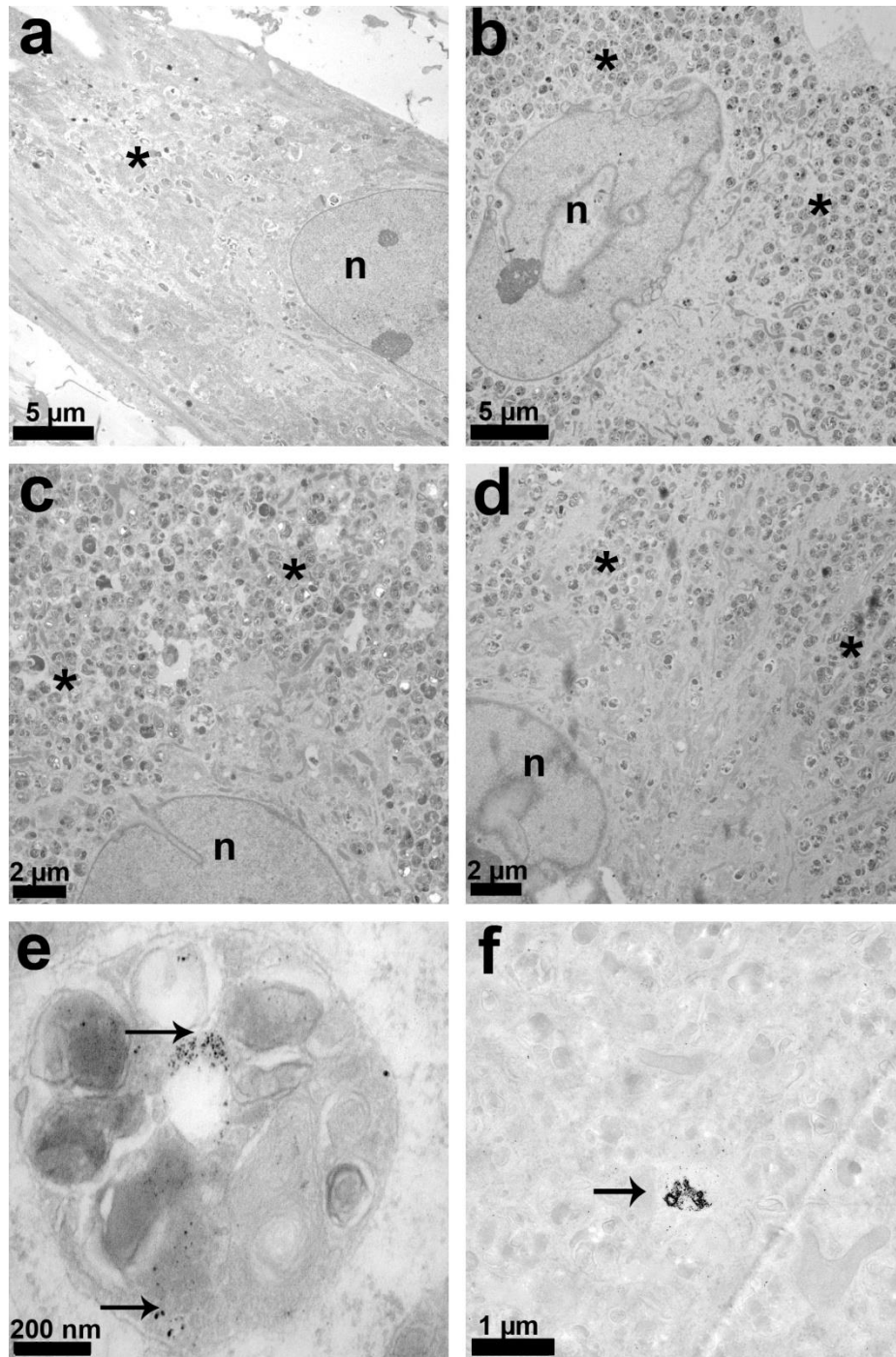
Figure 12. TEM analysis at day 21. **a.** Control. **b.** Mg2Ag. **c.** Mg10Gd. **d.** WE43. **e.** Lysosome of the HRD cultured with Mg2Ag. Note the degradation particles (arrows). **f.** Cytoplasm of the HRD cultured with Mg2Ag. Note the degradation particles (arrows). *Legend:* asterix = lysosomes/endocytotic vesicles, n = nucleus. Note the high amount of lysosomes and endocytotic vesicles in **b**, **c** and **d**.

5.2.5. SEM

Cellular attachment to magnesium specimens was studied under SEM after incubating the HRD with magnesium for 7 and 21 days. It was observed that the cells attached readily to the degradation layer and to the forming crystals on magnesium's surface (Fig. 13). The cell pseudopodia were numerous whenever the crystal formed on material's surface (Fig. 13). Few pseudopodia were seen on smoother surfaces (Fig. 13). No difference between 7 and 21 days was observed regarding the number of attached cells and their morphology.
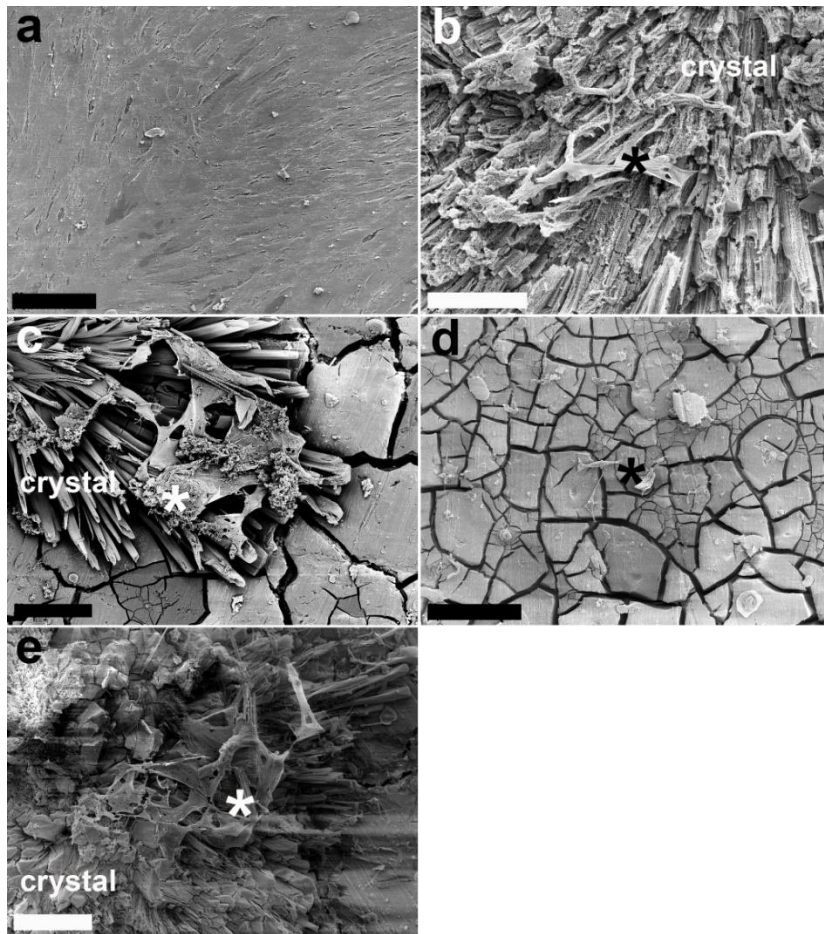
Figure 13. SEM analysis at day 7. **a.** Control densely covered with HRD. **b.** Pure Mg. **c.** Mg2Ag. **d.** Mg10Gd. **e.** WE43. Note the crystal formation on material's surface in **b**, **c** and **e** and the cell attachment to the crystal compared to the smooth surface in **d**. The cells are marked with an asterix. Scale bar represents 20 μm.

5.2.6. Ca²⁺ Consumption

Calcification induced by magnesium specimens was studied by measuring Ca^{2+} consumption from the surrounding medium. The results are presented in Fig. 14. A decrease in free calcium ions was observed around all magnesium materials from day 1 to day 7. Between day 7 and day 28 the Ca^{2+} ions were released into the medium for all tested samples. Mg2Ag's values were closest to the control out of all groups at day 21 and 28. Control group had significantly lower values compared to all tested alloys at day 1 ($p \le 0.01$), day 7 ($p \le 0.05$), day 14 ($p \le 0.01$), and significantly lower than WE43, pure Mg and 10Gd at days 21 ($p \le 0.01$) and 28 ($p \le 0.01$). Pure Mg had significantly higher values than all other samples at days 1 to 21 ($p \le 0.01$). At day 21 pure Mg behaved similarly to Mg10Gd and these values were significantly higher than WE43, Mg2Ag and control ($p \le 0.01$).
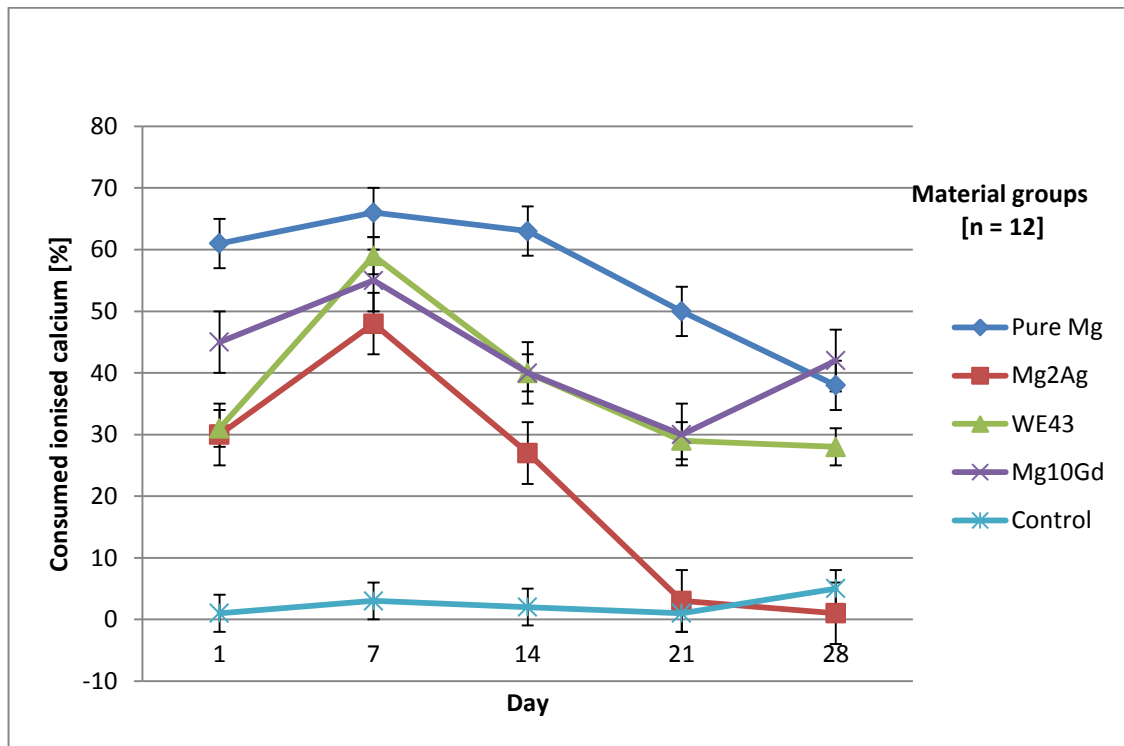

Figure 14. Consumed ionised calcium at different observation points. Note the low values for the control group and high values for pure Mg.

5.2.7. pH – measurements

Figure 15 represents pH changes. It was seen that all magnesium materials increased the pH of the medium compared to the control group. The following general pattern was observed for all

groups: the pH values were stable up to day 7, a sudden pH drop occurred on day 14 and then the pH tended to increase slightly up to day 28. The pH values for Mg2Ag were the closest to the control. Pure Mg caused the highest increase in pH of all groups, and this increase was statistically significant compared the control group at all time points ($p \leq 0.005$) but not statistically significant compared to the other alloys throughout the study ($p \geq 0.01$). No correlation between the pH and Ca^{2+} consumption was found in this study.
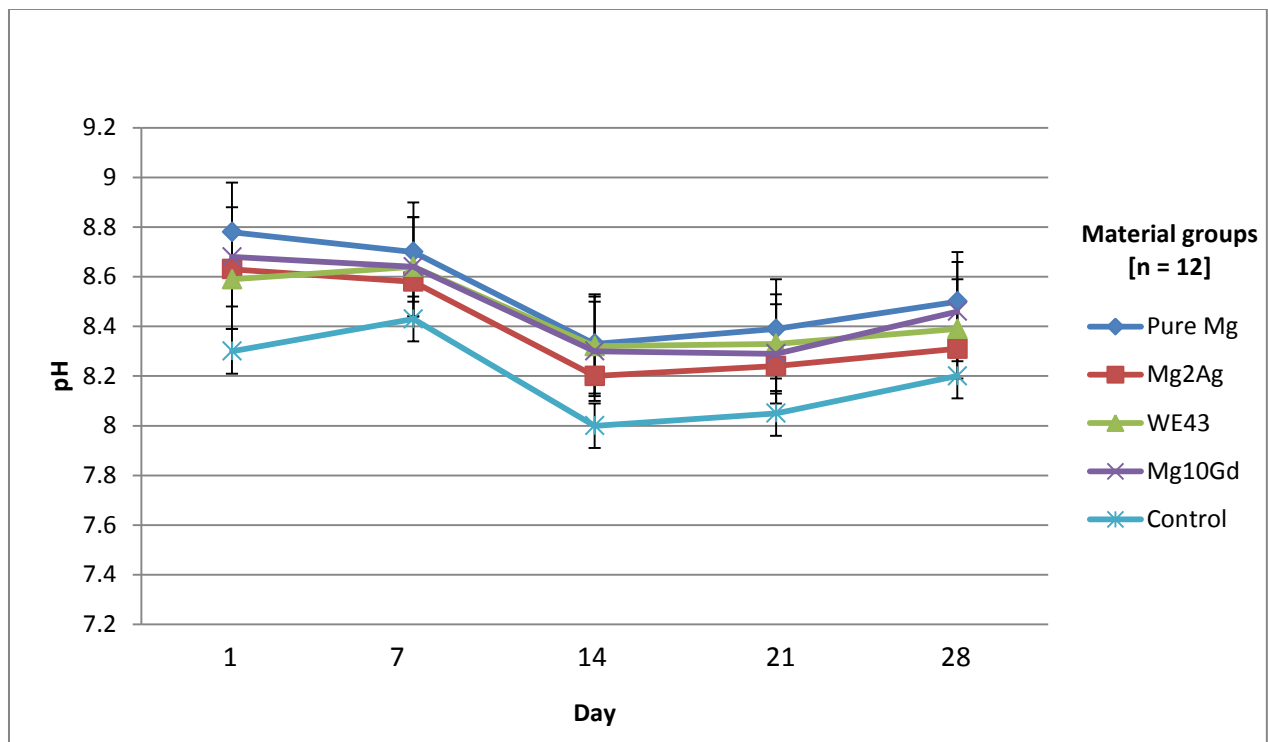
Figure 15. pH of the solution after placement to different materials over time. Note significantly higher pH of pure Mg compared to the control att all time points ($p \leq 0.005$).

5.3. Early Stages of Biofilm Formation

The next study looks at ability of *S. epidermidis* and *E. faecalis* to form early biofilm on magnesium implants, and furthermore investigates how the surface changes during the degradation influence the early stages of biofilm formation.

5.3.1. Adhesion of *S. epidermidis* and *E. faecalis* to Magnesium Surfaces

Comparison between adhesion of *S. epidermidis* and *E. faecalis* to magnesium materials after 2 h of incubation is presented in Figure 16.
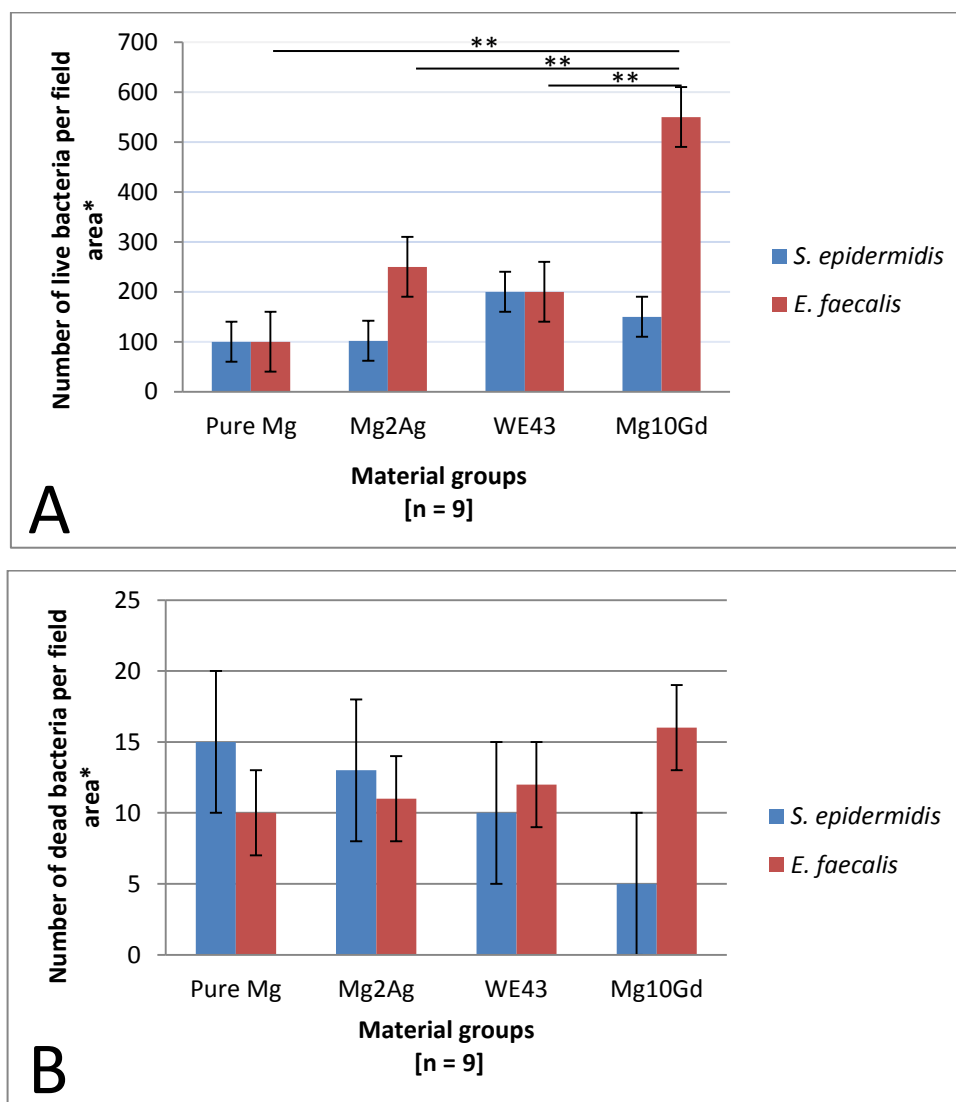
Figure 16 Adhesion of *S. epidermidis* and *E. faecalis* to magnesium materials after 2 h of incubation. **A.** Live *S. epidermidis* and *E. faecalis*. **B.** Dead *S. epidermidis* and *E. faecalis*. * Field area represents 15600 μm^2.

The viability of the adhered cells of both *E. faecalis* and *S. epidermidis* was high (> 95 % for both strains). *E. faecalis* was significantly more prevalent on Mg10Gd surface than on other alloys' surfaces (Fig. 16). The magnesium samples were densely covered with *E. faecalis*, whereas *S. epidermidis* colonies were scarcely spread over the surface (Fig. 17).
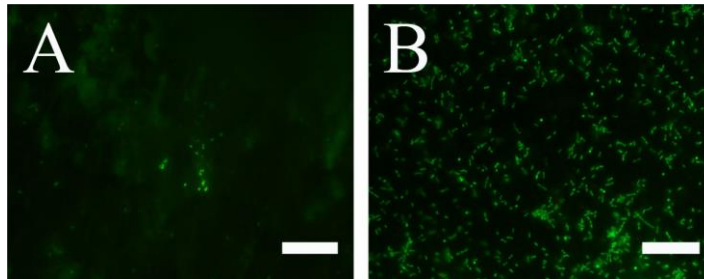

Figure 17. A. *S. epidermidis* on Mg2Ag's surface at 2 h. **B.** *E. faecalis* on Mg2Ag's surface at 2 h. Scale bar represents 30 μm.

5.3.2. *S. epidermidis* Growth over Time

Biofilm growth of *S. epidermidis* on magnesium materials over time is presented in Figure 18 A. In general, Mg2Ag and WE43 had similar pattern of the biofilm growth, whereas pure Mg was comparable to Mg10Gd. The number of adherent bacteria increased at 72 h of incubation for all tested samples and this increase was significant (p = 0.003) for all but Mg10Gd group (Fig. 18 A). Significantly more bacteria were found on Mg10Gd surface at 168 h compared to 2 h (p = 0.004). Between 72 h and 168 h, the biofilm reached its plateau for pure Mg and Mg10Gd. For Mg2Ag and WE43, the amount of adhered *S. epidermidis* decreased between 72 and 168 h and this decrese was significant for both samples (p = 0.004).

The viability of the cells remained high (> 95 %) at all time-points as shown by the low number of dead cells. There was found a significant difference between pure Mg at 24 and 72 h compared to the other groups at all time points (p ≤ 0.01) in the amount of dead *S. epidermidis* (Fig. 18 B). The pattern of *S. epidermidis* growth over time is shown in Fig. 18.
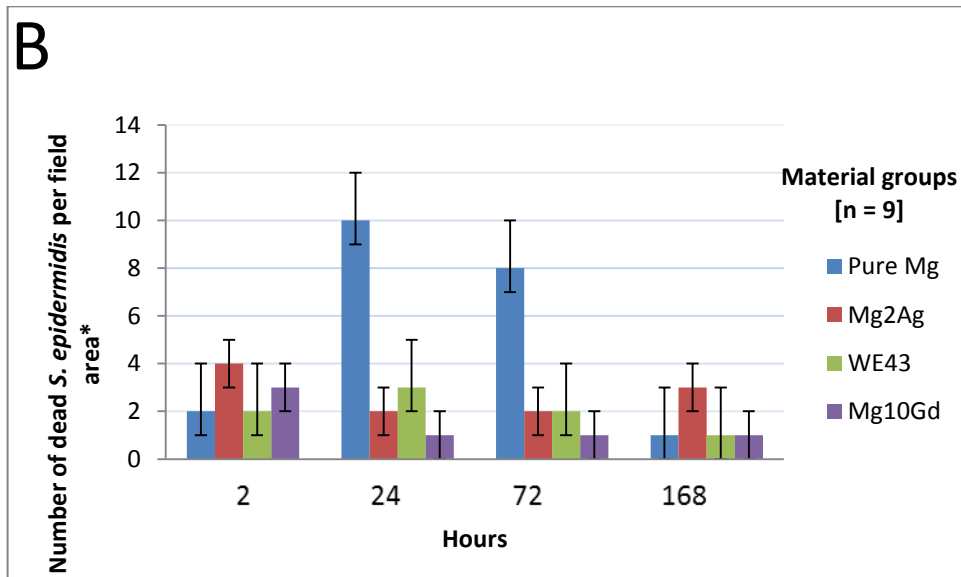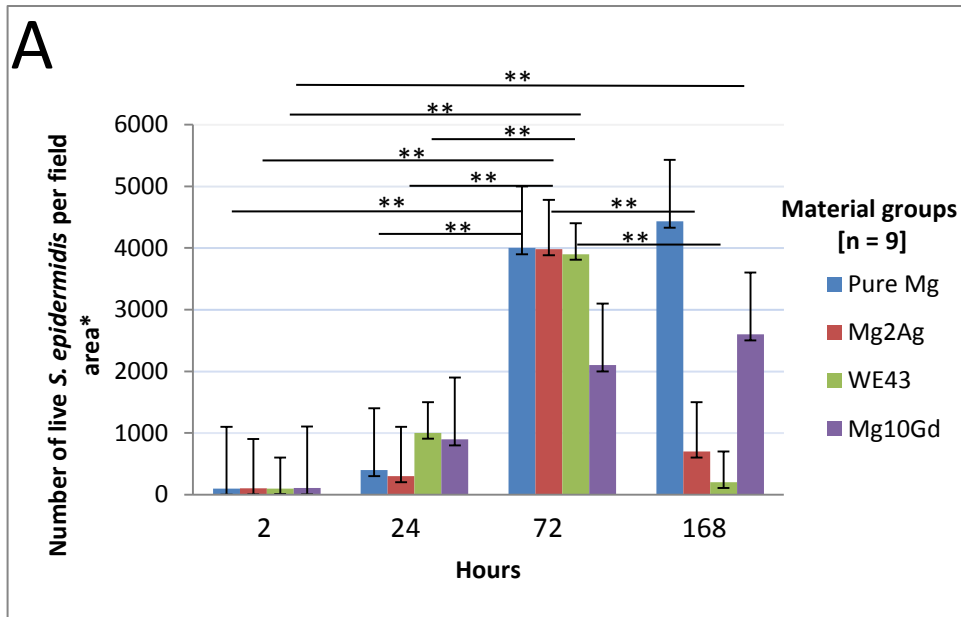
Figure 18. A. Adherence of live *S. epidermidis* to magnesium surfaces over time. **B.** Adherence of dead *S. epidermidis* to magnesium surfaces over time; note significantly higher values for pure Mg compared to all other groups at 24 and 72 h ($p \leq 0.01$). * Field arearepresents 15600 μm^2.
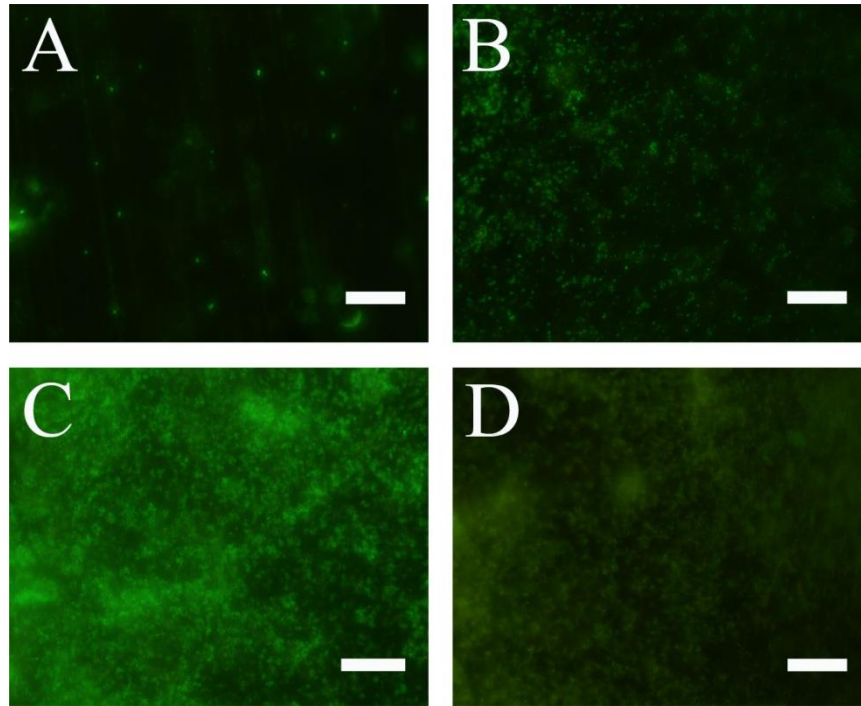
Figure 19. Adherence of *S. epidermidis* to pure Mg at **A.** 2 h, **B.** 24 h, **C.** 72 h, **D.**168 h. Scale bar represents 30 μm.

5.3.3. Characterisation of Surface Roughness

Surface topology was quantified starting from 0 h when bacteria were seeded onto the samples. It was observed that S_a values for pure Mg significantly increased from 0 to 2 h, and then slightly decreased at 168 h (Fig. 20). This increase was significantly higher than in all other samples ($p \leq 0.001$). The surface of Mg2Ag stayed stable over time with no significant changes in S_a. WE43 was comparable to Mg2Ag in respect to S_a changes. Significant decrease in S_a was observed for Mg10Gd at 0 and 168 h ($p = 0.005$).

The pattern of S_{dr} change over time was very similar to S_a and is presented in Figure 21. At 2 h there was observed a significant increase of S_{dr} for pure Mg compared with the initial value ($p \leq 0.001$) as well as in relationship with all other groups ($p \leq 0.001$). S_{ds} behavior was similar for all tested materials (Fig. 22). In general, S_{ds} decreased from 0 h to 2 h but then stayed quite stable over time. No correlation between the surface topology and amount of adherent bacteria were found in this study.
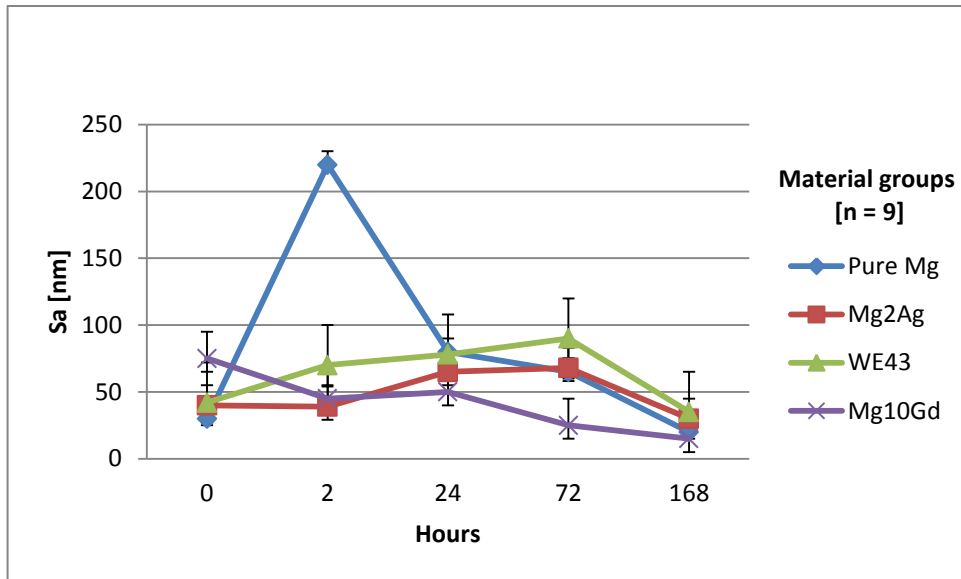
Figure 20. S_a, average surface roughness, of magnesium alloys over time. Note significant increase in S_a for pure Mg at 2 h compared to the other groups ($p \leq 0.001$). Observe Mg10Gd's significant decrease in S_a from 0 to 168 h ($p = 0.005$).
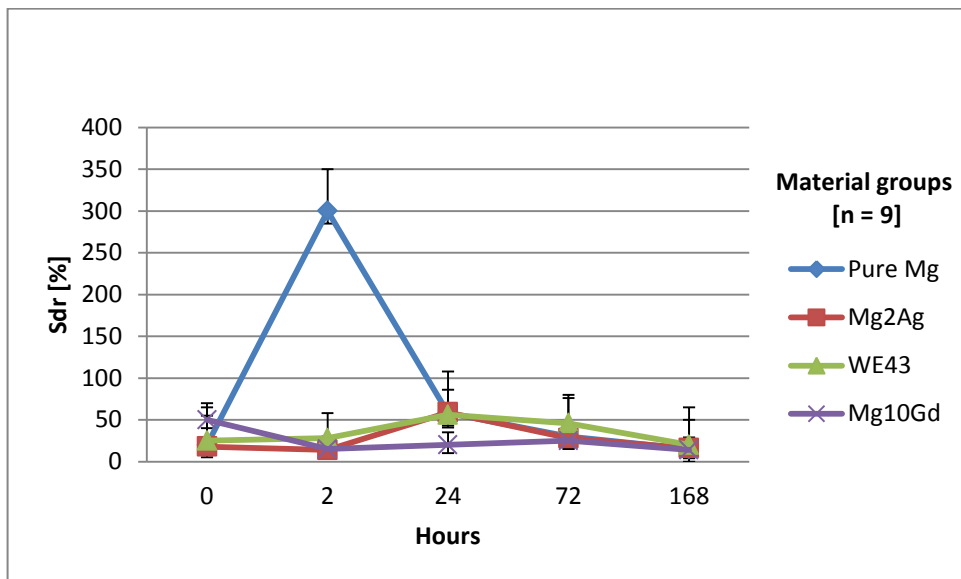
Figure 21. S_{dr}, a ratio between the 3-D measurement and a 2-D reference plane, of magnesium alloys over time. Note a similar pattern with S_a over the studied period: a significant increase of S_{dr} for pure Mg at 2 h compared with the initial value and with all other groups ($p \leq 0.001$).
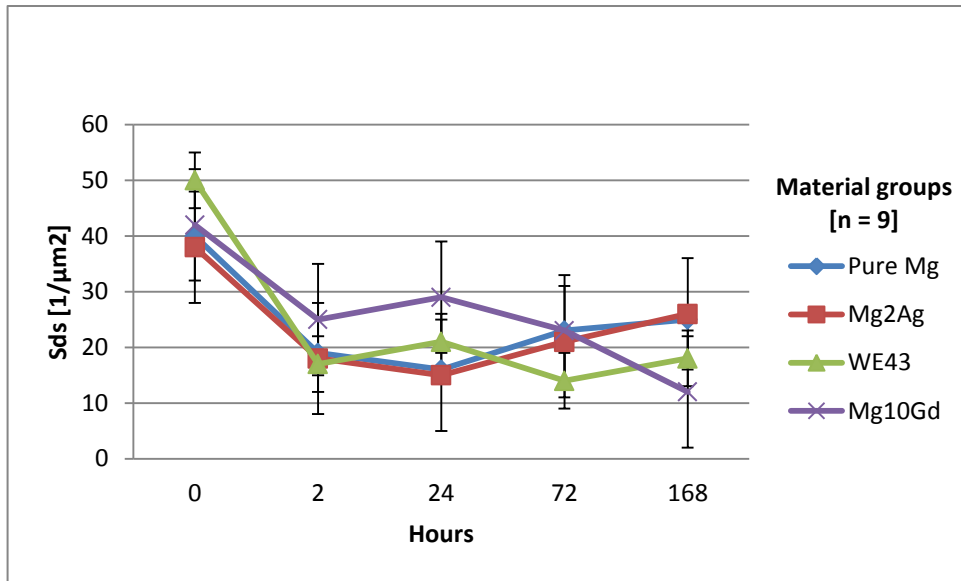
Figure 22. S_{ds}, the number of summits per unit area making up the surface, of magnesium alloys over time.

5.4. Histology

The next study's aim is to determine the bone response to pure Mg, Mg-HA and W4 as well as to evaluate the amount of gas in the bone tissue and the implant resorption behavior.

5.4.1. Bone Response

A total of 24 female New Zealand white rabbits were used for this in vivo study. There were 8 rabbits in each group. The animals were sacrificed at 6 and 12 weeks post-implantation and W4, Mg-HA and pure Mg were evaluated histologically.

There was no significant difference between the pure Mg and W4 in the amount of new bone formation ($p = 0.011$), and these two materials showed similar appearance histologically (Fig. 23 A-D). Both materials were often surrounded by host bone (Fig. 23 B), with few areas with newly formed bone in direct contact to corrosion layer at 6 and 12 weeks (Fig. 23 C-D). The least new bone was observed in Mg-HA group compared to all other materials both at 6 and 12 weeks (Fig. 23 E-F). This difference was statistically significant ($p = 0.03$).

What was similar for all groups is that the clusters of new bone typically formed on the circumference of gas bubbles, encircling the gas (Fig. 24 A-B). These newly formed bone clusters grew and appeared more matured and developed at 12 weeks (Fig. 24 C-D). Mean bone contact to the implant surface was more extensive in Mg-HA group both at 6 and 12 weeks (Fig. 25). Pure Mg and W4 had the lowest mean values for bone-implant contact (Fig. 25).
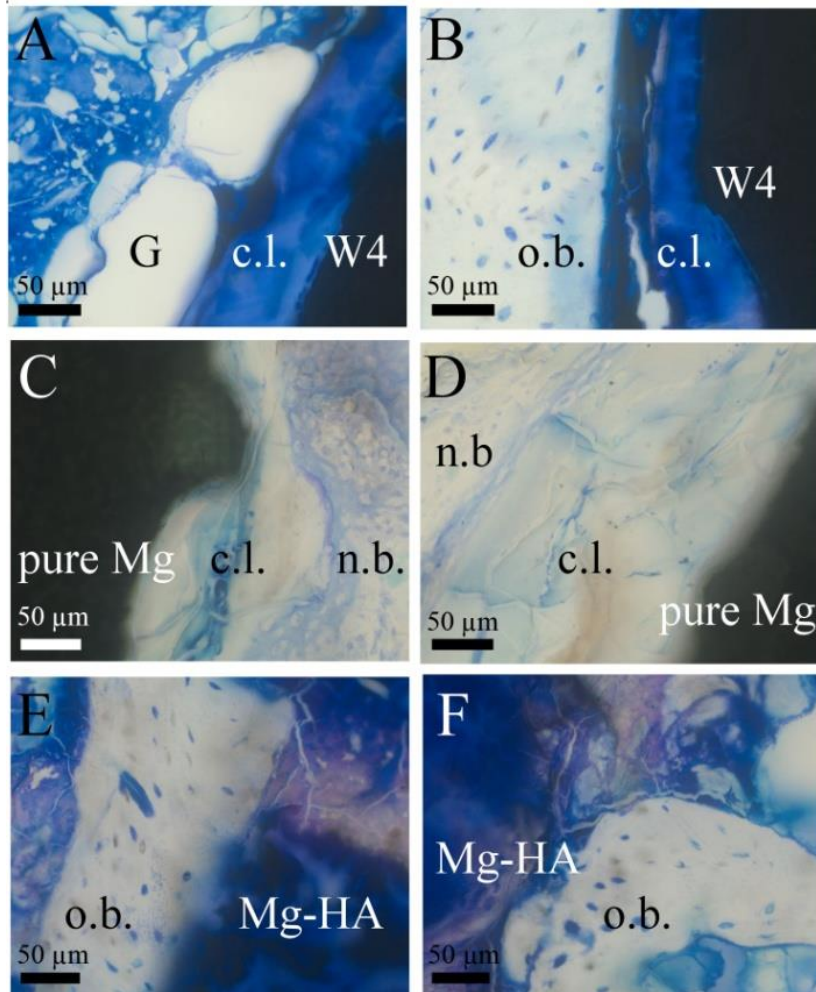
Figure 23. New bone formation patterns at implants' surfaces. TB staining. **A.** W4 at 6 weeks. Gas voids (G) and corrosion layer (c.l.) were observed on material's surface. **B.** W4 at 12 weeks. Bone-implant interface, corrosion layer (c.l.) formed next to host bone (o.b.). **C.** Pure Mg at 6 weeks. New bone (n.b.) formed in direct contact to corrosion layer (c.l.). **D**. Pure Mg at 12 weeks. New bone formed around corrosion layer (c.l.). Corrosion layer (c.l.) was thicker at 12 weeks than at 6 weeks. E. Mg-HA at 6 weeks. The material was mostly surrounded by older bone (o.b.) and there were no signs of new bone formation. F. Mg-HA at 12 weeks. Material had irregular shape and spread into the tissues. Still mostly old host bone (o.b.) was observed.
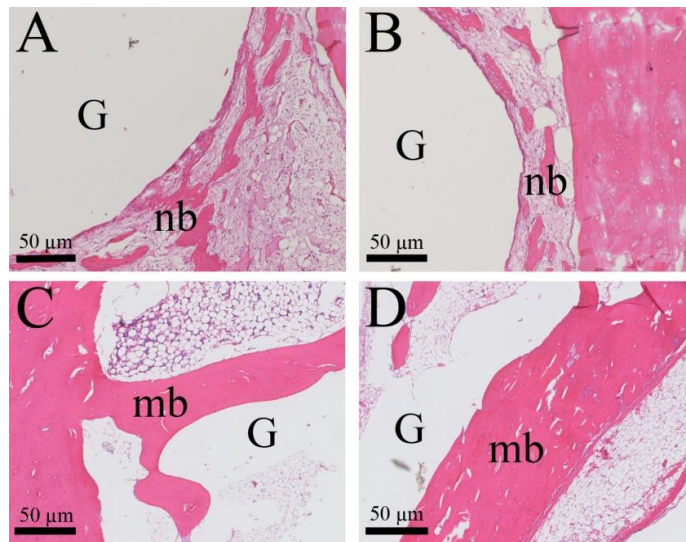
Figure 24. New bone formation patterns around gas voids. HE staining. **A** and **B.** New bone (nb) clusters surrounding the gas void (G) at 6 weeks. C and D. The bone grows stronger and matures (mb) at 12 weeks post-operation.

TRAP-positive multinucleated cells were found in all groups. The highest mean prevalence of TRAP-positive cells was seen in Mg-HA group at 6 weeks. There was no significant difference between the groups at 12 weeks post-operation, and the number of TRAP positive cells was similar in Mg-HA and pure Mg groups (Fig. 26).
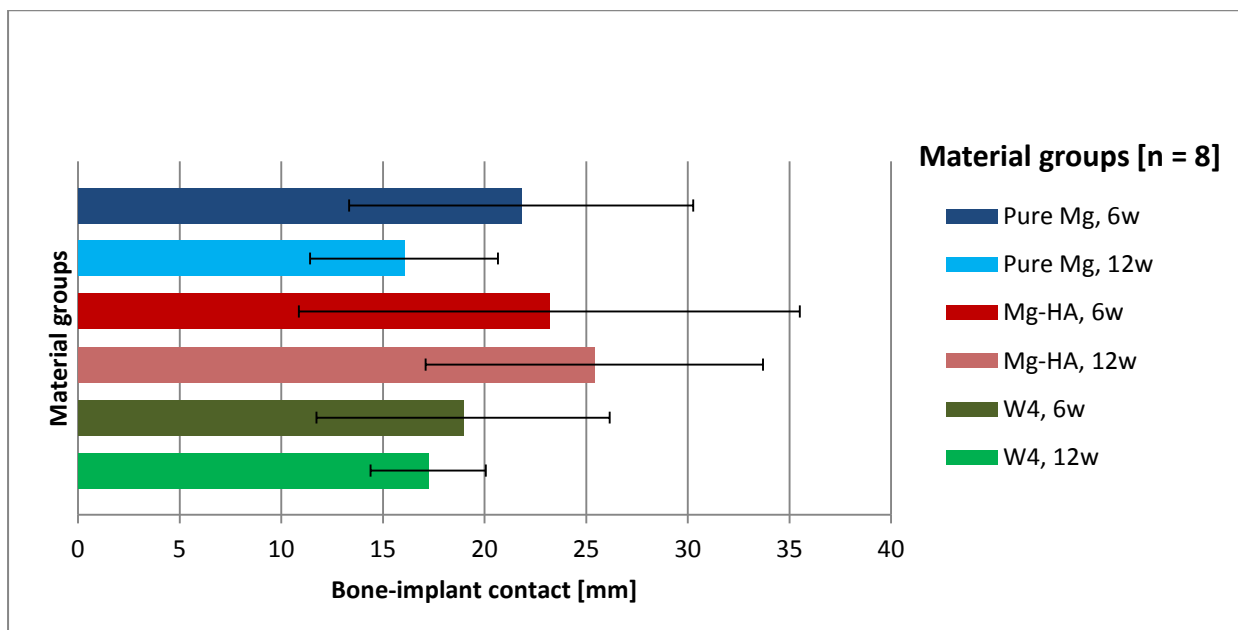
Figure 25. Bone-to-implant contact [mm] at 6 and 12 weeks (6 w and 12 w respectively).
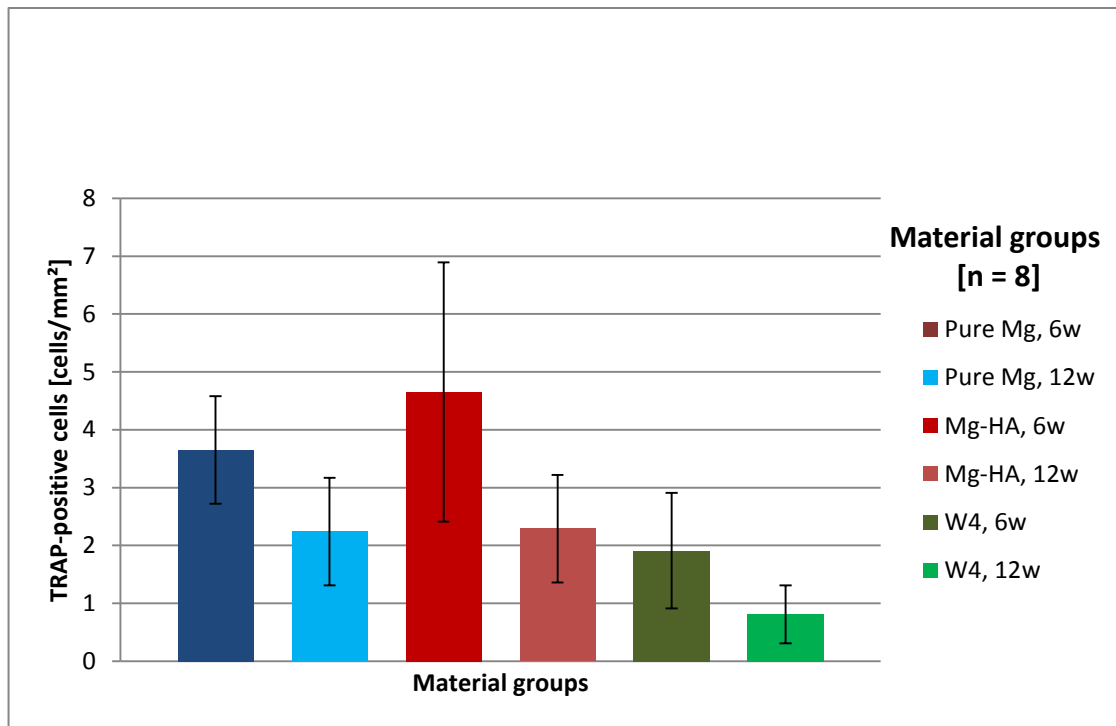
Figure 26. TRAP-positive cells [cells/mm²] around tested materials at 6 w and 12 w.

5.4.2. Gas Voids

In general, the gas voids' diameter was biggest at some distance from the implants. The bubbles were smallest at material surface. Pure Mg and W4 were normally surrounded by huge bubbles up to 4 mm in diameter whereas Mg-HA implants were producing smaller gas volumes. The gas was spread in the bone marrow, not affecting trabecular or cortical bone. Least gas was seen in the bone surrounding Mg-HA biomaterial both at 6 and 12 weeks, whereas W4 produced the most gas of all groups (Fig. 27).
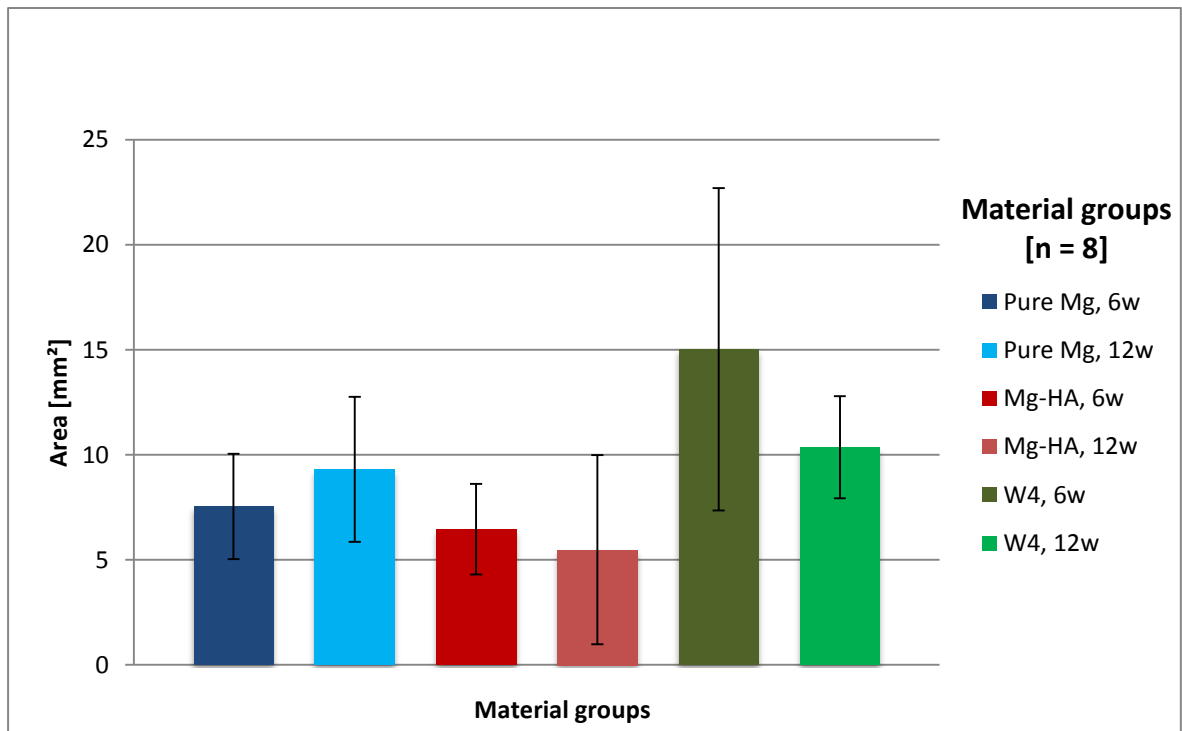
Figure 27. Graph showing the area of gas voids [mm²] around the tested materials at different time points.

5.4.3. Implant Resorption Behaviour

Mg-HA implants had the fastest corrosion rate of all evaluated materials (Fig. 28). Already at 6 weeks most implants lost their integrity, and degradation products together with the implant pieces were seen in the tissues. At 12 weeks the implants were even more degraded. Unlike Mg-HA, both pure Mg and W4 retained their round shape and density. Corrosion process was happening on their surface, whereas in Mg-HA corrosion was more uneven and uncontrollable.
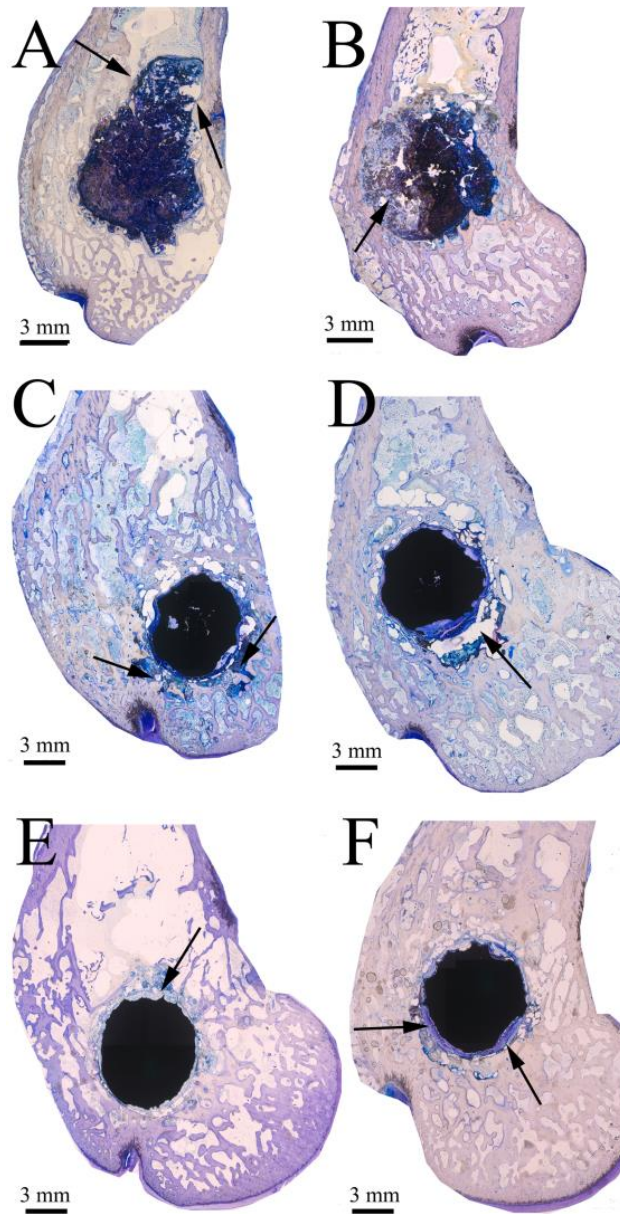
Figure 28. Implants' resorbtion behaviour at 6 and 12 weeks. TB staining. Arrows represent degradation products. **A.** Mg-HA at 6 weeks. **B.** Mg-HA at 12 weeks. **C.** Pure Mg at 6 weeks. **D.** Pure Mg at 12 weeks. **E.** W4 at 6 weeks. **F.** W4 at 12 weeks.

5.4.4. TEM

Bone remodeling was observed in direct proximity to implants' surface. In W4 group osteoclasts were seen at implants interface (Fig. 29 A). The signs of bone remodeling with typical rough boarders at bone-implant interface were also seen at gas voids' periphery in W4 (Fig. 29 B). Osteocytes were evenly spread in the bone tissue (Fig. 29 B). W4's degradation particles which

otherwise were not seen at light microscope magnifications were observed in the tissues at 12 weeks (Fig. 29 C).

Few osteoblasts were seen in Mg-HA group, and often these cells exhibited abnormal morphology (Fig. 29 D). Unlike, other materials, bone remodeling around gas voids was not observed in Mg-HA (Fig. 29 E). However, new bone-ingrowth into the material was found (Fig. 29 F).
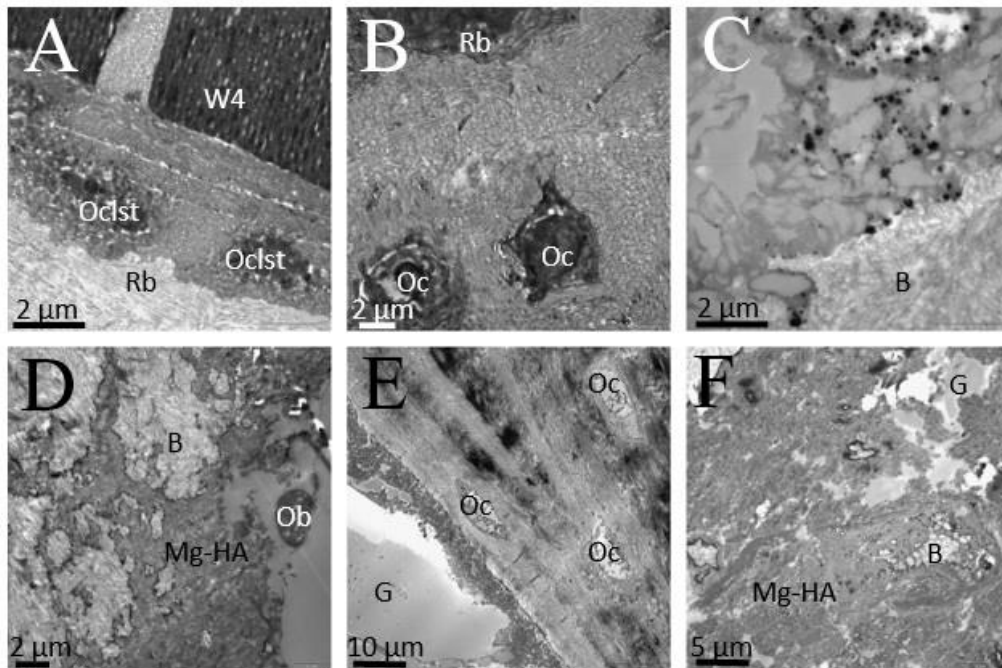
Figure 29. Images from TEM at 12 weeks. **A.** Osteoclasts (Oclst) produced typical rough boarders (Rb) on bone around W4. **B.** Host bone rich in osteocytes (Oc) with typical appearance of rough boarders (Rb). **C.** Degradation particles (black dots) of W4 seen in the tissue. **D.** Few osteoblasts (Ob) were seen in direct contact with Mg-HA, and their morphology was disturbed. Mg-HA's degradation products covered host bone (B). **E.** Gas (G) inside bone marrow in Mg-HA group. No active bone remodeling was observed. Numerous osteocytes (Oc) in host bone. **F.** View into Mg-HA material. Isles of newly formed bone (B) together with gas voids (G) were observed.

6. Discussion

Degradation, cellular reactions, early stages of biofilm formation and histology have been investigated in this work. The results and possible future applications of magnesium will be discussed in this chapter.

6.1. Degradation

This study had the aim to determine corrosion rate, osmolality, pH and surface changes of four magnesium-based materials developed for medical applications.

It was shown that WE43 had the highest, whereas Mg2Ag had the lowest corrosion of all materials. Corrosion rates of Mg10Gd and pure Mg were comparable. It is important for degradable metal implants to have slow, uniform and thus predictable degradation. Bone healing usually takes around 12 weeks (Steiger et al. 2006), but this can vary on individual basis depending on patients' age, general health and medications. Therefore, Mg2Ag with the lowest corrosion rate seems to be the most promising for medical purposes of all tested materials.

Two methods were used to observe corrosion in this study. Immersion test more closely resembles in vivo conditions since it was performed under cell culture condition under constant temperature, oxygen and carbon dioxide. Moreover, medium was constantly changed every second day. Gas evolution test had a few considerations. The experiment was performed in a closed system so the gas would not escape, thus the medium was not changed and the access to oxygen was limited. Therefore, gas evolution method shows corrosion of magnesium-based materials under anaerobic conditions while immersion method represents corrosion under aerobic state. In a clinical situation when the implant is placed into the bone the conditions are aerobic, with more or less constant body temperature, oxygen and fluid transportation to and from the healing site. Thus, the immersion test design is closer to a clinical set-up while the gas evolution test is very demonstrative of the amount of hydrogen gas that magnesium-based materials produce.

Theoretically, osmolality should be high when corrosion rate is high because degradation products and ions are released from the material (Feyerabend et al. 2012). However, this was not the case in this study. Although the corrosion rate of WE43 and Mg2Ag differed by a factor of about 2, there was no highly statistical difference between the groups (p = 0.009). This is because corrosion is a multi-factorial process characterized by the release of certain ions (e.g. magnesium and alloying elements) from the alloy to solution and incorporation of other ions into the

degradation layer (e.g. calcium and phosphate). As it was shown by earlier studies, Mg^{2+} facilitates calcification by stimulating formation of calcium phosphates and thus decreases the amount of free Ca^{2+} in the surrounding medium (Shaw et al. 2003). In fact, all magnesium-based materials decreased the amount of Ca^{2+} in the solution. Pure Mg and Mg10Gd had a similar effect on Ca^{2+}: first high decrease and then only slow further reduction, whereas WE43 and Mg2Ag had a constant rate of depletion. Calcification is beneficial for potential bone implants that are to be used in orthopedic, dental or maxillofacial fields (Reid 2014).

It was shown in previous research that calcification is promoted at basic pH whereas acidic pH leads to dissolving of calcium crystals (Feyerabend et al. 2012). In our study no statistical correlation was found between pH and free Ca^{2+} ions in the solution. However, it was shown that pH increased and Ca^{2+} concentration decreased with time for all tested samples.

This study showed that magnesium makes pH more basic, and that there is a sudden pH drop after day 7. This drop towards more neutral values can be explained by the formation of the corrosion layer. Corrosion layer consists of calcium, phosphorous, magnesium and oxygen and is osseoinductive, permeable and corrosion protective (Willumeit et al. 2011, Feyerabend et al. 2012). While high pH is a sign of fast magnesium degradation due to pitting corrosion, lower pH indicates that corrosion is either more uniform or reduced (Reid 2014).

Since magnesium alloys are designed as temporary implants, the fixture will resorb slowly over time resulting in the surface change. This resorbtion is mainly the result of pitting corrosion (Feyerabend et al. 2012). This means that the surface of magnesium alloys is not uniform during degradation and is challenging to control. We have seen that S_a and S_{dr} tended to increase when the alloys are placed into the medium which represents the body conditions. This increase is probably due to pitting corrosion making the surface rougher. After day 3 both S_a and S_{dr} decrease which might be due to formation of corrosion layer which is unstable and tends to break away because the crystalline lattice is easily cleaved (Hornberger et al. 2012). This might explain why S_a and S_{dr} values slightly increase after day 7, although this increase is not significant.

S_{ds} tended to decrease reaching its absolute minimum at day 3 for Mg10Gd and at day 5 for pure Mg and Mg2Ag. Such decrease in the number of summits per unit area is due to the cleavage of the surface peaks and irregularities which weaken as corrosion proceeds. For pure Mg a rapid increase of S_{ds} was observed at day 7 and 10, which might be due to deposition of calcium phosphate crystals (Feyerabend et al. 2012). Thus, it can be summarized that when magnesium alloys resorb in vitro, the summits become lower with time, while the pitting corrosion

progresses. Formation of corrosion layer makes the surface more uniform, while precipitation of calcium phosphates contributes to surface roughness.

Based on the results from this study, it can be hypothesized that formation of corrosion layer not only improves conditions in the surrounding environment such as osmolality, pH and Ca^{2+} concentration, but also makes the surface more uniform. Limitation of this study is that it looked at corrosion properties of magnesium in absence of cells. Since these implants are to be used in medical applications, the effect of cells on corrosion is desirable to know. Further studies examining corrosion properties in presence of cells are required to see the possible interactions. It is also desirable to compare in vitro corrosion rate with in vivo degradation in future research.

6.2. Cellular Reactions

This study looked at direct long-term effect of magnesium alloys on primary human HRD. The cell viability, differentiation, morphology as well as pH and calcium uptake were analyzed in order to assess the overall biocompatibility of the tested materials. We evaluated the long-term effects of magnesium on human cells to simulate as closely as possible the in vivo situation.

All magnesium specimens impaired cell viability in this study. Previous studies have shown higher values for cell viability measured by MTT test compared to the present study (Feyerabend et al. 2010, Tie et al. 2013, Yang et al. 2013). The difference between this work and previous publications is that the present study applies the longest in vitro incubation times for magnesium alloys tested up to now. The HRD were kept in the direct contact with magnesium samples and not in magnesium extract as conducted in most studies (Feyerabend et al. 2010, Tie et al. 2013, Yang et al. 2013).

An important drawback of the tetrazolium-based tests is that the difference between cytotoxic (cell death) and cytostatic (reduced growth rate) effects cannot be distinguished (Plumb et al. 2004). We have thus looked at the cell morphology under light microscope, TEM and SEM.

After examination under SEM and light microscope it was revealed that the number of cells decreased in the presence of pure Mg, Mg10Gd and WE43. These materials seem to have long-term cytotoxic effect on HRD when put in direct contact with the cells. This explains the low viability values.

The cell number was high and the cells had normal morphology in Mg2Ag groups. However, the cell viability was unexpectedly low for this alloy. The TEM analysis revealed elevated amount of lysosomes which contained degraded magnesium particles. Degradation particles were also

found in the cytoplasm. The presence of high amounts of degradation products inside the HRD could explain the low cell viability values for Mg2Ag. It was shown in previous studies that the uptake of the material particles leads to the induction of cell stress which triggers the cytotoxicity (Pauksch et al. 2014).

The ALP content in HRD is an important factor in bone mineral formation and shows a range of changes during differentiation. The inhibition of ALP content in osteogenic differentiating HRD was caused by pure Mg at day 14 and 28. All other magnesium alloys did not affect the ALP content. In this respect our study shows similar results as previous research in this area (Li et al. 2014) despite the fact that we observed osteogenic differentiation under much longer period and in direct contact of cells with magnesium.

The SEM analysis revealed that the cellular attachment was generally more apparent to the crystals generated by degradation products on material's surface. The crystals have been seen forming on magnesium alloys in previous studies as well (Tie et al. 2013). In this sense our results are similar to earlier findings. The fact that the cells attached to the crystalline structures more readily than to the overall material surface and developed numerous pseudopodia can be explained by the rough structure of crystals, and by the chemical composition of these crystals. It was previously shown that the cells attach better to certain surfaces with the preferable average surface roughness of ~ 0.5 μm up to ~ 8.5 μm (Stout et al. 1993). Values under or above this range diminish the cells' ability to bind to the surface.

The chemical composition of the crystals and the degradation layer formed on magnesium's surface can also explain the better attachment of the cells to these structures. Their chemical composition consists of calcium, phosphorous, magnesium and oxygen (Willumeit et al. 2011). Thus, the cells attach to already reacted material where they are not mechanically disturbed by hydrogen gas produced as a by-product of degradation. The formation of the degradation layer could also explain an increase in cell density around Mg10Gd and WE43 after 21 days of incubation.

All magnesium-based materials decreased the amount of Ca^{2+} in this study. As was shown by previous publications, Mg^{2+} promotes the formation of calcium phosphates and consequently decreases the amount of free Ca^{2+} ions in the medium (Feyerabend et al. 2012. Willumeit et al. 2011). Consequently, our results are consistent with earlier works. A sufficient supply of calcium is vital to ensure that bone laid down by osteoblasts is normally mineralized (Reid. 2014). Calcification is thus advantageous for orthopedic and maxillofacial implants.

It was shown in previous works that magnesium increases the pH and that the high pH promotes Ca^{2+} binding (Witte et al. 2008. Willumeit et al. 2011). In this study, it was also revealed that pH shifts to alkali values in presence of magnesium but to somewhat different degree for different alloys. Yet no statistical correlation was observed between the pH and consumed Ca^{2+}.

In conclusion, our study displays a long-term effect of magnesium materials on human HRD seeded directly onto magnesium discs. In respect to cell morphology, cell density and the effect on the surrounding pH, Mg2Ag showed the most promising results. However, the mechanism of cell stress induction and cytotoxicity need to be further studied in order to be able to predict possible health risks.

6.3. Early Stages of Biofilm Formation

Implant-associated infections are the result of bacteria adhesion to an implant surface and subsequent biofilm formation at the implantation site. This study compared magnesium materials on their ability to resist bacterial adhesion as well as further biofilm formation. The surface changes were measured in order to find the possible correlation between the biofilm and surface characteristics.

Adhesion of *E. faecalis* was significantly better than adhesion of *S. epidermidis* to the same samples. This means that different bacterial strains have different ability to bind to magnesium surfaces under the same conditions which can be supported by previous studies on microbiology (Guo et al. 2014). In this study, no correlation was found between the surface topology and the ability of the bacteria to adhere to the magnesium surface, although this correlation was observed in previous research (Dorkhan et al. 2012). Resorbtion of magnesium is a very complex chemical process. Surface topology is one of many factors that might influence cell and bacteria adherence and there are many more aspects that should be taken into account when analyzing magnesium's performance in vitro.

It has been shown in previous research that magnesium changes the surrounding environment, it makes pH more basic (Witte et al. 2008, Willumeit et al. 2011), stimulates precipitation of Ca^{2+} ions from the solution (Feyerabend et al. 2012, Witte et al. 2008, Willumeit et al. 2011), changes the osmolality (Feyerabend et al. 2012) and reacts with the medium to form H_2 gas (Staiger et al. 2006). The surrounding environment also has effect on magnesium since it promotes formation of the protective layer on its surface (Staiger et al. 2006). Protective layer slows down further degradation but is brittle and cleaves off from the surface quite easily (Hornberger et al. 2012). This means that the surface topology of magnesium materials is constantly changing. In this

study it was observed that in the first hours of observation S_a increased which can be explained by removal of surface irregularities and particles that are present on the surface. Later, the summits start to resorb and their tops break off from the surface decreasing the $S_{ds.}$ At later stages, the protective layer consisting of calcium phosphates and precipitated proteins from the medium is formed on the surface decreasing S_a and S_{dr} values.

Bacterial adhesion to magnesium surfaces is lower compared to titanium surfaces (Tie et al. 2012). Antibacterial properties of magnesium might be explained by the changes that magnesium promotes in its surroundings. As stated previously, magnesium makes pH basic through the release of OH^- ions in contact with fluids (Staiger et al. 2006, Witte et al. 2008, Willumeit et al. 2011). The higher pH inhibits enzyme activities that are essential to bacterial life, i.e. metabolism, growth, and cellular division (Prabhakar et al. 2012).

It was shown in previous studies that *S. epidermidis* grows best in slightly more acidic pH close to around 6.35 but demonstrates the ability to growth in a range of pHs (McDonald et al. 1986, Korting et al. 1992). In this study *S. epidermidis* seemed to be resistant to alkali pH which magnesium creates since the number of bacteria increased up to 72 h for all samples tested. After 72 h Mg2Ag and WE43 suppress further bacterial growth on their surfaces. This might be due to release of Ag^{2+} ions which have known antibacterial properties (Tie et al. 2013). In case of WE43, the decreased number of adherent bacteria after 72 h might be due to high resorbtion rate of this alloy (Gu et al. 2010) and consequent formation of H_2 gas which acts as a physical barrier for further biofilm growth. Pure Mg and Mg10Gd both had bacteriostatic effect after 72 h which might be due to the change in the surrounding environment which became less favorable for *S. epidermidis*.

It was shown in previous studies that unlike *S. epidermidis*, *E. faecalis* can survive in highly alkaline pH, and some clinical isolates require 72 h at pH 12.5 to be killed (Weckwerth et al. 2013). Mild alkaline mediums had no effect on *E. faecalis* vitality and high alkaline condition (pH > 10) led to significant declines of survival rate of bacteria in one study (Yan et al. 2012). Also the biofilm cells of *E. faecalis* were more alkaline tolerant than corresponding planktonic cells (Yan et al. 2012). This can explain why there were more *E. faecalis* adhered to magnesium samples compared to *S. epidermidis* which are less resistant to alkali pH. Based on the previous research results it can be hypothesised that *E. faecalis* would have continued its biofilm growth if the experiment would have continued for several more h and days.

Dead *E. faecalis* and *S. epidermidis* were few in our study. The surface was predominantly occupied by live bacteria. Thus, magnesium seems to have no bactericidal effect. With time no increase in dead *S. epidermidis* was observed, their number was stable over the observation period.

Magnesium alloys seemed to suppress the adhesion of *S. epidermidis* in the first h of experiment. Unlike *S. epidermidis*, *E. faecalis* binded to magnesium more readily at 2 h. One of the limitations of this study is that it does not compare magnesium to titanium surfaces and it is thus not possible to see whether magnesium is better in its ability to prevent biofilm adhesion than titanium. Resorption of magnesium alloys is a complex process which involves alterations of material's surface and changes to surrounding environment. Thus the task of the future research in this area would be determination of factors that suppresses bacterial vitality.

6.4. Histological Examination

The current Thesis is based on 3 R's principle. In vitro methods were first performed in order to evaluate the processes which happen to magnesium-based alloys without involving animals. The last stage was to see the tissue reaction to magnesium-based implants. The implants were carefully chosen and the animal number was kept to as low as possible. All animal experiments were conducted according to the European Commission Directive 86/609/EEC for animal experiments and it was ensured that the animal suffering is kept to minimal.

In this study three magnesium-based implants – pure Mg, W4 and Mg-HA – were compared qualitatively and quantitatively using such parameters as degradation behaviour, gas formation and bone response.

Formation of corrosion layer and implant resorbtion shows the rate of implant degradation. It is crucial that the implant starts resorbing after the bone has gained enough strength after the fracture. In this study, Mg-HA implants had the fastest corrosion rates. Already at 6 weeks these biomaterials lost their integrity, and degradation products together with the implant pieces spread in the tissue. At 12 weeks Mg-HA were even more disintegrated and spread outside the initial area of surgical placement. Hard-tissue repair typically requires implantation of the fixture for a minimum of 12 weeks (Steiger et al. 2006). Thus, Mg-HA tested in this study does not meet these criteria, most likely due to high concentration of HA reaching 20 % by wt. It was shown in one publication by Schaffler et al. that the corrosion rate of calcium-containing magnesium implants was highly dependent on the amount of calcium in the alloy: the higher the calcium

concentration, the faster the degradation rate (Schaffler et al. 2012). Based on these results it can be assumed that decreasing the amount of HA might improve resorbtion properties of Mg-HA. Unlike Mg-HA, pure Mg and W4 held their original round shape during the whole period of investigation. These two materials were covered by even corrosion layer, meaning that degradation was quite uniform. W4 had the most even degradation behaviour in this study. Material was covered by uniform corrosion layer and degradation products were rarely seen breaking off the surface unlike in the other implants. This means that the surface corrosion is more homogeneous and thus more predictable. This, of course, is more beneficial for the screws and plates that are to be used in bone augmentation procedures.

In this study we have observed an interesting pattern of new bone formation around magnesium-based implants. The bone formed not only around material itself, but also around the gas voids. Osteocytes, the principal sensors for mechanical loading of bone, regulate the onset of bone formation and resorbtion (Frost et al. 1994). Moderate mechanical stress stimulates bone formation by osteoblasts, whereas high loads or no loads at all lead to bone resorbtion by osteoclasts (Frost et al. 1994). It can be hypothesized that the gas produced by degradation process of magnesium acted as a moderate mechanical stress and stimulated osteocytic activation of bone remodeling process in this study. This could explain why the clusters of new bone were often seen forming around the gas voids.

When comparing the values for implant-bone contact (Fig. 24 A) and the amount of gas (Fig. 25), a certain pattern between these two parameters could be observed: the less gas, the higher the implant-bone contact. Thus, for Mg-HA the highest mean bone-implant contact was most probably due to the lowest mean gas amounts compared to the other groups.

Several publications describe the gas formation by magnesium implant degradation in vivo (Witte et al. 2005, Li et al. 2008). Li et al. detected gas around the binary Mg-Ca implants during the early implantation period. The gas disappeared two months after implantation, and no adverse effects were observed (Li et al. 2008). Zhang et al. showed that the subcutaneous gas bubbles generated by a Mg-6Zn alloy disappeared 6 weeks after implantation (Zhang et al. 2010). In our study we have seen that the mean amount of gas was less at 12 weeks compared to 6 weeks for W4 and Mg-HA. In this our results are consistent with previous findings.

TRAP is an enzyme that is expressed in high amounts by osteoclasts, but even by inflammatory macrophages and dendritic cells (Noordin et al. 2012). TRAP-staining is widely used as a marker of osteoclasts. High amount of TRAP-positive cells, which in most cases are osteoclasts, is a first

sign of bone remodeling since resorption by osteoclasts precedes bone formation by osteoblasts. Mg-HA group had the highest mean number of TRAP-positive cells at 6 weeks both surrounding the implant and in direct contact to material, compared to pure Mg and W4. This is probably because of fewer and smaller gas bubbles which, hypothetically, do not push out the cells from the implant resulting in higher cell counts in the ROI. Another explanation to such high numbers of the TRAP-positive cells could be the osteolysis caused by high degradation rate of Mg-HA and an increase in metal particulates in the bone. This immunological response can cause the loss of bone and lead to implant failure. Macrophages, fibroblasts, lymphocytes and osteoclasts are recruited to the implantation site and secrete proinflammatory and osteoclastogenic cytokines, exacerbating the inflammatory response. This chronic cell activation can break the balance between bone formation and bone resorption resulting in the osteolysis (Noordin et al. 2012).

Numerous publications suggest that magnesium alloys promote bone attachment to implant surfaces compared to conventional materials (Cecchinato et al. 2015, Zreiqat et al. 2002, Castellani et al. 2011, Witte et al. 2007). New bone formation was shown for MgYREZr, Mg-Mn-Zn, WE43, MgCa0.8, AX30, LANd 442, ZEK100 and LAE442 (Waizy et al. 2012, Willumeit et al. 2011, Witte et al. 2007, Waizy et al. 2014). Castellani et al. observed greater bone-implant contact with a magnesium alloy based on WE43 compared to a titanium implant (Castellani et al. 2011). It was also observed that magnesium significantly promotes the osteopontin gene expression compared to titanium, this is an essential gene for the early biomaterial-cell osteogenic interaction (Cecchinato et al. 2015). Witte et al. reported a greater mineral apposition rate on magnesium alloys compared to a degradable polymer (Witte et al. 2007).

Our results are hard to compare with previous research since slightly different alloy compositions and manufacture methods are used in various in vivo studies. However, also in this investigation it was observed that new bone can form directly on corrosion layer of pure Mg and W4. The least new bone formation was seen in Mg-HA. This material had the fastest degradation of all implants and thus its release of corrosion products was the highest. These products might have changed the internal environment and interfered with the normal tissue healing. This could also explain the abnormal appearance of osteoblasts coming in direct proximity to Mg-HA. As a result, new bone was not readily forming in Mg-HA group.

In previous research it was stated that magnesium might stimulate bone formation since magnesium ions enhance cell attachment and proliferation (Witte et al. 2005). In our study, new bone was seen forming in direct contact to the materials, as well as around the gas voids. We did

not observe fibrous tissue formation around tested materials. Fibrous tissue in-growth was observed in commercially available MagneZix (Waizy et al. 2014). In this respect our tested materials seem to have more positive effect on bone healing. Magnesium itself seems to be biocompatible. It is its product of degradation – gas – which causes mechanical barrier for the cells.

To conclude, pure Mg and W4 were shown to be the most promising materials in this study in respect to the bone response to the implant material. Mg-HA did not enhance much new bone formation, had fast degradation and high amount of TRAP-positive cells which might be the sign of the osteolysis. Future research should look at mechanical performance of such materials in vivo. The possible applications of pure Mg and W4 could be the screws and plates for fixing minor bone fractures as well as for bone augmentation procedures in order to avoid the secondary surgery on screw removal.

6.5 Possible Applications of Magnesium as Implant Material

Steel- and titanium-based implants are frequently used in orthopedic and maxillofacial surgery. While they provide excellent stability, they may persuade stress shielding, and supplementary secondary surgery for implant removal may be required since these materials are non-degradable (Waizy et al. 2013, Sumitomo et al. 2008). Alternatively, degradable polymer materials are mechanically weaker and might provoke foreign body reactions (Bostman et al. 1992). The idea behind magnesium implants is to combine degradability (similar to polymers) with good mechanical properties (similar to or better than conventional titanium-based materials). Modern magnesium alloys show improved anti-corrosive and mechanical properties (Waizy et al. 2013).

From the studies performed within our project, Mg2Ag alloy was the most promising in respect to the cellular reactions, degradation rates, the effect on the surrounding environment and the ability to withstand biofilm growth after 72 h. It is thus of interest to conduct in vivo experiment with Mg2Ag alloy screws and pins and evaluate degradation, tissue reaction and mechanical properties of degrading implants.

Another possible application for magnesium, and specifically for Mg2Ag, which showed positive results in our investigations, are bone cements and fillers with magnesium microparticles, magnesium reinforced polymers, as well as magnesium-based coating materials for titanium implants.

Calcium phosphate cement (CPC) has been successfully used in clinics as bone repair biomaterial for many years. However, poor mechanical properties, low intrinsic porosity limiting bone in-growth and a low biodegradation rate restrain any further applications. Incorposating Mg2Ag particles into CPC cement should theoretically improve CPC's intrinsic porosity, stimulate bone in-growth and improve mechanical properties. Wu et al. has shown good results in vivo by combining CPC with magnesium phosphate cement (MPC) and developing calcium-magnesium phosphate cement (CMPC). Histological evaluation showed that the introduction of MPC into CPC enhanced the efficiency of new bone formation. CMPC also showed good biocompatibility, biodegradability and osteoconductivity with host bone in vivo (Wu et al. 2008). Similar results were presented by Zeng et al. who applied CMPC for sinus floor elevation (Zeng et al. 2012). According to the authors, CMPC's excellent osteoconductivity, which may be attributed to Ca and Mg ion composition, and the tissue-engineered bone constructed of CMPC and HRD might be a potential alterative graft for maxillofacial bone regeneration (Zeng et al. 2012).

In future, not only the bone cements might be improved with magnesium micro particles, but also polymers' mechanical properties. According to the study by Wong et al., incorporation of magnesium micro-particles into the polycaprolactone (PCL) matrix yields mechanical properties close to those of human cancellous bone, and in vitro studies show that the silane-coated Mg/PCL composites have good cytocompatibility and osteoblastic differentiation qualities (Wong et al. 2013). The bulk mechanical properties could be maintained for 2 months before degradation takes place. The new bone formation on the silane-coated Mg/PCL composites was significantly larger compared to conventional polymethyl methacrylate (PMMA) and pure PCL and the results suggest potential clinical applications of the silane-coated Mg/PCL composites (Wong et al. 2013).

Magnesium was suggested as possible surface coating material on titanium implants (Cecchinato et al. 2015). It was shown that magnesium coated surfaces significantly promote the osteopontin gene expression compared to conventional titanium implants, this is an essential gene for the early biomaterial-cell osteogenic interaction (Cecchinato et al. 2015). Thus, testing Mg2Ag as a coating material should be the scope of future research.

7. Conclusion and Future Prospects

7.1. Conclusion

Resorption of magnesium materials is a complex process which causes the shift of the surrounding pH to alkali values, increases the osmolality, changes the outer surface and decreases the amount of free Ca^{2+} which is beneficial for bone applications. The general pattern of magnesium alloys' surface change is as follows: the summits become lower with time, while the pitting corrosion progresses.

In the cellular reaction experiment it was shown that exposure of HRD to magnesium increases the intracellular counts of lysosomes and endocytotic vesicles. Cellular attachment is generally best to the crystals and irregularities that form on material's surface. All magnesium materials induce calcification and apart pure Mg do not affect the normal ALP content which is beneficial for orthopedic and maxillofascial applications.

With regard to bacterial adhesion to magnesium alloys it was detected that various bacterial strains have different adherence capacity. There is no difference between the tested magnesium materials in their ability to withstand biofilm formation at early stages up to 72 h. After 72 h Mg2Ag and WE43 had more favorable properties than pure Mg and Mg10Gd in their ability to suppress bacterial growth. The changes in biofilm growth and adherence were not due to the changes in surface topology.

As a result, Mg2Ag alloy seems to be the most promising in respect to the cellular reactions, degradation rates, the effect on the surrounding environment and the ability to withstand biofilm growth after 72 h.

Histological study revealed that the new bone was seen forming in direct contact to the magnesium materials, as well as around the gas voids. Mg-HA did not cause any adverse biological reaction but had too fast resorption in vivo probably due to the high levels of HA comprising 20 % of the material's composition.

7.2. Future Prospects

This Thesis along with the previous findings supports the idea of using magnesium materials as implants for bone application. Despite the interesting results from this study, there are still scopes to investigate.

The alloy of Mg2Ag has shown the most promising results in vitro, thus an animal study would be the next step to perform. It is of great interest to investigate Mg2Ag's degradation under long observation period of up to 24 months. In vivo investigation should consist of micro-CT to study gas production under degradation, histological analysis of tissue reaction to the implant, blood sample analysis to detect any abnormal values of magnesium in the blood, analysis of organs including kidneys, liver and brain for the presence of elevated levels of magnesium and other degradation products. It is also essential to perform mechanical strength tests at different stages of degradation to evaluate support that the implant gives to the bone at different time points.

As discussed in Chapter 6.5, magnesium has many application potentials in regeneration medicine. Thus, not only Mg2Ag screws can be designed and tested in vivo, but also Mg2Ag particles incorporated in CPC and PCL for improvement of mechanical properties of these biomaterials. It might further be of interest to see how Mg2Ag coating on conventional titanium implants can influence bone attachment to the materials' surface.

Furthermore, Mg-HA bone filling material has shown quite good results in vivo exept rather too fast degradation. Therefore, finding optimal proportions of components would be the next stage in product development. The amount of HA in our study was 20 % by wt. Future studies should look at Mg-HA with smaller HA amount.

Pure Mg and W4 had a good effect on new bone formation, however, gas voids were interfering with the normal tissue healing in this study. It is interesting to investigate the effect of surface coating on degradation properties of these materials. Surface coating would eventually assist the initial bone healing and thus initial stability of the implant in the bone. The coating would resorb with time exposing magnesium's surface, but than the implant would already have gained the initial stability in the bone and the gas production would not be as critical at that stage.

In addition, 12 weeks after biomaterial implantation might be a too short time gap for the study of new bone formation. Hence, analysis should be carried out over a prolonged time period in order to study the time related effects of magnesium on bone formation.

In spite of promising performance seen in magnesium materials, the main conclusion seems to be that there is still need for improvement of existing systems and testing promising alloys such as Mg2Ag in vivo in order to match the biological bone complexity. The task of tailoring the appropriate magnesium material for different purposes seems to be a feasible challenge in the future, and requires a synergistic interdisciplinary work of materials science, engineering, biology, chemistry, physics and medicine.

8. Dissemination

8.1. List of Publications:

1. <u>Olga Charyeva</u>, Ulrich Thormann, Katrin S. Lips, Lydia Heimann, Ursula Sommer, Gabor Szalay, Volker Alt, Norbert Hort, Reinhard Schnettler, Michael Rauschmann, Sven Schmidt. *Histological Comparison of New Biodegradable Magnesium-Based Implants for Medical Applications.* Journal of Maxillofacial and Oral Surgery. 2015 Online publication ahead of print. DOI: 10.1007/s12663-015-0743-z.

2. <u>Olga Charyeva</u>, Ulrich Thormann, Sven Schmidt, Ursula Sommer, Katrin S.Lips, Lydia Heimann, Reinhard Schnettler. *In Vivo Comparison of New Biodegradable Magnesium-Based Implants for Orthopaedic Uses.* Bone & Joint Journal, Orthopaedic Proceedings Supplement. 2014,96(11):247.

3. <u>Olga Charyeva</u>, Frank Feyerabend, Regine Willumeit, Daniel Zukowski, Cyrille Gasqueres, Gabor Szakacs, Nezha Ahmad Agha, Norbert Hort, Felix Gensch, Francesca Cecchinato, Ryo Jimbo, Ann Wennerberg, Katrin Susanne Lips. *In Vitro Resorption of Magnesium Materials and its Effect on Surface and Surrounding Environment.* Open Journal of Toxicology. 2015. Online publication ahead of print. DOI: 10.15406/mojt.2015.01.00004.

4. <u>Olga Charyeva</u>, Jessica Neilands, Gunnel Svensäter, Ann Wennerberg. *Bacterial Biofilm Formation on Resorbing Magnesium Implants.* Open Journal of Medical Microbiology. 2015,(5): 1-11. DOI: 10.4236/ojmm.2015.51001.

5. <u>Olga Charyeva</u>, Olga Dakischew, Ursula Sommer, Katrin Susanne Lips. *Biocompatibility of Magnesium Implants in Primary Human Reaming Debris-derived cells Stem Cells in Vitro.* Journal of Orthopaedics and Traumatology. Online publication ahead of print. DOI: 10.1007/s10195-015-0364-9.

8.2. Presentations on the International Conferences:

- Combined Meeting of the Orthopaedic Research Societies (CORS), October 2013, Venice, Italy.
- Orthopaedic Research Society Congress (ORS), March 2014, New Orleans, USA.
- European Orthopaedic Research Societies Congress (EORS), July 2014, Nantes, France.
- Nordic Young Scientist Conference in Odontology (NYSCO), August 2014, Malmö, Sweden.

- SingHealth Scientific Congress on Academic Medicine, September 2014, Singapore, Singapore.
- European Congress of Clinical Microbiology and Infectious Disease (ECCMID), April 2015, Copenhagen, Denmark.

8.3. Presentations on the Local Conferences:

- Conference of the International Giessen Graduate Centre for the Life Sciences (GGL), September 2013, Giessen, Germany.
- Conference of the International Giessen Graduate Centre for the Life Sciences (GGL), September 2014, Giessen, Germany.

9. References

1. Aghion E, Levy G, Ovadia S. In vivo behavior of biodegradable Mg-Nd-Y-Zr-Ca alloy. J Mater Sci Mater Med. 2012,23(3):805-812.

2. Bergsma EJ, Rozema FR, Bos RR, de Bruijn WC. Foreign body reactions to resorbable poly (L-lactide) bone plates and screws used for fixation of unstable zygomatic fractures. J Oral Maxillofac Surg. 1993,51(6):666-670.

3. Bhat SV. Biomaterials. Kluwer Academic Publishers, Boston, MT, USA: 2002. p. 265.

4. Bostman OM, Paivarinta U, Partio E, Manninen M, Vasenius J, Majola A, Rokkanen P. The tissue-implant interface during degradation of absorbable polyglycolide fracture fixation screws in the rabbit femur. Clin Orthop Relat Res. 1992,285:263–272.

5. Brar HS, Platt MO, Sarntinoranont M, Martin PI, Manuel MV. Magnesium as a biodegradable and bioabsorbable material for medical implants. JOM. 2009,61(9):31-34.

6. Bürgers R, Gerlach T, Hahnel S, Schwarz F, Handel G, Gosau M. In vivo and in vitro biofilm formation on two different titanium implant surfaces. Clin Oral Implants Res. 2010,21(2):156-64.

7. Campoccia D, Montanaro L, Arciola CR. The significance of infection related to orthopedic devices and issues of antibiotic resistance. Biomaterials. 2006,27(11):2331-9.

8. Castellani C, Lindtner RA, Hausbrandt P, Tschegg E, Stanzl-Tschegg SE, Zanoni G, Beck S, Weinberg, AM. Bone-implant interface strength and osseointegration: bio-degradable magnesium alloy versus standard titanium control. Acta Biomater. 2011,7:432–440.

9. Cecchinato F, Karlsson J, Ferroni L, Gardin C, Galli S, Wennerberg A, Zavan B, Andersson M, Jimbo R. Osteogenic potential of human adipose-derived stromal cells on 3-dimensional mesoporous TiO_2 coating with magnesium impregnation. Materials Science and Engineering: C. 2015,52:225-234.

10. Delaney RA, Falvey E, Kalimuthu S, Molloy MG, Fleming P.Orthopaedic admissions due to sports and recreation injuries. Ir Med J. 2009,102(2):40-42.

11. Dorkhan M, Chávez de Paz LE, Skepö M, Svensäter G, Davies JR. Effects of saliva or serum coating on adherence of Streptococcus oralis strains to titanium. Microbiology. 2012,158(2):390-7.

12. Edwards RC, Kiely KD, Eppley BL. Fixation of bimaxillary osteotomies with resorbable plates and screws: Experience in 20 consecutive cases. J Oral Maxillofac Surg. 2001,59(3):271-6.

13. Erbel R, Di Mario C, Bartunek J, Bonnier J, de Bruyne B, Eberli FR, Erne P, Haude M, Heublein B, Horrigan M, Ilsley C, Böse D, Koolen J, Lüscher TF, Weissman N, Waksman R. Temporary scaffolding of coronary arteries with bioabsorbable magnesium stents: a prospective, non-randomised multicentre trial. Lancet. 2007,369(9576):1869-75.

14. Fernández Guerrero ML, Goyenechea A, Verdejo C, Roblas RF, de Górgolas M. Enterococcal endocarditis on native and prosthetic valves: a review of clinical and prognostic factors with emphasis on hospital-acquired infections as a major determinant of outcome. Medicine (Baltimore). 2007,86(6):363-77.

15. Feyerabend F, Drücker H, Laipple D, Vogt C, Stekker M, Hort N, Willumeit R. Ion release from magnesium materials in physiological solutions under different oxygen tensions. J Mater Sci Mater Med. 2012,23(1):9-24.

16. Feyerabend F, Fischer J, Holtz J, Witte F, Willumeit R, Drucker H. Evaluation of short-term effects of rare earth and other elements used in magnesium alloys on primary cells and cell lines. Acta Biomater. 2010, 6:1834–42.

17. Feyerabend F, Witte F, Kammal M, Willumeit R. Unphysiologically high magnesium concentrations support chondrocyte proliferation and redifferentiation. Tissue Eng. 2006, 12:3545–56.

18. Frank KL, Guiton PS, Barnes AM, Manias DA, Chuang-Smith ON, Kohler PL, Spaulding AR, Hultgren SJ, Schlievert PM, Dunny GM. AhrC and Eep are biofilm infection-associated virulence factors in Enterococcus faecalis. Infect Immun. 2013,81(5):1696-708.

19. Frost HM. Wolff's Law and bone's structural adaptations to mechanical usage: an overview for clinicians. Angle Orth. 1994,64(3):175-188.

20. Goyer RA, Clarkson TW. Toxicity of metals. Klaassen CD, editor. Casarett and Doull's Toxicology: The Basic Science of Poisons. USA: McGraw-Hill Book Company Inc. 2001:811–868.

21. Gu X, Zheng Y, Cheng Y, Zhong S, Xi T. In vitro corrosion and biocompatibility of binary magnesium alloys. Biomaterials. 2009,30:484–98.

22. Gu XN, Zhou WR, Zheng YF, Cheng Y, Wei SC, Zhong SP, Xi TF, Chen LJ. Corrosion fatigue behaviors of two biomedical Mg alloys - AZ91D and WE43 - In simulated body fluid. Acta Biomater. 2010,6(12):4605-13.

23. Guo L, He X, Shi W. Intercellular communications in multispecies oral microbial communities. Front Microbiol. 2014,1(5):328.

24. Hachenberg T, Sentürk M, Jannasch O, Lippert H. Postoperative Wundinfektionen. Pathophysiologie, Risikofaktoren, und Praventive Konzepte. [Postoperative wound infections. Pathophysiology, risk factors and preventive concepts]. Article in German. Anaesthesist. 2010,59(9):851-66.

25. Halleen JM, Tiitinen SL, Ylipahkala H, Fagerlund KM, Väänänen HK. Tartrate-resistant acid phosphatase 5b (TRACP 5b) as a marker of bone resorption. Clin Lab. 2006,52(9-10):499-509.

26. Haude M, Erbel R, Erne P, Verheye S, Degen H, Böse D, et al. Safety and performance of the drug-eluting absorbable metal scaffold (DREAMS) in patients with de-novo coronary lesions: 12 month results of the prospective, multicentre, first-in-man BIOSOLVE-I trial. The Lancet. 2013,381(9869):836-44.

27. He W, Zhang E, Yang K. Effect of Y on the bio-corrosion behavior of extruded Mg–Zn–Mn alloy in Hank's solution. Materials Science and Engineering: C. 2010,3(1):167–174.

28. Hemmer E, Kohl Y, Colquhoun V, Thielecke H, Soga K, Mathur S. Probing cytotoxicity of gadolinium hydroxide nanostructures. J Phys Chem B. 2010,114(12):4358-4365.

29. Hidron AI, Edwards JR, Patel J, Horan TC, Sievert DM, Pollock DA, Fridkin SK, National Healthcare Safety Network Team, Participating National Healthcare Safety Network Facilities. NHSN annual update: antimicrobial-resistant pathogens associated with healthcare-associated infections: annual summary of data reported to the National Healthcare Safety Network at the Centers for Disease Control and Prevention, 2006-2007. Infect Control Hosp Epidemiol. 2008,29(11):996-1011.

30. Hornberger H, Virtanen S, Boccaccini AR. Biomedical coatings on magnesium alloys - a review. Acta Biomater. 2012,8(7):2442-55.

31. Iizuka T, Mikkonen P, Paukku P, Lindqvist C. Reconstruction of orbital floor with polydioxanone plate. Int J Oral Maxillofac Surg. 1991,20(2):83-87.

32. Institute of Medicine Standing Committee on the Scientific Evaluation of Dietary Reference Intakes. Dietary Reference Intakes for Calcium, Phosphorous, Magnesium, Vitamin D, and Fluoride. Washington, DC: National Academy Press, 1997.

33. Jannasch O, Lippert H. Perioperative Prophylaxe und Therapie von Infektionen - Postoperative Wundinfektionen. [Surgical site infections]. Article in German. Anasthesiol Intensivmed Notfallmed Schmerzther. 2011,46(10):664-73.

34. Kang J, Sickbert-Bennett EE, Brown VM, Weber DJ, Rutala WA. Relative frequency of health care-associated pathogens by infection site at a university hospital from 1980 to 2008. Am J Infect Control. 2012,40(5):416-20.

35. Kawahara M. Effects of aluminum on the nervous system and its possible link with neurodegenerative diseases. J Alzheimers Dis. 2005,8(2):171-182.

36. Korting HC, Lukacs A, Vogt N, Urban J, Ehret W, Ruckdeschel G. Korting HC, Lukacs A, Vogt N, Urban J, Ehret W, Ruckdeschel G. Influence of the pH-value on the growth of Staphylococcus epidermidis, Staphylococcus aureus and Propionibacterium acnes in continuous culture. Zentralbl Hyg Umweltmed. 1992,193(1):78-90.

37. Kyker GC, Anderson EB. Rare Earths in Biochemical and Medical Research. Chemical toxicity of salts of lanthanum, yttrium and some other rare metals to animals. Oak Ridge Institute of Nuclear Studies, Inc., Conference Proceedings. 1955:91-101.

38. Li RW, Kirkland NT, Truong J, Wang J, Smith PN, Birbilis N, Nisbet DR. The influence of biodegradable magnesium alloys on the osteogenic differentiation of human mesenchymal stem cells. J Biomed Mater Res A. 2014 Feb 14. doi: 10.1002/jbm.a.35111. [Epub ahead of print]

39. Li Z, Gu X, Lou S, Zheng Y. The development of binary Mg-Ca alloys for use as biodegradable materials within bone. Biomaterials 2008,29(10):1329-44.

40. MagneZix Compression Screw 3.2. Product Information. Retrieved from http://syntellix.de/en/wp-content/uploads/2014/05/EN-Magnezix.
Date accessed: 06.01.2015.

41. McDonald JR, Olaison L, Anderson DJ, Hoen B, Miro JM, Eykyn S, Abrutyn E, Fowler VG Jr, Habib G, Selton-Suty C, Pappas PA, Cabell CH, Corey GR, Marco F, Sexton DJ. Enterococcal endocarditis: 107 cases from the international collaboration on endocarditis merged database. Am J Med. 2005,118(7):759-66.

42. McDonald WA, Watts J, Bowmer MI. Factors affecting Staphylococcus epidermidis growth in peritoneal dialysis solutions. J Clin Microbiol. 1986,24(1):104–107.

43. Moravej M, Mantovani D. Biodegradable metals for cardiovascular stent application: interests and new opportunities. Int J of Mol Sc. 2011,12(7): 4250-4270.

44. Mosmann T. Rapid colorimetric assay for cellular growth and survival: application to proliferation and cytotoxicity assays. J Immunol Methods. 1983,65(1-2):55-63.

45. Noordin, Shahryar, and Bassam Masri. Periprosthetic osteolysis: genetics, mechanisms and potential therapeutic interventions. CJS. 2012,55(6):408-417.

46. Paganelli FL, Willems RJ, Jansen P, Hendrickx A, Zhang X, Bonten MJ, Leavis HL. Enterococcus faecium biofilm formation: identification of major autolysin AtlAEfm, associated Acm surface localization, and AtlAEfm-independent extracellular DNA Release. MBio. 2013,4(2):e00154-13.

47. Park JB, Lakes RS. Biomaterials an Introduction. 3rd ed. Springer SpringerLink (Service en ligne), New York, NY, USA: 2007. p. 561.

48. Pauksch L, Hartmann S, Rohnke M, Szalay G, Alt V, Schnettler R, Lips KS. Biocompatibility of silver nanoparticles and silver ions in primary human mesenchymal stem cells and osteoblasts. Acta Biomater. 2014,10(1):439-49.

49. Peng Q, Huang Y, Zhou L, Hort N, Kainer KU. Preparation and properties of high purity Mg–Y biomaterials. Biomaterials. 2010,31(3): 398-403.

50. Pihl M, Chávez de Paz LE, Schmidtchen A, Svensäter G, Davies JR.Effects of clinical isolates of Pseudomonas aeruginosa on Staphylococcus epidermidis biofilm formation. FEMS Immunol Med Microbiol. 2010,59(3):504-12.

51. Plumb JA. Cell sensitivity assays: the MTT assay. Methods Mol Med. 2004,88:165-9.

52. Prabhakar AR, Savita Hadakar G, Raju OS. Comparative evaluation of pH and antibacterial effect of various calcium hydroxide combinations on E. faecalis and its effect on root strength: An in vitro study. Contemp Clin Dent. 2012,3(1):42-7.

53. Quereshy FA, Dhaliwal HS, El SA, Horan MP, Dhaliwal SS. Resorbable screw fixation for cortical onlay bone grafting: a pilot study with preliminary results. J Oral Maxillofac Surg. 2010,68(10):2497-502.

54. Quereshy FA, Goldstein JA, Goldberg JS, Beg Z.The efficacy of bioresorbable fixation in the repair of mandibular fractures: an animal study. J Oral Maxillofac Surg. 2000,58(11): 1263-1269.

55. Quinn A, Hill AD, Humphreys H. Evolving issues in the prevention of surgical site infections. Surgeon. 2009, 7(3):170-2.

56. Ratna SB, Sampath KTS, Chakkingal U, Nandakumar V, Doble M. Nano-hydroxyapatite reinforced AZ31 magnesium alloy by friction stir processing: a solid state processing for biodegradable metal matrix composites. J Mater Sci Mater Med. 2014,25(4):975-88.

57. Reardon KA, McIntosh AF, Shilling AT, Hagspiel KD, Al-Osaimi A, Berg C, Caldwell SH, Northup PG, Angle F, Mulder R, Rich TA. Treatment of primary liver tumors with Yttrium-90 microspheres (TheraSphere) in high risk patients: analysis of survival and toxicities. Technol Cancer Res Treat. 2009,8(1):71-7.

58. Reid IR. Should we prescribe calcium supplements for osteoporosis prevention? J Bone Metab. 2014,21(1):21-28.

59. Ribeiro M1, Monteiro FJ, Ferraz MP. Infection of orthopedic implants with emphasis on bacterial adhesion process and techniques used in studying bacterial-material interactions. Biomatter. 2012,2(4):176-94.

60. Russell, W. M. S., & Burch, R. L. The principles of humane experimental technique. London: Methuen, 1959.

61. Sandler G, Nguyen L, Lam L, Manglick MP, Soundappan SS, Holland AJ. Trampoline trauma in children: is it preventable? Pediatric Emergency Care. 2011,27(11):1052-6.

62. Sartori M, Giavaresi G, Tschon M, Martini L, Dolcini L, Fiorini M, Pressato D, Fini M. Long-term in vivo experimental investigations on magnesium doped hydroxyapatite bone substitutes. J Mater Sci Mater Med. 2014,25(6):1495-504.

63. Schaffler MB, Kennedy OD. Osteocyte signaling in bone. Curr Osteoporos Rep. 2012,10(2):118-25.

64. Seal, C. K., K. Vince, and M. A. Hodgson. Biodegradable surgical implants based on magnesium alloys–A review of current research. IOP Conf Ser: Mater Sci Eng. 2009,4(1):1-4.

65. Setyawati MI, Khoo PK, Eng BH, Xiong S, Zhao X, Das GK, Tan TT, Loo JS, Leong DT, Ng KW. Cytotoxic and genotoxic characterization of titanium dioxide, gadolinium oxide, and poly(lactic-co-glycolic acid) nanoparticles in human fibroblasts. J Biomed Mater Res A. 2013,101(3): 633-640.

66. Shadanbaz S, Dias GJ. Calcium phosphate coatings on magnesium alloys for biomedical applications:A review. Acta Biomaterialia. 2012(8):20–30.

67. Shalabi MM, Gortemaker A, Van't Hof MA, Jansen JA, Creugers NH. Implant surface roughness and bone healing: a systematic review. J Dent Res. 2006, 85: 496–500.

68. Shaw BA. Corrosion Resistance of Magnesium Alloys. D. Stephen, editor. ASM handbook, vol 13a, Corrosion: fundamentals, testing and protection. UK: ASM International. 2003:692-696.

69. Shcherbatykh I, Carpenter DO. The role of metals in the etiology of Alzheimer's disease. J Alzheimers Dis. 2007,11(2):191-205.

70. Sinikumpu JJ, Lautamo A, Pokka T, Serlo W. The increasing incidence of pediatric diaphyseal both-bone forearm fractures and their internal fixation during the last decade. Injury. 2012, 43(3):362-6.

71. Sinikumpu JJ, Lautamo A, Pokka T, Serlo W. The increasing incidence of paediatric diaphyseal both-bone forearm fractures and their internal fixation during the last decade. Injury. 2012,43(3):362-6.

72. Smyth ET, Emmerson AM. Surgical site infection surveillance. J Hosp Infect. 2000, 45 (3):173-84.

73. Smyth ET, McIlvenny G, Enstone JE, Emmerson AM, Humphreys H, Fitzpatrick F, Davies E, Newcombe RG, Spencer RC. Four country healthcare associated infection prevalence survey 2006: overview of the results. Journal of Hospital Infection. 2008,69(3):230-248.

74. Staiger MP, Pietak AM, Huadmai J, Dias G. Magnesium and its alloys as orthopedic biomaterials: a review. Biomaterials 2006, 27:1728–34.

75. Stout KJ, Sullivan PJ, Dong WP, Mainsah E, Luo N, Mathia T, Zahouani H. Development of Methods for Characterisation of Roughness in Three Dimensions. European Community Contract No 3374/1/0/170/90/2 Birmingham: Univ of Birmingham, 1993.

76. Sumitomo N, Noritake K, Hattori T, Morikawa K, Niwa S, Sato K, Niinomi M. Experiment study on fracture fixation with low rigidity titanium alloy: plate fixation of tibia fracture model in rabbit. J Mater Sci Mater Med. 2008,19:1581–1586.

77. Tennert C, Fuhrmann M, Wittmer A, Karygianni L, Altenburger MJ, Pelz K, Hellwig E, Al-Ahmad A. New bacterial composition in primary and persistent/secondary endodontic infections with respect to clinical and radiographic findings. J Endod. 2014,40(5):670-7.

78. Tie D, Feyerabend F, Müller WD, Schade R, Liefeith K, Kainer KU, Willumeit R. Antibacterial biodegradable Mg-Ag alloys. Eur Cell Mater. 2013,16(25):284-98.

79. Waizy H, Seitz JM, Reifenrath J, Weizbauer A, Bach FW, Meyer-Lindenberg A, Denkena B, Windhagen H. Biodegradable magnesium implants for orthopedic applications. J Mater Sci 2012. DOI: 10.1007/s10853-012-6572-2

80. Waizy H, Seitz JM, Reifenrath J, Weizbauer A, Bach FW, Meyer-Lindenberg A, Denkena B, Windhagen H. Biodegradable magnesium implants for orthopedic applications. J Mater Sci. 2013,48:39–50.

81. Waizy H, Diekmann J, Weizbauer A, Reifenrath J, Bartsch I, Neubert V, Schavan R, Windhagen H. In vivo study of a biodegradable orthopedic screw (MgYREZr-alloy) in a rabbit model for up to 12 months. J Biomater Appl. 2014,28(5):667-75.

82. Waksman R, Erbel R, Di Mario C, Bartunek J, de Bruyne B, Eberli FR. Early- and long-term intravascular ultrasound and angiographic findings after bioabsorbable magnesium stent implantation in human coronary arteries. J Am Coll Cardiol Intv. 2009,2(4):312-20.

83. Waksman R, Pakala R, Kuchulakanti PK, Baffour R, Hellinga D, Seabron R, Tio FO, Wittchow E, Hartwig S, Harder C, Rohde R, Heublein B, Andreae A, Waldmann KH, Haverich A. Safety and efficacy of bioabsorbable magnesium alloy stents in porcine coronary arteries. Catheter Cardiovasc Interv. 2006,68:607–617.

84. Weckwerth PH, Zapata RO, Vivan RR, Tanomaru Filho M, Maliza AG, Duarte MA. In vitro alkaline pH resistance of Enterococcus faecalis. Braz Dent J. 2013,24(5):474-6.

85. Wenisch S, Trinkaus K, Hild A, Hose D, Herde K, Heiss C, Kilian O, Alt V, Schnettler R. Human reaming debris: a source of multipotent stem cells. Bone. 2005, 36(1):74

86. Wennerberg A, Albrektsson T. Suggested guidelines for the topographic evaluation of implant surfaces. Int J Oral Maxillofac Implants. 2000,1(5):331–344.

87. Williams D. New interests in magnesium. Med Device Technol 2006,17(3):9–10.

88. Willumeit R, Fischer J, Feyerabend F, Hort N, Bismayer U, Heidrich S, Mihailova B. Chemical surface alteration of biodegradable magnesium exposed to corrosion media. Acta Biomater. 2011,7(6):2704-15.

89. Windhagen H, Radtke K, Weizbauer A, Diekmann J, Noll Y, Kreimeyer U, Schavan R, Stukenborg-Colsman C, Waizy H. Biodegradable magnesium-based screw clinically equivalent to titanium screw in hallux valgus surgery: short term results of the first prospective, randomized, controlled clinical pilot study. BioMedical Engineering OnLine. 2013,12:62-72.

90. Witte F, Feyerabend F, Maier P, Fischer J, Störmer M, Blawert C, Dietzel W, Hort N. Biodegradable magnesium-hydroxyapatite metal matrix composites. Biomaterials. 2007,28(13):2163-74.

91. Witte F, Hort N, Vogt C, Cohen S, Kainer KU, Willumeit R, Feyerabend F. Degradable biomaterials based on magnesium corrosion. Curr Opin Solid State Mater Sci. 2008,12:63–72.

92. Witte F, Kaese V, Haferkamp H, Switzer E, Meyer-Lindenberg A, Wirth CJ, Windhagen H. In vivo corrosion of four magnesium alloys and the associated bone response. Biomaterials. 2005,26(17):3557-63.

93. Witte F. The history of biodegradable magnesium implants: a review. Acta Biomater. 2010,6:1680–1692.

94. Witte F, Ulrich H, Palm C, et al. Biodegradable magnesium scaffolds: Part II: peri-implant bone remodeling. J Biomed Mater Res A. 2007,81:757–765.

95. Wong HM, Wu S, Chu PK, Cheng SH, Luk KD, Cheung KM, Yeung KW. Low-modulus Mg/PCL hybrid bone substitute for osteoporotic fracture fixation. Biomaterials. 2013,34(29):7016-32.

96. Wu F, Wei J, Guo H, Chen F, Hong H, Liu C. Self-setting bioactive calcium-magnesium phosphate cement with high strength and degradability for bone regeneration. Acta Biomater. 2008,4(6):1873-84.

97. Xin Y, Hu T, Chu PK. In vitro studies of biomedical magnesium alloys in a simulated physiological environment: A review. Acta Biomater. 2011,7(4):1452-9.

98. Xu L, Yu G, Zhang E, Pan F, Yang K. In vivo corrosion behavior of Mg-Mn-Zn alloy for bone implant application. J Biomed Mater Res A. 2007,83(3):703-11.

99. Yan PF, Liang JP, Jiang YT. [The influence of different alkaline pH conditions on Enterococcus faecalis in planktonic and biofilm mode].Shanghai kou qiang yi xue= Shanghai J Stomat. 2012,21(1):6-8.

100. Yang L, Hort N, Laipple D, Höche D, Huang Y, Kainer KU, Willumeit R, Feyerabend F. Element distribution in the corrosion layer and cytotoxicity of alloy Mg-10Dy during in vitro biodegradation. Acta Biomater. 2013,9(10):8475-87.

101. Zhang S, Zhang X, Zhao C, et al. Research on an Mg-Zn alloy as a degradable biomaterial. Acta Biomater. 2010,6:626–640.

102. Zreiqat H, Howlett CR, Zannettino A, et al. Mechanisms of magnesium-stimulated adhesion of osteoblastic cells to commonly used orthopaedic implants. J Biomed Mater Res. 2002, 62: 175–184.

103. Zeng D, Xia L, Zhang W, Huang H, Wei B, Huang Q, Wei J, Liu C, Jiang X. Maxillary sinus floor elevation using a tissue-engineered bone with calcium-magnesium phosphate cement and bone marrow stromal cells in rabbits. Tissue Eng Part A. 2012,18(7-8):870-81.

10. Summary

Background. Clinical problems like postoperative infection and increased incidence of pediatric trauma requiring surgical intervention raised the need for temporary medical implants that would resorb after the bone healing is complete. This would decrease high costs associated with repeated surgeries, minimize recovery times, decrease the risk of postoperative infections, and thus promote higher quality of life to the patients. The concept of biodegradation is already known in medical practice: resorbable sutures are successfully used in surgery. However, a bone implant that would resorb after the fracture heals is a new concept. Magnesium was suggested as a suitable material for these purposes because it is biocompatible and stimulates new bone formation. This doctoral Thesis evaluates both *in vitro* and *in vivo* behaviour of magnesium-based implants and consists of four parts: degradation, cellular reaction, early biofilm formation and histology study.

Materials and Methods. Degradation properties of Mg2Ag, Mg10Gd, WE43 and 99.99 % pure Mg were studied by immersion and gas evolution tests. The corrosion rate (CR), osmolality, pH, Ca^{2+} concentrations, and surface changes were determined. Biocompatibility was studied by exposing primary human reaming debris-derived cells (HRD) to described magnesium alloys and assesing cell viability, morphology, differentiation to osteoblasts, along with evaluation of pH changes and Ca^{2+} concentration induced by magnesium. Mg2Ag, Mg10Gd, WE43 and 99.99 % pure Mg were further tested for their ability to resist biofilm formation. *S. epidermidis* and *E. faecalis* were allowed to adhere to the magnesium surfaces for 2 hours (h) followed by rinsing and, for *S. epidermidis*, further incubation of 24, 72 and 168 h was carried out. Furthermore, an animal study was performed and consisted of histological and histomorphometrical analysis of three magnesium-based materials: magnesium-hydroxyapatite (Mg-HA), W4 (96 % magnesium, 4 % yttrium), and pure magnesium (pure Mg). Bone response to magnesium and implants' resorption behaviour was studied.

Results. **Degradation.** WE43 showed the highest CR of all materials tested – 1.057 mm/year – which is almost twice as high as in the other samples. The lowest mean CR was in Mg2Ag group. All alloys made pH more alkaline and decreased concentration of free Ca^{2+} in the solution. Osmolality decreased in all samples after day 7. Pure Mg had the most constant S_a and S_{dr} of all materials over the observation period. **Cellular Reaction.** The number of viable cells in presence of all magnesium samples was stable over the observation period of 21 days. The inhibition of ALP content in osteogenic differentiating HRD was caused by pure Mg at day 14

and 28. All other magnesium alloys did not affect the ALP content. Exposure of HRD to magnesium increased the amount of lysosomes and endocytotic vesicles. **Early Stages of Biofilm Formation.** *E. faecalis* were significantly more prevalent on all magnesium surfaces compared to *S. epidermidis* (p = 0.001). Biofilm growth of *S. epidermidis* was different on various magnesium materials: the amount of bacteria increased up to 72 h but interestingly a significant decrease was seen at 168 h on Mg2Ag and WE43 surfaces. For pure Mg and Mg10Gd the biofilm formation reached plateau at 72 h. No correlation was found between the surface topology and the amount of adherent bacteria. **Histology.** Mg-HA had the highest mean amount of tartrate-resistant acid phosphatase (TRAP) positive cells at the implantation site of all groups. It had shown the fastest degradation rate already at 6 weeks. New bone was observed in direct contact to pure Mg and W4. The mean gas volume was highest in W4 compared to pure Mg and Mg-HA but this difference was not statistically significant.

Conclusions. In vitro. Mg-Ag alloys seem to be the most promising in respect to the cellular reactions, degradation rates, the effect on the surrounding environment and the ability to withstand the biofilm growth after 72 h in vitro. *In vivo.* Pure Mg and W4 were the most promising material in the in vivo experiment. Mg-HA had too fast resorption probably due to the high levels of HA comprising 20 % of the material's composition. The level of HA should be reduced in future studies.

11. Zusammenfassung

Hintergrund. Die erhöhte Inzidenz von pädiatrischen Verletzungen sowie postoperativen Infektionen, die eine chirurgische Intervention erfordern, lassen die Entwicklung von temporären Implantaten zunehmend notwendig erscheinen. Es werden darunter Implantate verstanden, die nach abgeschlossener Frakturheilung vollständig resorbiert werden. Ihre Verwendung würden die hohen Operationskosten zur Implantatentfernung und das Risiko von postoperativen Infektionen reduzieren sowie die Lebensqualität der Patienten steigern. Das Konzept des biologischen Abbaus ist in der medizinischen Praxis bereits bekannt: resorbierbare Nähte werden in der Chirurgie erfolgreich eingesetzt. Ein Knochenimplantat, das sich nach der Frakturheilung auflöst, wäre jedoch ein völlig neues Konzept. Magnesium könnte für die Herstellung von bioresorbierbaren Implantaten geeignet sein, da es biologisch gut verträglich ist und die Knochenbildung stimuliert. Ziel der vorliegenden Dissertation war es sowohl in vitro als auch in vivo das Verhalten von Implantate auf Magnesium (Mg)-Basis zu untersuchen. Hierbei standen vier biologische Teilprozesse im Vordergrund: Abbau, zelluläre Reaktion, frühe Bildung von Biofilmen und die histologische Beurteilung der Verträglichkeit von Magnesiumimplantaten.

Materialien und Methoden. Die Degradation von Mg2Ag, Mg10Gd, WE43 und 99,99 % reinem Mg wurde durch die Analyse der Gasentwicklung, der Korrosionsgeschwindigkeit (CR), der Osmolarität, des pHs, der Ca^{2+} Konzentration und der Oberflächenveränderungen bestimmt. Zur Untersuchung der in vitro Biokompatibilität wurden primäre vom humanen Bohrmehl abgeleitete mesenchymalen Stammzellen (HRD) und folgende zellbiologische Methoden verwendet: MTT-Assay, Transmissions- und Rasterelektronenmikroskopie zur Bestimmung der zellulären Vitalität, Calcium-Verbrauch und Gehalt an alkalischer Phosphatase (ALP) zur Beurteilung der Differenzierung der HRD zu Osteoblasten und pH-Änderungen zum Nachweis einer möglichen Induktion der Knochenbildung durch Magnesium-Ionen. Weiterhin wurde die Bildung von Biofilm durch *S. epidermidis* und *E. faecalis* auf der Oberfläche von Mg2Ag, Mg10Gd, WE43 und 99,99 % reinem Mg untersucht, wofür die Implantatoberflächen über mehrere Stunden mit den Bakterien inkubiert wurden. In vivo erfolgte eine Untersuchung von Implantaten aus Magnesium-Hydroxyapatit (Mg-HA), W4 (96 % Magnesium, 4 % Yttrium) und reinem Magnesium (reines Mg), die in ein künstlich erzeugtes Bohrloch (5,5 mm) in die laterale Femurkondyle des linken Femurs von 24 weiblichen Kaninchen eingebracht wurden. Das Resorptionsverhalten der Implantate sowie die zelluläre Reaktion des Knochens wurde nach Extraktion der Knochen nach einer postoperativen Zeit von 6 und 12 Wochen histologisch, histomorphometrisch und enzymhistochemisch untersucht.

Ergebnisse. Degradation. WE43 zeigte die höchste CR aller getesteten Materialien (1,057 mm/Jahr), die damit fast doppelt so hoch war wie die der anderen Proben. Die niedrigste durchschnittliche CR wurde in der Mg2Ag-Gruppe gemessen. Bei allen Mg-Legierungen wurde ein Anstieg des pHs und eine Reduktion der freien Ca^{2+}-Ionen nachgewiesen. Nach einer 7-tägigen Inkubationszeit sank die Osmolarität in allen Proben. Reines Mg hatte die konstanteste Oberfläche (S_a und S_{dr}) von allen untersuchten Materialien während des gesamten Beobachtungszeitraums. **Zelluläre Reaktion.** Die Zahl der lebensfähigen Zellen in Anwesenheit aller Magnesiumproben war über den Beobachtungszeitraum von 21 Tagen stabil. Die osteogene Differenzierung der HRD (ALP-Gehalt) wurde von reinem Mg gehemmt (Tag 14 und 28). Die Magnesiumlegierungen beeinflussten den ALP-Gehalt nicht. Durch die Exposition mit Magnesium wurde die Menge an Lysosomen und Endocytosevesikeln erhöht. **Frühe Phase der Biofilmbildung.** Bakterien des Stammes *E. faecalis* waren signifikant häufiger auf den Magnesiumoberflächen zu finden als *S. epidermidis* ($p = 0,001$). Die Biofilmbildung von *S. epidermidis* war abhängig vom verwendeten Magnesiumwerkstoff: Nach einer anfänglichen generellen Erhöhung der Bakteriendichte (72 Stunden), wurde interessanterweise eine signifikante Abnahme nach 168 Stunden auf Mg2Ag und WE43 beobachtet, während für das reine Mg und Mg10Gd die Biofilmbildung nach 72 Stunden ein Plateau erreichte. Es wurde keine Korrelation zwischen der Oberflächentopologie und der Menge der adhärierenden Bakterien gefunden. **Histologie.** Am Interface des Mg-HA Implantats konnte die höchste durchschnittliche Menge von Tartrat-resistenten saure Phosphatase (TRAP) positiven Zellen nachgewiesen werden. Die höchste Abbaurate wurde bereits nach 6 Wochen erzielt. Die Bildung von neuem Knochen konnte in direktem Kontakt mit reinem Mg und W4 beobachtet werden. Das durchschnittliche Gasvolumen war nach Implantation von W4 am höchsten, während reines Mg und Mg-HA eine geringere aber nicht signifikante Reduktion der Gasbildung aufwiesen.

Schlussfolgerungen. *In vitro.* Mg-Ag-Legierungen scheinen am vielversprechendsten zu sein in Bezug auf die Zellreaktionen, Abbaurate, die Auswirkung auf die Umwelt und die Fähigkeit, dem Biofilmwachstum nach 72 Stunden in vitro zu widerstehen. *In vivo.* Reines Mg und W4 sind die vielversprechendsten Materialien im in vivo Experiment. Mg-HA zeigte eine zu schnell Resorption, vermutlich aufgrund des hohen HA-Gehalts (20 % der Materialzusammensetzung). Das Niveau des HA-Gehalts sollte in zukünftigen Studien reduziert werden.

12. Declaration

I declare that I have completed this dissertation single-handedly without the unauthorized help of a second party and only with the assistance acknowledged therein. I have appropriately acknowledged and referenced all text passages that are derived literally from or are based on the content of published or unpublished work of others, and all information that relates to verbal communication. I have abided by the principles of good scientific conduct laid down in the charter of the Justus Liebig University of Giessen in carrying out the investigations described in the dissertation.

- *Olga Wetterlöv Charyeva*

13. Acknowledgements

This thesis would not have been possible without all the inspiring and generously supporting people around me. I wish to express my sincere gratitude to:

My supervisor at *Justus-Liebig University Giessen (JLU)* professor **Katrin Sussane Lips** for her expert guidance in academic thinking, writing and performing. Your technical and editorial advice was essential to the completion of this dissertation and has taught me innumerable lessons and insights on the workings in academic research. Danke für alles Katrin!

My supervisor at *aap Biomaterials GmbH (aap)*, Dieburg, Dr **Daniel Zukowski** for his encouragement and believing in me, as well as giving me this chance to do my PhD. I have been given a unique opportunity to learn cutting-edge research at one of the best European research groups for which I am very grateful. Thank you Daniel for always being there for me, vielen vielen dank.

This journey would not been possible without professor **Ryo Jimbo** and my co-supervisor professor **Ann Wennerberg** from the *Faculty of Odontology, Malmö University Sweden* (MAH) who saw my desire to go to academy and advised me to apply for this PhD position. Kära Ann och Ryo, tack så mycket för all hjälp, jag kommer alldrig glöma er, mina lärare!

My research group *MagnIm* for all inspiring discussions, meetings and workshops. It has been a memorable journey for me where I met friends for life. Special thanks to the group leader professor **Regine Willumeit** for building such a strong group of the early stage researchers.

I am greatful to my fellow PhD students from *MagnIm*: **Francesca Cecchinato** from Malmö University (MAH), **Nezha Agha** from *Helmholz Zentrum Geesthacht* (HZG), **Gabor Szakacs** (HZG) and **Sepideh Mostofi** from *Medical University Graz* (MUG) for valuable disscusions. Thank you **Silvia Galli** (MAH), **Anastasia Myrissa** (MUG), **Sriveena Srinivasaiah** (MUG), **Maria Costantino** (HZG), **Inigo Marco** and **Andrea Gil** from *KU Leuven*, **Marian Vlcek and Frantisek Lukas** from the *Charles University Prague* for inspiring me during the project. Special thanks to my friend and collegue **Dr Seemun Ray** (JLU) for valuable advices on doing PhD.

I thank all my co-authors for valuable discussions especially Dr **Jessica Neilands** and professor **Gunnel Svensätter** (MAH), Professor **Christian Heiß**, Dr **Ursula Sommer** and Dr **Ulrich Thormann** (JLU), Dr **Frank Feyerabend** and Dr **Norbert Hort** (HZG), Dr **Cyrille Gasqueres** and Dr **Lydia Heimann** (aap). I have learned a lot from you.